CERN Yellow Reports: Monographs CERN-2020-006

Linac4 design report

Editor: Maurizio Vretenar

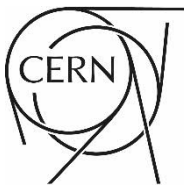

CERN Yellow Reports: Monographs
Published by CERN, CH-1211 Geneva 23, Switzerland

ISBN 978-92-9083-579-0 (paperback)
ISBN 978-92-9083-580-6 (PDF)
ISSN 2519-8068 (Print)
ISSN 2519-8076 (Online)
DOI https://doi.org/10.23731/CYRM-2020-006

This volume should be cited as:
Linac4 design report,
CERN Yellow Reports: Monographs, CERN-2020-006 (CERN, Geneva, 2020),
doi:10.23731/CYRM-2020-006

Editor: Maurizio.Vretenar@cern.ch
Accepted by the CERN Reports Editorial Board (contact Carlos.Lourenco@cern.ch) in September 2020.
Published by the CERN Scientific Information Service (contact Jens.Vigen@cern.ch).
Indexed in the CERN Document Server and in INSPIRE.
Published Open Access to permit its wide dissemination, as knowledge transfer is an integral part of the mission of CERN.

Linac4 design report

M. Vretenar (editor), J. Bauche, P. Baudrenghien, Y. Body, O. Brunner, M. Buzio, M. Calviani, N. Dos Santos, J.F. Fuchs, A. Funken, F. Gerigk, J. Hansen, I. Kozsar, J.B. Lallement, J. Lettry, A. Lombardi, L.A. Lopez-Hernandez, C. Martin, S. Mathot, R. Mompo, D. Nisbet, B. Puccio, U. Raich, S. Ramberger, F. Roncarolo, C. Rossi, R. Scrivens, J. Vollaire, T. Zickler
CERN, Geneva, Switzerland

Abstract
Linear accelerator 4 (Linac4) is designed to accelerate negative hydrogen ions for injection into the Proton Synchrotron Booster (PSB). It will become the source of proton beams for the Large Hadron Collider (LHC) after the long shutdown in 2019–2020. Linac4 will accelerate H^- ions, consisting of a hydrogen atom with an additional electron, to 160 MeV energy and then inject them into the PSB, which is part of the LHC injection chain. The new accelerator comprises an ion source and four types of accelerating structures. The particles are accelerated first to 3 MeV energy by a Radio-Frequency Quadrupole (RFQ), then to 50 MeV by three Drift Tube Linacs (DTL) tanks, then to 100 MeV by seven Cell-Coupled Drift Tube Linac (CCDTL) modules, and finally to 160 MeV by twelve Pi-Mode Structures (PIMS). A chopper line placed between the RFQ and the first DTL tank modulates the linac beam at the PSB injection frequency. Linac4 includes transfer and measurement lines up to the PSB injection, where the ions are stripped of their two electrons to leave only protons. Linac4 is 76 metres long and located 12 metres below ground. The first low-energy beams were produced in 2013 and after the commissioning of all accelerating structures the milestone energy of 160 MeV was reached in 2016. Linac4 will be connected to the PSB during the long shutdown of 2019–20, after which it will replace the 50 MeV Linac2 as source of protons for the LHC. The Linac4 is a key element in the project to increase the luminosity of the LHC during the next decade.

Keywords
Linear accelerators; injectors; the CERN accelerator complex.

Table of Contents

1 Introduction and general design

1.1 From Linac2 to Linac4

The idea of building a new linear accelerator to make the Large Hadron Collider (LHC) injectors capable of producing higher brightness beams dates back to the late 1990s [1]: at that time the LHC construction was progressing quickly and a high luminosity upgrade after about 10 years of operation was considered as a logical evolution of this unique facility. From this perspective, the construction of some new accelerators was unavoidable: although successful, the programme for the upgrade of the LHC injectors that took place between 1993 and 2000 in view of enabling the nominal LHC luminosity (10^{34} $cm^{-2}s^{-1}$) showed inherent limitations in the LHC injection chain that would not allow a significant progression beyond nominal [2]. In particular, the beam current upgrade of Linac2 that was part of the programme allowed a record proton current of 180 mA to be reached [3], but with limited benefits in the downstream Proton Synchrotron Booster (PSB) because of the limitations related to the multi-turn injection of protons at the relatively low energy of 50 MeV.

One of the main components of the LHC luminosity is the beam brightness (ratio between current and emittance) generated by the injectors, generally limited by space charge effects. In the LHC injection chain, the main limitations are related to transverse emittance blow-up due to incoherent space charge tune shift at injection into the first two synchrotrons of the chain, PSB and proton synchrotron (PS). The incoherent self-field detuning in the horizontal and vertical planes can be expressed in a simplified form as

$$\Delta Q_{x,y} \propto \frac{I_p}{\varepsilon^*_{x,y}\,\beta\gamma^2},$$

where I_p is the bunch peak current, $\varepsilon^*_{x,y}$ are the normalized emittances, and β, γ are the usual relativistic parameters; the beam brightness is the ratio $I_p/\varepsilon^*_{x,y}$. It appears from this relation that increasing the injection energy to achieve a higher $\beta\gamma^2$ is the only way to increase brightness while limiting tune shift to acceptable values. In particular, for the injection in the PSB a significant increase in Linac2 energy is not possible within the limited space available, and construction of a new injector linac is the only viable scenario for an increase in brightness [4].

Following these considerations, the first proposal to increase the LHC injector brightness had a broader scope and consisted of the construction of a 2 GeV high-energy linac, the SPL (superconducting proton linac), injecting directly into the PS [5]. This largely superconducting accelerator reusing part of the cavities and Radio Frequency (RF) equipment from the decommissioned Large Electron Positron (LEP) collider intended to simultaneously address the increase of the luminosity for the LHC and new demands for high-intensity proton beams at CERN for production of intense neutrino or radioactive ion beams. Replacing the PSB and injecting into the PS at an energy higher than the original 1.4 GeV the SPL was expected to eliminate at the same time brightness limitations related to injection into both the PSB and the PS. Production of the extreme proton intensities required to deliver intense secondary beams would have been made possible by pulsing the linac at a higher repetition frequency than what required by the PS. Additionally, the SPL was designed for the acceleration of H^- ions instead of protons, to benefit from the advantages of charge-exchange injection in a synchrotron using a stripping foil, a technique already in use in the major accelerator laboratories but never applied at CERN.

The idea of replacing only Linac2 with a new linac at higher energy came out in the early 2000s, following the refocusing of CERN resources on the LHC and the reduced priority given to the high-intensity programme. At that moment, the scope of the initial SPL proposal was reduced and its implementation was planned in a staged version, with an initial step consisting of replacing Linac2 with a new Linac4, whose design was based on the normal-conducting low-energy section of the SPL [6, 7].

The new linac was called Linac4 because it was the fourth linac to be built at CERN, following the heavy-ion Linac3 commissioned in 1994; its main goals were to remove the brightness limitations at PSB injection and to allow the implementation of the H^- injection in the PSB. After Linac4, the construction of a low-power version of the SPL was foreseen to replace the PSB as injector to the PS. This had to be followed at a later stage by a high beam power upgrade of the facility obtained by increasing the pulse repetition frequency [8].

Together with the increase in performance, Linac4 was expected to reduce maintenance effort and increase beam availability with respect to Linac2. In particular, it was intended to mitigate the risks for LHC operation related to persistent vacuum problems of Linac2 due to the obsolete mechanical construction technology of its large accelerating tanks [9].

After an extensive R&D phase, the Linac4 Technical Design Report (TDR) was published at the end of 2006 [10]. Part of the R&D effort was carried out within an international collaboration supported by the CARE (Coordinated Accelerator Research in Europe) project of the 6th European Commission Framework Programme [11].

The TDR was the basis for the decision to approve the Linac4 construction taken by the CERN Council in its June 2007 Session, as part of a programme to prepare a future upgrade of the LHC and of its injectors in line with the recommendations of the first European Strategy for Particle Physics that took place in 2006. The approved programme included the upgrade of the PSB injector region for H^- injection but other interventions in the injector complex remained at the level of design studies; the exact location of Linac4 on the CERN site was still under discussion. Following the approval, an analysis of the possible options led to the decision to build Linac4 in an underground tunnel at the position of the so-called 'Mount-Citron', an artificial hill close to Linac2 created in the 50s with the spoil from the PS excavation. This site provides an adequate natural shielding, an easy connection to the existing Linac2-PSB transfer line, and the possibility to extend the tunnel to reach higher energies; the overall layout including the possible extension to an SPL is shown in Fig. 1.1. The Linac4 ground-breaking ceremony took place at this location on October 16th 2008.

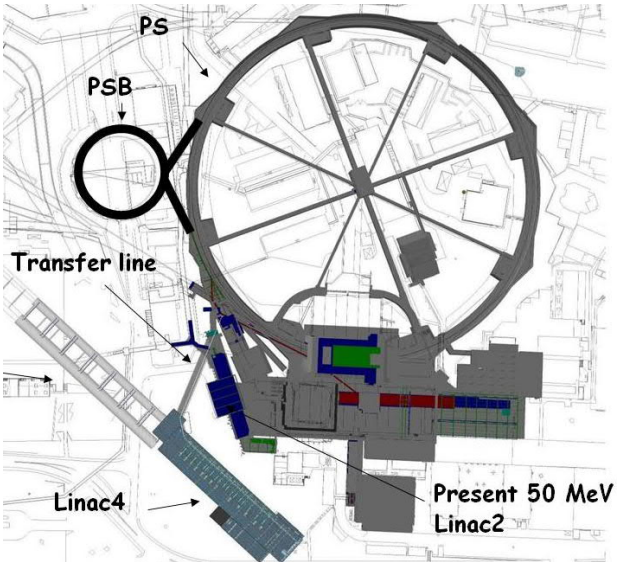

Fig. 1.1: Location of Linac4 (and possible high-energy extension) in the PS accelerator complex.

The strategy for the upgrade of the LHC injectors went through a revision in 2010, leading to the decision to consolidate the PSB and increase its energy to 2 GeV instead of building a new injector for the PS. The Linac4 design is entirely compatible with this new scenario, which resulted in the definition of an extensive project called the LHC Injector Upgrade (LIU) encompassing the entire LHC injection

chain composed by Linac4, PSB, PS, and the Super Proton Synchrotron SPS. This project integrates the Linac4 construction into a broad and coherent set of actions along the injection chain to increase the brightness of the beams delivered to the LHC [12].

The civil engineering works for Linac4 were completed in December 2010; Fig. 1.2 shows the original situation of Mount-Citron and the same position with the Linac4 building. The installation of all infrastructure in the building and tunnel took place in 2011 and 2012, and from 2013 onwards the accelerator components started to be installed and progressively commissioned. Most of the installation and commissioning of the linac took place after the 2013/14 LHC long shutdown to avoid interference with the LHC activities; the installation of the PSB H^- injection and the connection of Linac4 in front of the LHC injection chain is scheduled for the second long LHC shutdown.

Fig. 1.2: Mount-Citron in 2008 (left) and the same position in 2010 (right), after construction of the Linac4 building.

1.2 Parameters and layout

The main Linac4 beam parameters (Table 1.1) are based on the PSB requirements for the high-luminosity LHC upgrade, reported in Table 1.2 as specified in the LIU Technical Design Report [12].

Table 1.1: Main Linac4 beam parameters.

Ion species	H^-
Output kinetic energy	160 MeV
Bunch frequency	352.2 MHz
Maximum rep. frequency	2 Hz
Maximum beam pulse length	600 μs
Chopper beam-on factor	65 %
Source current[a], nominal	40 mA
Linac current[b], nominal	25 mA
Linac current[c], maximum	40 mA
Transverse emittance, root-mean-square (rms) normalised	0.4 π mm mrad

[a] Current at LEBT exit inside the radio frequency quadrupole (RFQ) acceptance

[b] Average beam current in the linac pulse, after chopping

[c] After chopping, for a source current of 62 mA

Table 1.2: PSB proton beam characteristics for LHC, from LIU TDR [11].

Kinetic energy	Number of bunches	Bunch intensity	Transverse emittance	Longitudinal emittance	Bunch length
160 MeV	4 (1 / ring)	2.96×10^{12} protons	1.5 μm	1.4 eVs	650 ns

Together with the LHC beams, Linac4 is designed to allow the PSB to provide a higher intensity to the ISOLDE post-accelerator and experiments. The maximum intensity delivered so far by the PSB for ISOLDE is 3.5×10^{13} protons/pulse; the planned high intensity and energy (HIE) ISOLDE upgrade, which requires important modifications to the ISOLDE dumps and shielding, sets the maximum intensity expected with Linac4 to 6.4×10^{13} protons/pulse [13].

The Linac4 energy of 160 MeV has been chosen to increase by a factor of two the relativistic $\beta\gamma^2$ factor of the particles at injection in the PSB with respect to the present 50 MeV injection from Linac2. This will allow the same incoherent space charge tune shift at injection in the PSB with twice the present 50 MeV brightness to be kept and, finally, the intensity that can be accumulated within a given emittance doubled.

The RF frequency of 352.2 MHz, selected to make the reuse of some klystrons, circulators, waveguides, and other RF components from the decommissioned LEP accelerator possible, is well matched to the requirements of a modern proton linear accelerator. With respect to lower frequencies, the 300–400 MHz frequency range offers the advantages of reduced cavity dimensions, simpler fabrication techniques, higher RF efficiency and achievable gradients, and at the same time allows for standard fabrication tolerances, excellent beam quality and the possibility of keeping the same frequency for the whole linac, from low to high energy.

Linac4 is pulsed at the repetition frequency required by the PSB, with some limited margin available for future upgrades or tests. While the PSB usually operates at 1.2 s bunch spacing (0.83 Hz), the transfer line elements can pulse at 1.1 Hz, corresponding to a pulse spacing of 0.9 s considered as the minimum achievable by the PSB following a major upgrade. The linac without the transfer line can pulse at a maximum frequency of 2 Hz to be able, if needed, to interlace the pulses going to the PSB with some additional pulses for beam measurements directed towards the beam dump. Further increases of the pulse repetition frequency, up to the limiting value of 50 Hz permitted by the RF cavities, would be possible only after a major upgrade of power converters, cooling system, and ion source. The maximum length of the beam pulse is 600 μs, limited by the PSB distributor. The maximum duty cycle achievable by the linac in limit conditions is therefore 0.12%, although it is not foreseen to operate simultaneously at maximum pulse length and repetition frequency.

Within the pulse, the beam can be chopped to provide empty sections corresponding to the edges of the PSB longitudinal acceptance (‘bucket’). Chopping is provided by a fast deflector placed at 3 MeV energy, which eliminates individual bunches or trains of bunches on a beam dump. The required bunch length of 650 ns in the PSB for a 1 MHz RF frequency at capture means that only 65% of the 352 MHz bunches of the linac will be injected in the PSB bucket, the remaining 35% are removed at low energy.

The transverse normalized rms emittance of 0.4 π mm mrad expected at PSB injection corresponds to the minimum considered as achievable by the ion source, about 0.3 π mm mrad, with some margin for emittance growth in the linac and in the transfer line. This emittance is lower than what was provided by Linac2 and leaves a margin for painting the PSB emittance.

A beam current of 40 mA inside the RFQ acceptance is considered as a realistic objective for the Linac4 caesiated RF ion source, in particular considering that this current has to be provided reliably over long running periods. With a chopping factor of 65%, this current translates to 25 mA inside the linac, averaged along the beam pulse. Further ion source developments could allow higher source currents. The maximum beam current in the linac allowed by initial RF configuration, mixing old LEP

klystrons with new higher power klystrons, is 40 mA; the ultimate current corresponding to the space charge limit is 52 mA, after chopping.

The PSB requirements for the LHC and ISOLDE beams define the length of the linac pulse. While the present multi-turn injection from Linac2 is associated with a beam loss of about 50%, the new H^- charge-exchange injection is virtually loss free, except for a few percent lost due to stripping efficiency. Similarly, the chopping of the beam at the PSB injection frequency will suppress most of the PSB capture losses. A margin of 5–10% between the intensity delivered by Linac4 in the different configurations and the PSB requirements has therefore been considered as largely sufficient. Table 1.3 presents the nominal pulse length and the corresponding number of turns to be injected in each of the four PSB rings to achieve the required intensity for three types of PSB beams.

Table 1.3: Linac4 beam parameters for nominal PSB beams.

	LHC maximum	ISOLDE present	ISOLDE maximum	
Linac current[a]	25	25	25	mA
Number of turns per ring	20	60	110	–
Linac pulse length	80	240	440	μs
Number of protons per pulse	1.24	3.72	6.82	$\times 10^{13}$

[a] Average beam current in the linac pulse, after chopping

The Linac4 basic architecture is shown in Fig. 1.3. The ion source is followed by a low energy beam transport (LEBT) section that prepares the beam for injection into the RFQ accelerator. The chopping line (also called medium energy beam transport, MEBT) that houses the chopper structures and matches the beam to the subsequent accelerating structures is placed between the RFQ and the ensuing accelerating sections. Acceleration is provided by three sections, the first two being equipped with drift tube linac (DTL) structures, the first of a conventional Alvarez type, and the second with a new design with external coupling cells connecting short DTL sections called the cell-coupled drift tube linac (CCDTL). In the third section, a sequence of Pi-mode structure (PIMS) cavities accelerates the beam to the final energy. All the accelerating structures operate at 352.2 MHz frequency; their RF designs allow for a conventional F0D0 beam optics, required to minimize emittance growth in the linac. The overall length of Linac4, from the ion source to the end of the last PIMS, is 76.33 m.

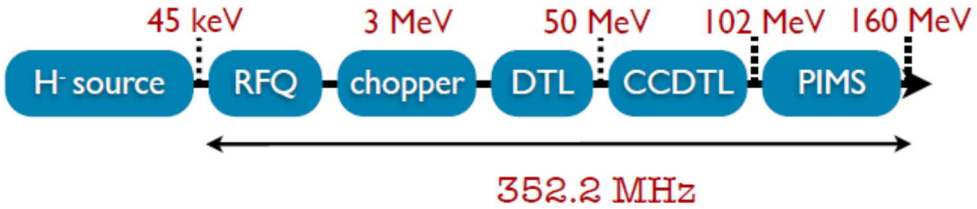

Fig. 1.3: Linac4 basic architecture.

The transition energies between the different sections have been carefully optimized. The 45 keV extraction energy from the ion source minimizes the length of the RFQ limiting simultaneously the space charge defocusing in the LEBT and in the first part of the RFQ [14]. The RFQ energy of 3 MeV has been selected to limit the voltage on the chopper deflector and to keep the activation from beam loss in the chopper line components and dump at acceptable levels, considering that the RFQ and the line need long commissioning times in an environment that should be easily accessible. Although the first nuclear reactions take place below 3 MeV energy, their cross-sections are still very small if materials with low activation thresholds are avoided in the construction of the line components. Three different

accelerating sections are needed to allow for a progressive increase in the length of the focusing periods, required to limit the number of quadrupoles and to maximize the RF conversion efficiency (shunt impedance) along the linac. The transition energies between the sections have been defined based on shunt impedance and beam dynamics considerations. As an additional advantage, fixing the DTL energy at 50 MeV made possible the use of the initial section of Linac4 as a backup in case of a Linac2 vacuum failure during the Linac4 commissioning.

Although the duty cycle of Linac4 is only 0.12%, the accelerating structures and the high-power RF systems have been designed for a maximum duty cycle of 10%, to provide the option of a future high-intensity upgrade with a minimum investment cost. The shielding is also dimensioned to cope with higher beam loss, thus providing a welcome margin for the normal Linac4 operation. Instead, all elements that can be replaced when going to a higher duty cycle, as power supplies, electronics, and all electromagnets, have been dimensioned only for the low duty cycle. The cooling system, including the piping and the cooling stations, would also need upgrading for a higher duty cycle.

At the end of the linac, the beam can go to the main dump or be deflected towards a 70.9 m long transfer line connecting Linac4 to the present Linac2 to PSB transfer line, at the position of the bending magnet LT.BHZ20 (Fig. 1.4). The line comprises a debunching cavity to reduce the beam energy spread at PSB input and a 2.5 m vertical chicane to bring the beam at the same horizontal level as the accelerators of the PS complex. From LT.BHZ20, the Linac4 beam follows the old transfer line from Linac2 to the PSB (called LT and LTB); the beam measurement lines placed at the entrance of the PSB need an extensive upgrade to cope with the higher energy of the Linac4 beam.

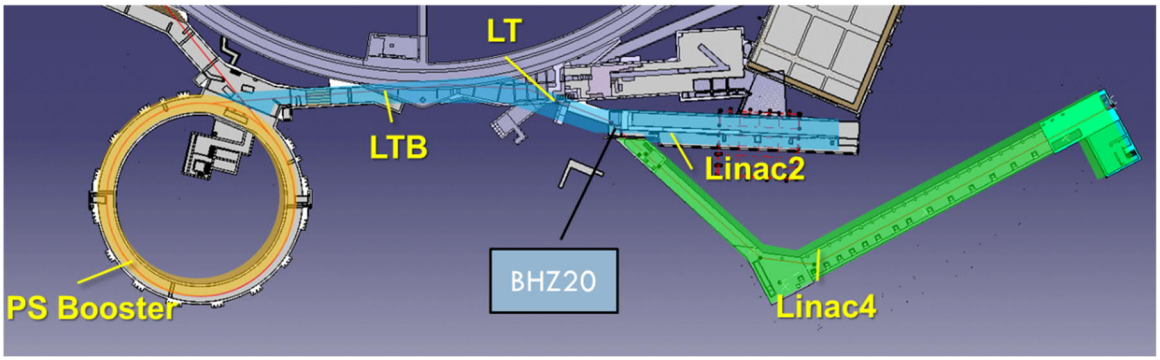

Fig. 1.4: Layout of Linac4, Linac2, and PSB showing the transfer lines LT, LTB, and the connection point LT.BHZ20.

1.3 Beam dynamics

1.3.1 Layout

The first element of Linac4 is a RF volume source followed by a two-solenoid low-energy beam transport (LEBT), which matches the beam to the entrance of the 3 m long RFQ providing the first RF acceleration (from 45 keV to 3 MeV). At 3 MeV the beam enters the 3.6 m long chopper line, consisting of 11 quadrupoles, 3 bunchers and two sets of deflecting plates. The beam is then further accelerated to 50 MeV in a 19 m long drift tube linac (DTL). Each of the 111 DTL drift tubes is equipped with a permanent magnet quadrupole (PMQ). A cell-coupled drift tube linac (CCDTL) accelerating the beam to 104 MeV follows the DTL. It is made of 21 tanks of 3 cells each, with focusing is provided by seven electromagnetic quadrupoles (EMQ) placed outside each tank, and 14 PMQs between coupled tanks. The final acceleration to 160 MeV is provided by a 22 m long PI-mode structure (PIMS), made of 12 tanks of 7 cells separated by EMQs.

The integrated gradient of the 150 quadrupoles (2/3 of which are permanent quads) and the phase and amplitude of the 260 RF accelerating gaps are shown in Figs. 1.5–1.7.

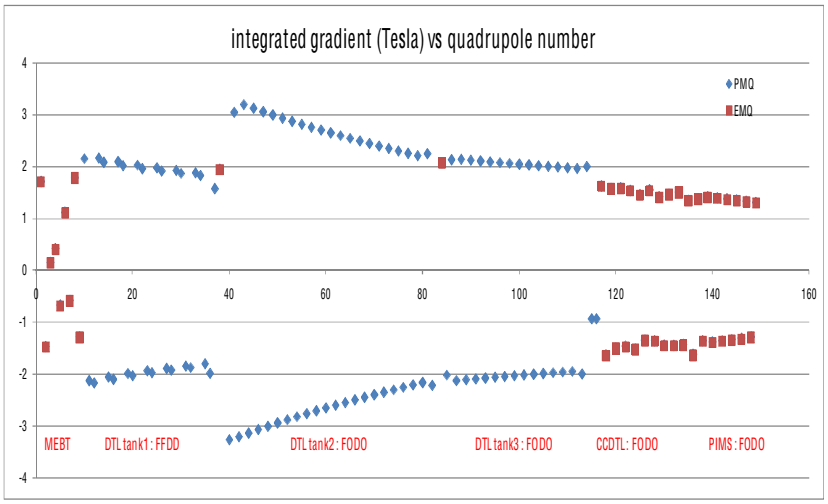

Fig. 1.5: Integrated gradient vs. quadrupole number. Blue diamonds = PMQ; red square = EMQs.

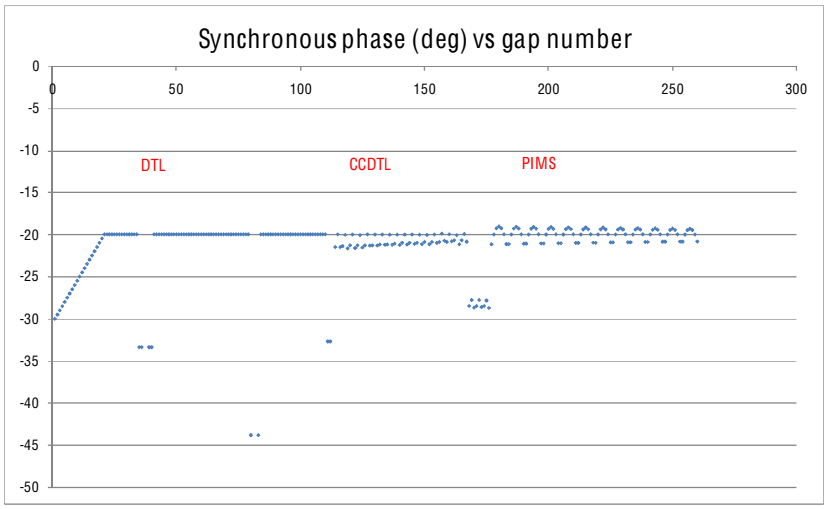

Fig. 1.6: RF phase vs. gap number.

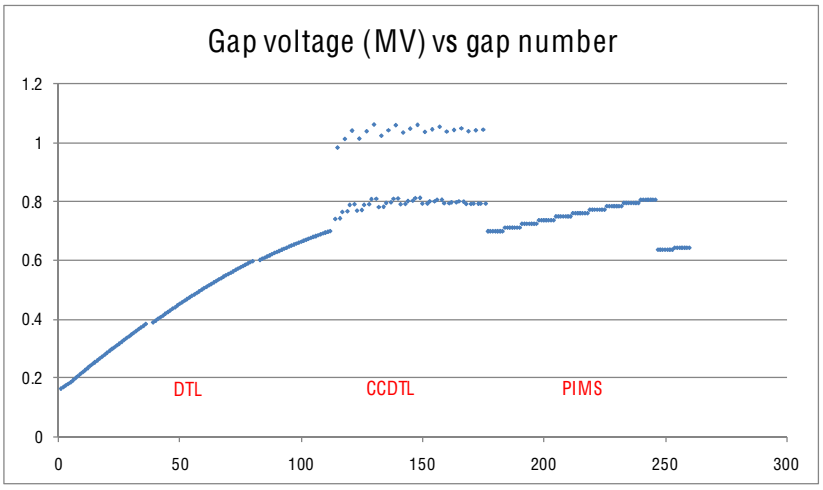

Fig. 1.7: RF voltage vs. gap number.

1.3.2 Nominal beam dynamics

The beam dynamics in each of the 4 accelerating structures has been optimized to guarantee the minimum emittance growth together with the maximum transmission. Efforts have been made to control the transverse and longitudinal phase advance in order to avoid resonances and sharp transitions at any time [15], and to be able to accept a wide range of beam currents in a focusing system of which 2/3 is made of permanent magnet quadrupoles. In general, the best beam quality is obtained when the focusing is as extended as possible and drift spaces without active elements are minimized, thus minimizing the time when space charge forces are left unbalanced. This approach, especially at the low energy end, leads to limited space for passive elements like diagnostics that are necessary for the good functioning of the machine. The integration of the accelerating structures in a real beam line has caused therefore a general degradation of the emittance accompanied by formation of halo. The two sections where most of the emittance increase is localized are the 45 keV LEBT and the 3MeV chopper line. In the LEBT (1.9 m long) the beam is assumed to be 90% neutralized, therefore the emittance increase is not due to space charge but mostly to the very high divergence (about 200 mrad) with which the beam comes out of the source. In fact such a divergence is almost comparable to the transverse momentum given by the entrance fringe field of the first solenoid, making it impossible to completely cancel out the azimuthal component at the solenoid exit fringe field. Such an effect amounts for 15% emittance increase, but most importantly leads to the distortion of the transverse phase space (see Fig. 1.5) that pushes a few percent of the particles outside the RFQ transverse acceptance.

A chopper capable of removing a defined number of micro-bunches from the linac pulse is housed in the space between the RFQ and the DTL, to tailor the 352 MHz time structure of the linac pulse to the 1 MHz CERN PSB bucket [16]. It provides an electric field perpendicular to the direction of propagation of the beam, applied between two parallel plates. The requirement to limit the chopper rise time to less than the time between two consecutive beam pulses (2 ns) to minimize beam loss in case of possible future operation at high repetition frequency (50 Hz) limits the maximum applicable voltage to the kV range. The consequence is that the chopper plates need to have an active length of the order of one metre to achieve the separation needed to remove the unwanted bunches on an off-axis beam dump. To house this long object the only solution is to increase (in this case by a factor of 10) the length of the focusing period in the transition between the RFQ and the DTL. Because of this increase, detrimental to the continuity of the phase advance and to transverse and longitudinal beam emittance conservation in presence of space charge forces, the transverse emittance increase in the chopper line is of the order of 20%. This value has to be compared with an overall emittance increase over the whole Linac4 of about 40%; after 12 MeV there is virtually no emittance increase, within the statistical fluctuations.

Figure 1.8 shows the rms transverse emittances along Linac4, the transition between structures being indicated with a triangular marker. The emittance decreases at z = 8 m, corresponding to the 3 MeV off-line beam dump, is due to a controlled beam clean up that is removing halo particles coming from source, LEBT, and RFQ. Figure 1.9 shows the transverse emittance evolution.

In case of a possible high-duty cycle operation, control of the losses to minimize activation of the accelerator was an important design criterion. The minimum ratio between rms beam size and vacuum chamber has been fixed at 6 after the point where the beam reaches the energy of 3 MeV, considered as the threshold for neutron production in copper. Figure 1.10 shows the ratio between the bore aperture and the rms beam size in Linac4. The bottlenecks are at low energy, in the LEBT and in the MEBT, whereas from 3 MeV the ratio is always above 6 and from 100 MeV is above 8. In simulations no losses are observed in the LEBT, whereas in the MEBT losses are located on the chopper plates and on the dump, where activation is not an issue. The nominal transmission from the source to the end of the PIMS is 85%, not including H^- stripping losses. The loss pattern is shown in Fig. 1.11.

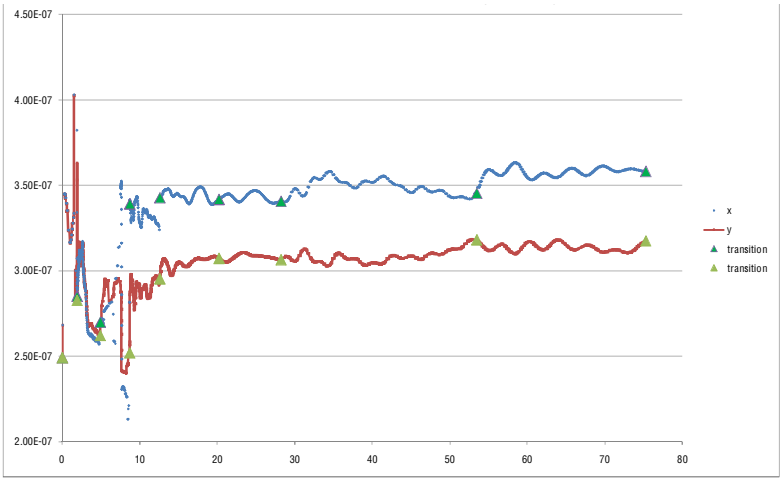

Fig. 1.8: Normalized transverse emittances along Linac4. The triangles indicate the transition between the different structures.

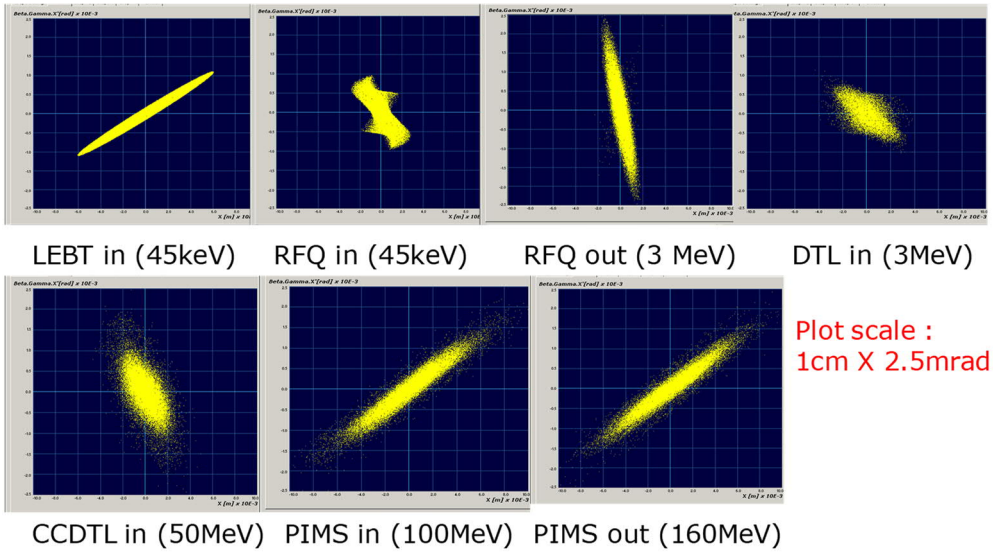

Fig. 1.9: Normalized transverse phase space at the transition between structures in Linac4.

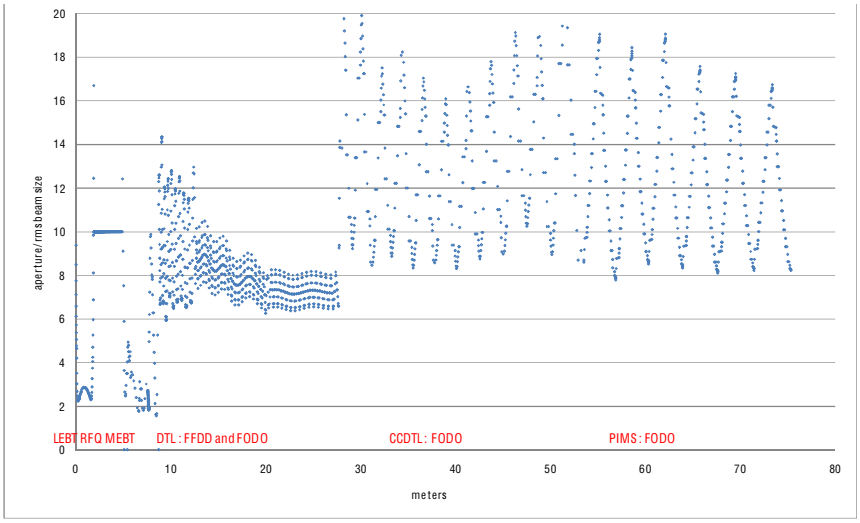

Fig. 1.10: Ratio between the bore aperture and the rms beam size in Linac4.

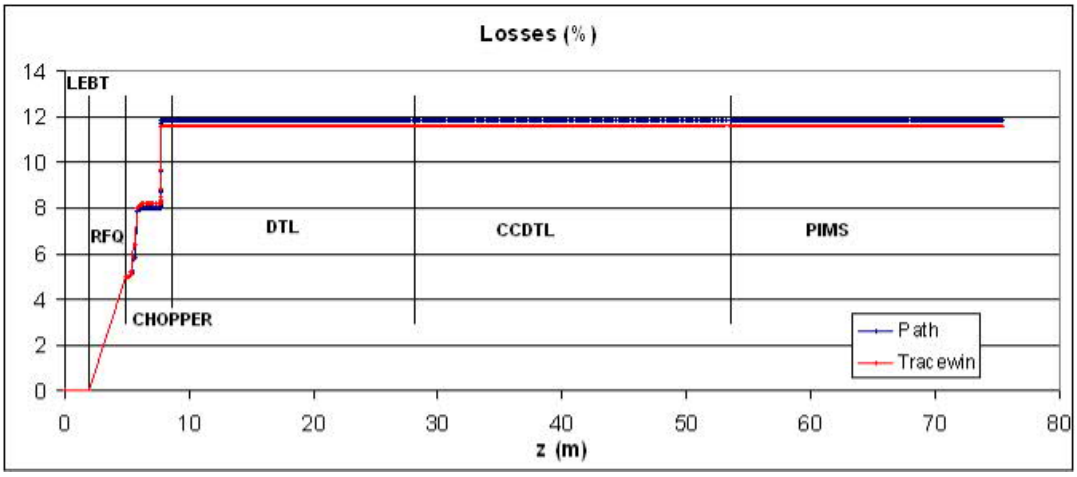

Fig. 1.11: Nominal losses in Linac4, predicted by two different beam dynamics codes.

1.3.3 Chopping

The chopper line houses the fast-switching electrostatic device able to remove 150/352 micro-bunches (and ultimately 3/8 micro-bunches) and a conical-shaped dump to dispose of the chopped micro-bunches [17]. The device is embedded in a quadrupole, to limit beam quality deterioration. An effective applied voltage of 500 Volts translates in a kick of 6.6 mrad, which guarantees an almost complete separation of the wanted and unwanted micro-bunches: a mere 0.03% of the chopped beam is not intercepted at the dump and is lost in the DTL. A higher voltage (550 V) would completely separate the two beams. The transverse phase space in the plane of chopping at the end of the chopper and at the end of the dump are shown in Fig. 1.12 (a) and (b).

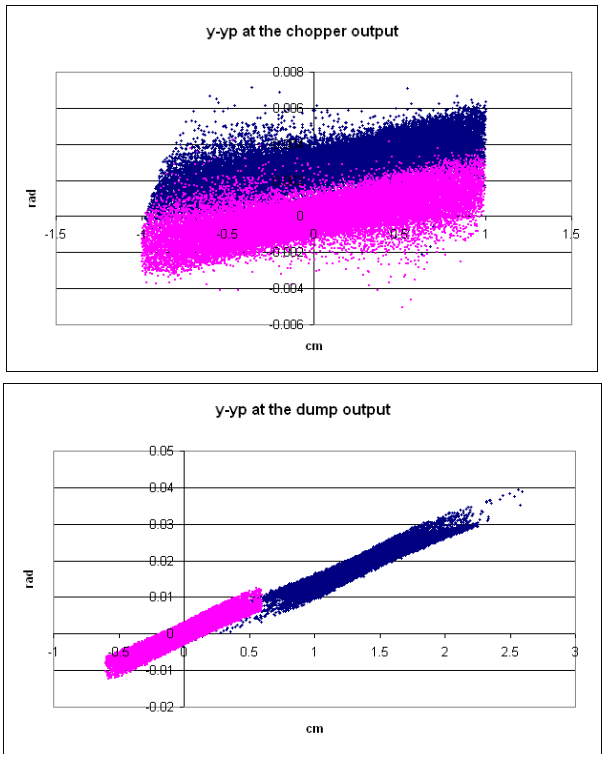

Fig. 1.12: Chopped and unchopped beam at the end of the chopper (a) and at the end of the dump (b).

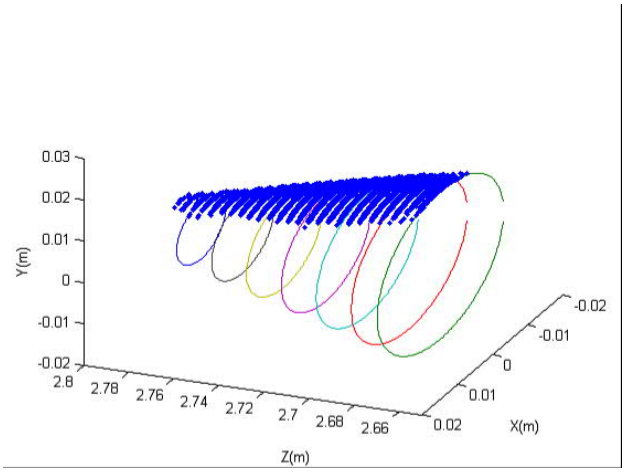

Fig. 1.13: Footprint of the beam on the dump conical surface. The rings indicate the size of the dump cross- section and the dots represent the beam. The beam travels from right to left.

The chopped beam will be intercepted by a conical shaped dump [17], 120 mm in length and with a minimum radius of 6 mm. The power deposition on the dump is as uniform as possible, in order to minimize the power per unit surface. This is an issue only for high duty cycle operation as the dump can stand up to 2 MW/m^2. The mark of the chopped beam on the dump can be seen in Fig. 1.13.

1.3.4 Energy ramping

In order to have a more uniform longitudinal distribution inside the PSB bucket, the average energy of the linac is varied over 20 injection turns by 1 MeV (up and down) [18]. In this way the longitudinal bucket is 'painted' as shown in Fig. 1.14. From the linac dynamics and hardware point of view this operation implies varying linearly (up and down) the field in the last two tanks of the PIMS by 10% over 10 + 10 μs (20 turns). In order to ease this task the last two tanks of the PIMS operate at a lower nominal gradient than the maximum attainable (2.9 instead of 3.8 MV/m). The field distribution in the PIMS tanks is shown in Fig. 1.15. Figure 1-16 shows the effect on the longitudinal beam phase space: the beam distribution is unmodified and the average energy is changed by ± 1 MeV.

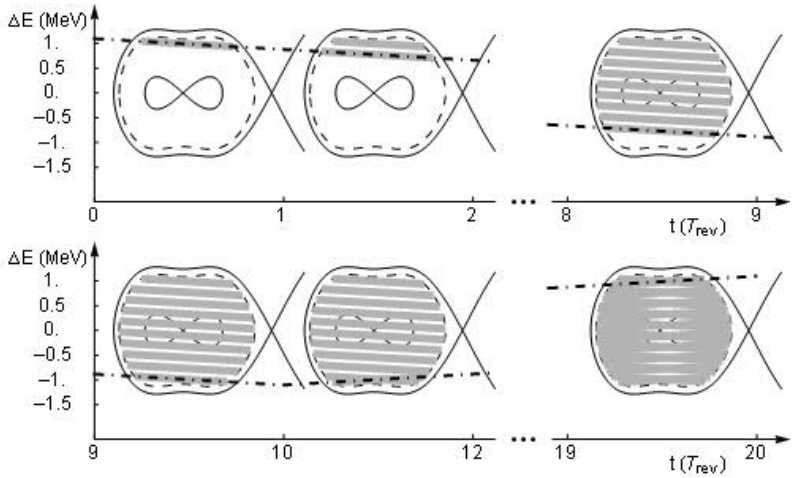

Fig. 1.14: Sketch of the energy painting in the PS booster (courtesy of C. Carli).

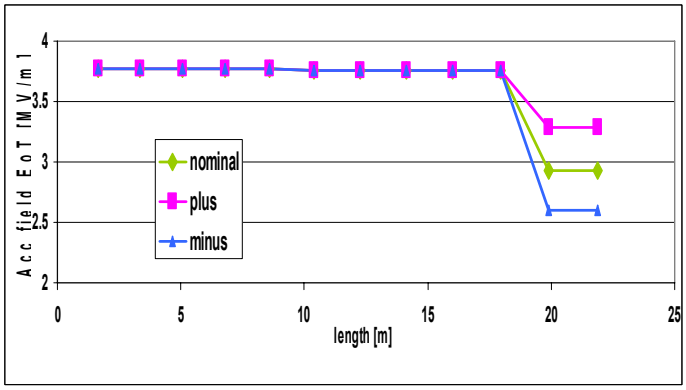

Fig. 1.15: Accelerating field in the PIMS: the last two tanks are varied for energy ramping.

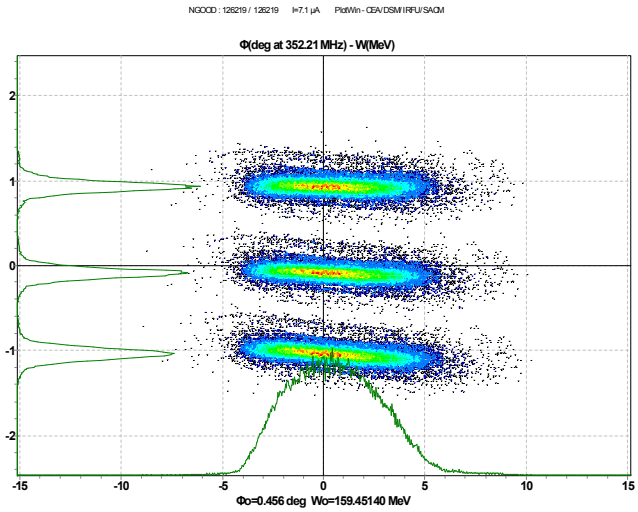

Fig. 1.16: Longitudinal phase space (energy in MeV vs. phase in deg) of the beam with nominal beam energy (centre) and the two extremes of the energy ramping.

1.3.5 Error studies

The behaviour of the accelerator under the influence of beam alignment errors, quadrupole alignment errors, quadrupole gradient errors, beam energy jitters, and RF phase and amplitude errors has been evaluated in a dedicated series of statistical runs. Errors were divided into the two main categories, transverse and longitudinal. Transverse errors include alignment errors (beam and quadrupoles) and quadrupole gradient errors. Longitudinal errors include beam energy jitter, RF phase and RF amplitude errors. Transverse errors affect transmission, transverse emittance and the orbit of the beam, whereas longitudinal error have an effect on the 'effective' transmission, i.e., the percentage of accelerated particles, as well as longitudinal emittance and energy jitter. It has been verified that the effects of transverse and longitudinal errors sum up and that in first approximation there is no strong cross-correlation.

1.3.5.1 Transverse error studies procedure

Transverse error studies were used to probe the stability of the machine under the influence of errors, to define alignment tolerances for the focusing elements and finally to defining the number, position and strength of the dipole correctors (steerers) and monitors needed to control the remnant trajectory errors in the machine. The procedure was to first perform a series of about 2000 simulations with different errors settings and to log for each run beam losses, emittance growth and beam trajectory. This first phase allows to observe the sensitivity of the machine, identify the weak spots and the sensitive

parameters and possibly make modification to the optics to reduce the sensitivity. The correction system is then applied on the worst cases and a steering procedure identical to the one that would be used in the operations of a real accelerator is put in place. An optimizing routine cycles over the steerers in order to find the minimum orbit excursion at the position of the monitors, together with the maximum transmission. Often the maximum transmission is not achieved with the minimum orbit excursion, due to the possible misalignment of the focusing elements. The number of steerers and monitors was increased until the maximum average losses are below 1 W/m at 6% beam duty cycle and the transverse additional emittance growth at 2 σ is limited to 15–20% with respect to the nominal case.

The results of these studies [19] show that errors as detailed in Table 1.4 can be compensated by a system composed of 15 independent horizontal and vertical steerers with an integrated field of 3.5×10^{-3} T·m and 15 beam position monitors with an accuracy of at least 0.5 mm. An example of beam trajectory in the DTL before and after steering can be seen in Fig. 1.17 and the corresponding transmission in Fig. 1.18.

Table 1.4: Transverse errors.

Error	Amplitude	Distribution
Quadrupole transverse position	± 0.1 mm; 1 σ	Gaussian
Quadrupole angles (3)	± 1 mrad; 1 σ	Gaussian
Quadrupole gradient	± 0.5% total	Uniform
Beam transverse position	± 0.3 mm; 1 σ	Gaussian
Beam angles	± 0.3 mrad; 1 σ	Gaussian

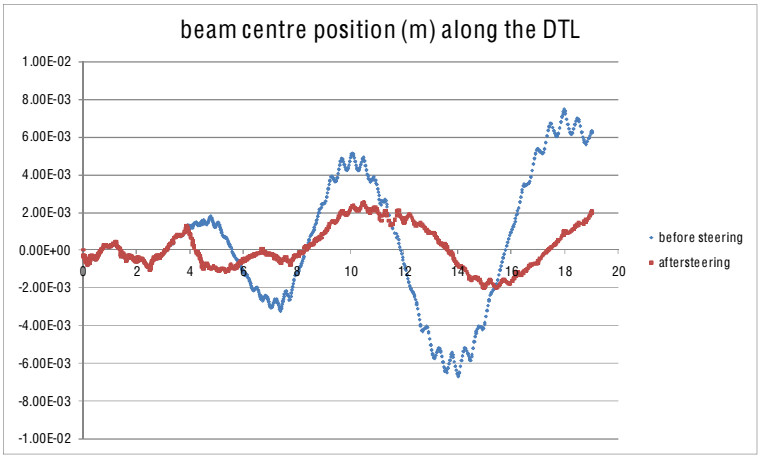

Fig. 1.17: Beam centre position under the effect of one possible set of transverse errors before and after steering in the DTL.

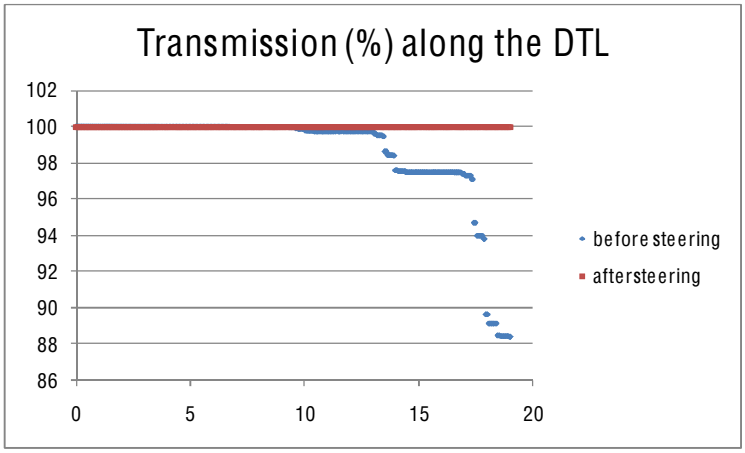

Fig. 1.18: Transmission under the effect of one possible set of transverse errors before and after steering in the DTL.

The several thousand runs with 500 000 macro-particles representing the beam and different error distribution provided a comprehensive map of the losses along the linac, to be used for radiation protection calculations. In all the runs the location and energy of the particle lost has been recorded and the maximum losses have been calculated at the highest foreseeable beam duty cycle, i.e., 6% (Fig. 1.19).

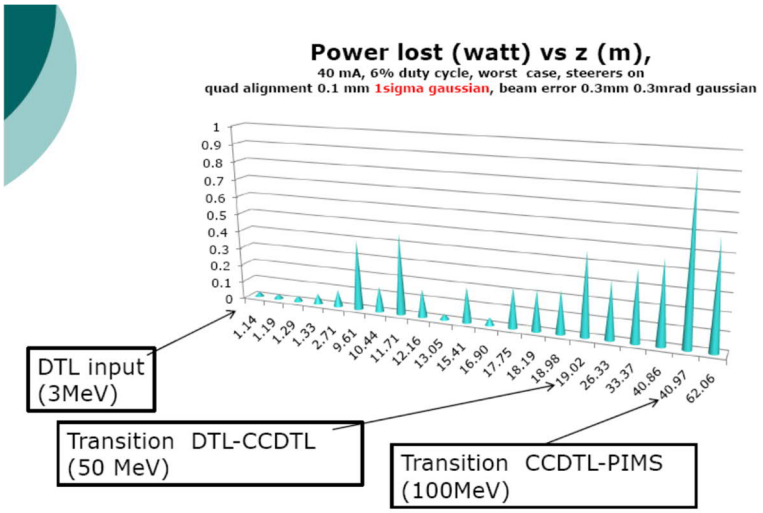

Fig. 1.19: Loss map of Linac4, starting from the DTL input (3 MeV).

1.3.5.2 Longitudinal error studies

The longitudinal errors considered in the studies are 'dynamic' (klystron errors) and 'static' (gap errors). Klystron phase and amplitude errors come from a jitter in the amplitude and phase of the RF power source. They affect mostly the output beam energy and phase and are correlated over many gaps (all the gaps powered by the same klystron, up to 40 in Linac4).

Gap amplitude errors are due to tuning and/or manufacturing imperfections, they are static and they affect mostly the longitudinal emittance. They are uncorrelated between one gap and the next one or, if they are, their average is zero over several gaps. Their effect can be generally mitigated by increasing the RF power above nominal.

Klystron errors between ± 0.5% and ± 2% for amplitude, and between 0.5 and 2° for the phase were considered in the simulations. A uniform input energy jitter coming from the previous stage of

acceleration was introduced, estimated at 6 keV at the input of the DTL, 90 keV at the input of the CCDTL and 250 keV at the input of the PIMS.
Table 1.5 reports the results of the effect of a klystron error on the beam phase and energy jitter and rms emittance at the end of the DTL. The amplitude error has more effect than the phase errors; a variation of ± 2% in amplitude causes an emittance growth and an energy jitter above what is acceptable. The conclusion of these studies is that a control of the amplitude and phase within ± 0.5% and ± 0.5° would be ideal but a control within ± 1% and ± 1° is acceptable.

Table 1.5: Effects of Klystron errors in the DTL.

Klystron amplitude and phase errors	Phase jitter [deg] 1 σ	Energy jitter [keV] 1 σ	rms emittance [deg MeV]
nominal			0.167
0.5% and 0.5°	0.8	13	0.169 ± 0.003
0.5% and 1°	0.9	18	0.171 ± 0.004
0.5% and 2°	1.1	31	0.175 ± 0.009
1% and 0.5°	1.6	23	0.1707 ± 0.005
1% and 1°	1.6	28	0.1719 ± 0.006
1% and 2 deg	1.8	36	0.1772 ± 0.011
2% and 0.5 deg	5.1	43	0.179 ± 0.014
2% and 1 deg	5.7	46	0.180 ± 0.017
2% and 2 deg	8.6	49	0.187 ± 0.024

Equivalent runs have been done for the CCDTL and the PIMS (Tables 1.6 and 1.7) and the results confirm that klystron amplitude and phase should be controlled ideally to 0.5% and 0.5° but that values of 1% and 1° are still acceptable. For the PIMS the value of 1% and 1° is a hard limit, as the maximum energy jitter acceptable for a successful energy painting is 125 keV (1 σ value).

Table 1.6: Effects of klystron errors in the CCDTL.

Klystron amplitude and phase errors	Phase jitter [deg] 1 σ	Energy jitter [keV] 1 σ	rms emittance [deg MeV]
nominal			0.196
0.5% and 0.5°	0.5	39	0.196 ± 0.003
1% and 1°	1	63	0.196 ± 0.005
2% and 2°	2	115	0.198 ± 0.009
5% and 2°	4	237	0.200 ± 0.015

Table 1.7: Effects of klystron errors in the PIMS.

Klystron amplitude and phase errors	Phase jitter [deg] 1 σ	Energy jitter [keV] 1 σ	rms emittance [deg MeV]
nominal			0.180
0.3% and 0.3°	0.3	65	0.181 ± 0.00088
0.5% and 0.5°	0.4	78	0.181 ± 0.00094
1% and 1 deg	0.66	126	0.181 ± 0.0012
2% and 1 deg	0.85	220	0.181 ± 0.0013

The effects of the static errors were evaluated independently of the dynamic errors. In the DTL gap amplitude errors were assigned randomly and independently to the 111 gaps with a uniform distribution over ± 1% to ± 10% of the nominal voltage of each gap. In the CCDTL a tilt inside each tank, correlated over the module was applied with amplitudes varying from ± 1% to ± 5%. In the PIMS two types of error distribution were applied: a tilt over each tank as well as an elliptical distribution with variations from ± 1% to ± 10%. In all cases the average of the individual errors has been readjusted to be equal to the nominal value, which in practical terms is equivalent to adjusting the RF power in each tank to achieve the nominal average field. In all cases the result is that the structures of Linac4 are quite insensitive to static errors, and that amplitude of 2% in DTL and CCDTL and tilt of up to 5% in PIMS can be tolerated by adjusting the average field to the nominal value.

All the results of the simulation are reported in Ref. [20]. Beam losses were never observed in any of the cases analysed.

References

[1] R. Garoby and M. Vretenar, Proposal for a 2 GeV linac injector for the CERN PS, PS-RF-Note- 96-27 (1996).

[2] M. Benedikt *et al.*, The PS complex produces the nominal LHC beam, EPAC00, Vienna, Austria, pp. 527–529.

[3] C.E. Hill *et al.*, Performance of the CERN Linac2 with a high intensity proton RFQ, LINAC94, Tsukuba, Japan, 1994, pp. 175–177.

[4] M. Benedikt *et al.*, Report of the high intensity protons working group, CERN-AB-2004-022-OP-RF (2004).

[5] M. Vretenar (ed.), Conceptual design of the SPL, a high-power superconducting H^- linac at CERN, CERN-2000-012 (2000), doi:10.5170/CERN-2000-012.

[6] F. Gerigk and M. Vretenar, Design of a 120 MeV H^- linac for CERN high-intensity applications, LINAC02, Gwangju, Korea, 2002, pp. 73–75.

[7] M. Vretenar *et al.*, Design of Linac4, a new injector for the CERN booster, LINAC04, Lübeck, Germany, 2004, pp. 291–293.

[8] F. Gerigk (ed.), Conceptual design of the low-power and high-power SPL: a superconducting H^- linac at CERN, CERN-2014-007 (2014), doi:10.5170/CERN-2014-007.

[9] E. Mahner, Risk analysis for Linac2 vacuum system, CERN-ATS-Note-2011-051 TECH (2011).

[10] F. Gerigk and M. Vretenar (eds.), Linac4 technical design report, CERN-AB-2006-084 (2006).

[11] O. Napoly *et al*., The CARE accelerator R&D programme in Europe, PAC05, Knoxville TN, USA, pp. 749–751, doi:10.1109/PAC.2005.1590550.

[12] H. Damerau (ed.) *et al*., LHC injectors upgrade, technical design report, vol. I: Protons, CERN-ACC-2014-0337 (2014).

[13] M. Lindroos and T. Nilsson (eds.), HIE-ISOLDE: the technical options, CERN-2006-013 (2006), doi:10.5170/CERN-2006-013.

[14] A.M. Lombardi, C. Rossi and M. Vretenar, Design of an RFQ accelerator optimised for Linac4 and SPL, CERN-AB-Note-2007-027 (2007).

[15] I. Hofmann *et al*., Review of beam dynamics and space charge resonances in high intensity linacs, EPAC02, Paris, France, 2002, pp.74–78.

[16] F. Caspers *et al*., The CERN-SPL chopper concept and final layout, EPAC04, Lucerne, Switzerland, 2004, pp. 1141–1143.

[17] J-B. Lallement *et al*., Measurement strategy for the CERN Linac4 chopper line, 39th ICFA Advanced Beam Dynamics Workshop on High Intensity High Brightness Hadron Beams, Tsukuba, Japan, 2006, CARE-Conf-06-038-HIPPI (2006).

[18] C. Carli and R. Garoby, Active longitudinal painting for the H-charge exchange injection of the Linac4 beam into the PS booster, CERN-AB-Note-2008-011 (2008).

[19] A.M. Lombardi *et al.,* Loss control and steering strategy for the CERN Linac4, CERN-AB-Note-2007-033 (2007).

[20] G. Bellodi *et al*., Alignment and field error tolerance in Linac4, CERN-ATS-Note-2011-021 (2011).

2 Linac4 sections

2.1 Ion source and LEBT

The Linac4 ion source is intended to deliver at 2 Hz repetition rate an H^- pulse of 45 ± 0.5 keV energy, with intensity of the order of 80 mA (45 mA after RFQ) required for a future upgrade of the ISOLDE facility and maximum pulse duration of 600 μs, within a transverse rms emittance of 0.25 π·mm·mrad. Utmost reliability and very high availability are mandatory to match LHC-operation requirements. A trade-off with the number of turns in the PSB charge exchange injection scheme allows for operating the Linac4 at a lower beam intensity.

The low energy beam transport (LEBT) aims at matching the beam from the ion source to the RFQ, measuring its intensity via a Faraday cup and its horizontal and vertical beam profiles via two sets of secondary emission grids (SEM Grid). An electrostatic pre-Chopper is installed in the middle of the LEBT to deflect the head and tail of the beam to the desired pulse duration or to supress the beam following safety or machine protection interlocks. A pressure regulated gas injection installed in the LEBT provides optimum space charge compensation conditions.

2.1.1 H^- ion source

The ion source development is based on H^- beam intensity stages expected to deliver 25 and 45 mA within RFQ acceptance. The source is of the inductive surface plasma (ISP) type where a few mg of Caesium are deposited in the plasma chamber and on the Molybdenum plasma electrode at intervals of a few weeks or in a continuous Cs-loss compensation mode [1]. The design is inspired from ion source developments at the Spallation Neutron Source facility at Oak Ridge (US) [2]. An offset Hallbach octupole magnetic cusp [3] can be mounted around the ceramic plasma chamber. The plasma is ignited and sustained by inductive coupling of an external 2 MHz RF solenoid to the hydrogen plasma. The RF amplifier at a frequency of 2 ± 0.1 MHz [4] is driven by arbitrary function generators defining the evolution of the RF pulse power and frequency [6]. The RF frequency is tuned to match the fast evolution of the load during plasma ignition. The RF power is transmitted to the plasma chamber via a matching network presented in Fig. 2.1. By design, a consumption of Cs of the order of 0.1 g/year and multi month mean time between maintenance were expected and demonstrated. H^- current of 40–50 mA is achieved in the LEBT and matches LHC operation requirements (25 mA after RFQ). R&D is in progress to meet the 45 mA after the RFQ deliverable.

The ion source consists of a front-end vacuum chamber that encompasses the main high voltage insulator, equipped with survey targets. It is mounted on a support table and connected to a pumping unit. The front end is equipped with a fine alignment system with two rotation axes of ± 3° and a horizontal movement of ± 3 mm to compensate for the tilt and alignment effects induced by the source dipole magnetic fields. Different types of plasma generators can be mounted on the front end, via dedicated flanges suited for volume, surface or discharge modes of H^- production. The layout and assembly of the Linac4 ion source are presented in Figs. 2.1–2.2.

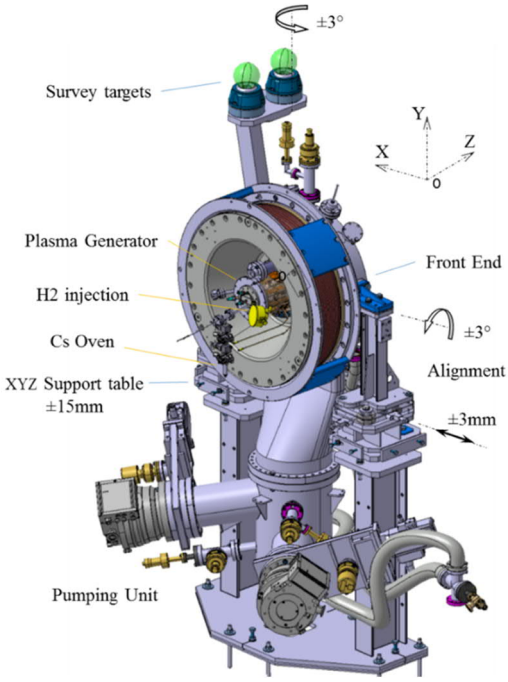

Fig. 2.1: Layout of the Linac4 ion source.

Hydrogen injection, Caesium distribution, RF plasma heating, and pulsed high voltages are essential components of the ion source. The hydrogen feed line is density regulated close to 1.5 bar ± 0.5 mbar [7], it feeds piezo or electromagnetic valves that releases a burst of hydrogen during 0.5 ms. The high voltage system provides the electrostatic acceleration of the ion beam, and a multistage extraction allows fine tuning of the beam optics. For the low repetition rate of Linac4, a pulsed high voltage system was developed based on pulsed generators and high voltage transformers located close to the ion source [8]. An important feature of the system is identification of overcurrent and diversion of the remaining High-Voltage pulse energy that allows a very effective protection against sparks induced damages.

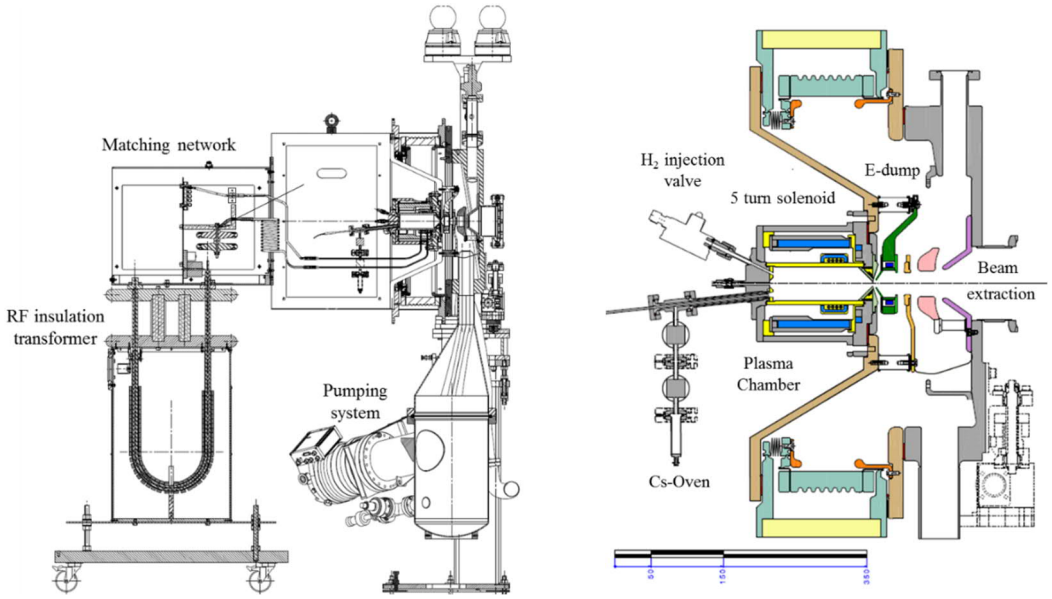

Fig. 2.2: Assembly of the Linac4 ion source plasma generator mounted onto its front end. The Cs oven, the pulsed H_2 injection valve, the plasma generator, and the puller-electron dump and einzel lens electrodes are shown.

The RF field was calculated [9] for homogeneous plasma density conditions. The electrical load resulting from the plasma can be effectively represented as the secondary of a transformer where the primary is the solenoidal coil [10]. Ignition of the hydrogen into a plasma occurs via capacitive coupling of the RF field in a very well defined pressure domain. Then, effective plasma heating occurs via inductive coupling of the RF field to the plasma [11–14]. The plasma ignition conditions were studied for purely inductive coupling [15]. The hottest plasma is located within the solenoid; a 20–30 mT dipole magnetic 'filter' field sufficiently strong to magnetize 30 eV electrons is located before the plasma electrode. The effect of the filter field is to reduce the average energy of the electrons located in the extraction region down to eV energies; this was confirmed via Langmuir gauge measurements [16].

The geometries of the extraction electrodes and of the magnetic separation of the co-extracted electrons from the space charge dominated H^- ion beam were designed based on simulations of the beam transport code IBSIMU [17–20]. A control software was developed to ensure stability of the source current and to automatize the caesiation process [21].

The ion source is contained in a Faraday cage designed for rapid maintenance or repair interventions, the safety of which is ensured via access and lockout procedures, dedicated handling tools and training. The operation and exchange of the Cs oven must follow a very detailed procedure to mitigate the risks inherent to its highly reactive chemical nature.

2.1.2 LEBT

The low energy beam transport (LEBT) is the region from the Linac4 source to the entrance of the RFQ. Its function is to transport and match the beam from the source and match it to the RFQ input parameters, which is achieved using two solenoid magnets and two horizontal and vertical correction magnets. The layout of the LEBT is shown in Fig. 2.3.

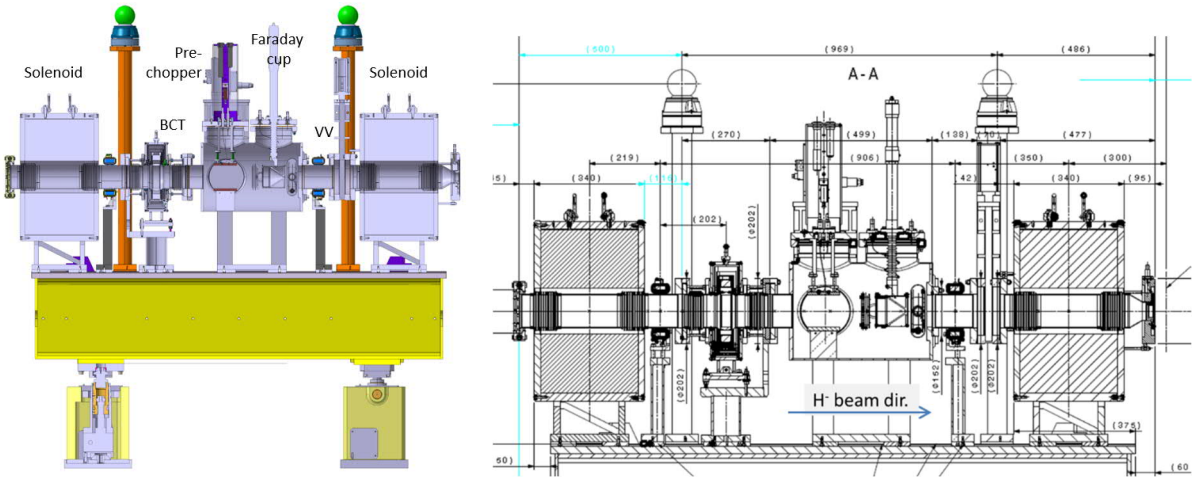

a) b)

Fig. 2.3: Layout of the Linac4 LEBT. a) 3D model on support, b) cut through drawing.

The full list of equipment housed in the LEBT is reported here. More details on these devices can be found in the relevant sections of this report.

- Two solenoid magnets: perform the beam focusing and matching to the RFQ.
- Two steerers: horizontal and vertical dipole correcting magnets.
- Sector valve: separates the source vacuum sector from the RFQ.
- Instrumentation:

  - Beam current transformer: beam current measurement.
  - SEM Grid: profile measurement system.
  - Faraday cup: beam current measurement (destructive to the beam).

- Pre-chopper: pulse electrostatic deflection system that deflects the beam away from the RFQ entrance aperture. It is used to reduce the amount of head beam sent to the RFQ, to cut the end of the beam pulse from the source when it is no longer required for injection to the PSB, and as one of the redundant devices to cut the beam when the Linac4 Beam interlock system is activated.
- Ion/electron trap: electrode to control the potential at the RFQ entrance, to keep secondary particles in the beam.
- Vacuum pump and gauge: additional vacuum pump and pressure gauge, which make up part of the source vacuum sector.
- Gas injection: dosing valve to allow injection of gas into the LEBT, for controlling the space charge compensation.
- Beam stoppers: plates inserted into the beam path in order to block the beam. The source continues to run even with the beam-stoppers in their IN position, meaning they serve also as a beam dump for 45 keV ions. For the commissioning of Linac4, one of the beam stoppers uses a plate with a hole in it in order to produce a pencil beam if required. This will be removed before final connection, and the second beam stopper installed.
- Diagnostic tank: the tank in the centre of the LEBT on which the pumping, gas injection, SEM Grid, Faraday cup, beam stoppers, and pre-chopper are mounted.

All of these items are mounted on a single girder, which can be aligned to the Linac4 reference axis via alignment arms mounted on the girder. Alignment of individual items to the girder is given by their design tolerances and, where necessary, after metrology measurements, the mounting surface of individual items was adjusted in order to improve the alignment.

At low energy, the cross-section for gas stripping of H^- is very high (approximately 6×10^{-16} cm^2) which limits the pressure at which it is possible to transport the beam. Space charge neutralization was measured for various gases and pressures [22–24].

2.2 RFQ

The Linac4 RFQ (Fig. 2.4) has been designed for two different requirements, an initial operation to fill the PSB with beam pulses up to 600 μs at 0.9 Hz and a possible operation at a later stage to fill a Superconducting Proton Linac (SPL) with 400 μs pulses at 50 Hz. The accelerated beam characteristics at the RFQ output have been defined to match the already existent chopper line that was initially designed for operation with another RFQ [25]. Another constraint on the design was the requirements to keep the RFQ length at around 3 m, to divide the RFQ into three segments of one metre (the maximum allowed by the brazing furnace) while keeping the RFQ short enough to allow the direct coupling of the three sections without using coupling cells. The result of the design is a compact RFQ (3 m) with an intra-vane voltage of 78 kV and a peak surface field of 34 MV/m (1.84 times the Kilpatrick limit) [26,27]. The main beam dynamics parameters are summarized in Table 2.1.

2.2.1 RF design

The RF design principle was to aim for simplicity, keeping a constant section over the full length to simplify the mechanical fabrication and taking a constant inter-vane voltage of 78 kV. The tuning of the accelerating field profile is done with 12 tuners per quadrant distributed over the accelerator length. Table 2.2 shows the electrical parameters for the quadrupole cut-off frequency mode, i.e., without tuner and end-cell contributions.

The detailed RF design was done by a team from CEA (France), in the frame of a collaboration with CERN. The same team provided the thermomechanical calculations and was in charge of the RF measurements.

Table 2.1: Summary of the main beam dynamics parameters of the Linac4 RFQ. Emittances are rms values.

RFQ beam parameter	Value	Units
Beam input energy	0.045	MeV
Beam output energy	3.0	MeV
Nominal beam current	70	mA
Average aperture r_0	0.33	cm
Ratio ρ/r_0	3.0	–
Focusing parameter B	5.77	–
Input emittance (norm)	0.25	π mm mrad
Acceptance at zero current	1.7	π mm mrad
Longitudinal emittance (out)	0.13	π deg MeV
Transmission	95	%
Transverse emittance growth	0	%

Table 2.2: RFQ electrical parameters (2D simulation).

RFQ electrical parameter	Value	Units
Vane voltage	78	kV
Quality factor (unloaded)	10269	–
Stored energy	0.372	J/m
Dissipated power	78.738	kW/m
Magnetic field (max)	5444	A/m

At the design stage, the frequency separation between the accelerating quadrupole mode and the adjacent dipole modes was about 5 MHz, providing sufficient stability during operation in all conditions. The stability studies have shown that dipole rods are not required in the end cells due to the favourable length of this design (3.5 times the RF wavelength). The proper tuning of the end cells guarantees a voltage error in the RFQ not exceeding ± 1%.

Eight cooling channels are sufficient to allow temperature stabilization of the RFQ cavity. Two cooling circuits, one using the four channels in the vane pole tips and the other using the four channels in the RFQ body, assure the frequency stability. A dynamic tuning of the RFQ is obtained by regulating the water temperature difference between the two circuits. Thirty-two fixed tuners (80 mm diameter) plus the adjustable RF and the dummy RF ports allow achieving a flat electrical field for the quadrupole accelerating mode. The nominal tuner position has been set at 15 mm inside the cavity to allow linear frequency variations as a function of the tuner penetration. The limited power required by the efficient design enables the adoption of a single input RF coupling port, an iris coupled ridged waveguide connecting the WR2300 reduced height RF window to the RFQ cavity.

2.2.2 Mechanical design, fabrication, and assembly

Each of the three RFQ sections results from the assembly of two major vanes and two minor vanes. The structure is equipped with thirty-two circular apertures, 82 mm diameter, to host the fixed tuners; four rectangular apertures were designed in the central section for the RF input(s). The first and last sections hold eight circular apertures for the vacuum pumps. The gridded pumping ports are brazed onto the module in order to avoid the machining of the grids directly into the major vanes.

The vane modulation is machined by a milling machine using a wheel shaped cutting tool. The assembly of the RFQ cavity was done with a two-step brazing procedure developed at CERN. The first

assembly step of the four poles was done by brazing in the horizontal position at 825ºC. This allows a uniform diffusion of the brazing material by capillary action. The second assembly step, performed in a vertical oven at 790ºC, connected the stainless-steel flanges and end flanges to the RFQ body.

The OFE (Oxygen-Free Electronic grade) copper used for fabrication was submitted to a severe 3D forging in order to obtain a maximum homogeneity in the raw material. A detailed procedure, alternating machining phases to thermal annealing cycles was established in order to stabilize the material and avoid deformations and possible displacements of the vanes, especially for the first brazing step [28]. The machining and assembly tolerances were defined following an error study simulation campaign, which showed that the beam dynamics design adopted is relatively insensitive to errors. The most important contributions come from section tilts and electromagnetic field errors, as can be seen in Table 2.3 that summarizes the mechanical tolerances.

Table 2.3: Linac4 RFQ mechanical tolerances.

Linac4 RFQ tolerances	Value	Units
Machining errors	± 20	µm
Vane modulation error	± 20	µm
Vane tilt over 1 m	± 100	µm
Vane positioning error	± 30	µm
Vane thickness error	± 10	µm
Contiguous section gap	100 ± 15	µm
Section tilt over 1 m	± 30	µm

The manufacturing procedure, up to the first brazing step, includes the rough machining with 1 mm over thickness, first heat treatment, partial finishing with 0.15 mm over thickness only for the vane tips and the brazing surfaces, second heat treatment, and mechanical finishing. Reference holes have been used to align each vane by minimizing the error measured on the modulation profile. Metrology and RF measurements were extensively used to assess the quality of the machining and assembly.

The principle for the final assembly of the three modules was based upon very precise metrology measurements of the reference points located at the entrance and exit of each module. The connection between adjacent modules was realized by means of centring rings machined to bring the optimized beam axis of the two modules to coincide within ± 30 µm when bolted together. A key allowed establishing the right azimuthal orientation. After assembly the RFQ showed very small errors, within the ± 1% range, confirming the quality of the RFQ machining and assembly.

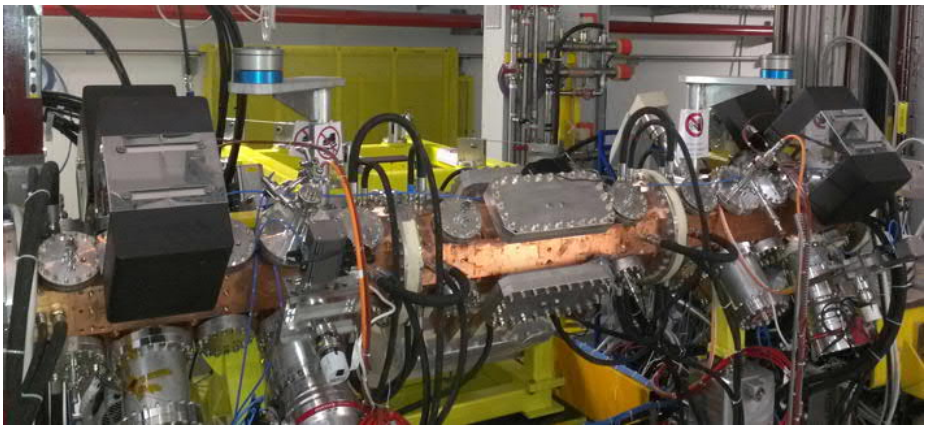

Fig. 2.4: RFQ installed in the Linac4 tunnel.

2.2.3 RF tuning, conditioning, and beam tests

The tuning procedure alternates measurement sessions where the longitudinal electric field profiles in the four quadrants are measured with the bead-pull technique, with fabrication steps where components like tuners and the RF coupler are built according to the indications provided by the measurements.

After the RFQ assembly, end cells were tuned first. Quadrupole rods of 53 mm length were brazed to the RFQ end plates to fine tune the two end cells and to increase separation between quadrupole and dipole modes to improve field stability against mechanical errors. The next step was the definition of the RF coupler geometry. The diameter of the ridged slotted waveguide iris was defined for optimum coupling, and the penetration of the waveguide in the cavity was defined to compensate for the RF field perturbation introduced.

The final tuning step aimed at bringing the accelerating field flatness within the specified range of ± 1%. This was obtained by an iterative procedure performed with 32 dummy aluminium tuners that finally converged providing the desired values of penetration for the final copper piston tuners. Figure 2.5 shows the final result of the field tuning with respect to quadrupole (Q) and dipole (S and T) components as a function of the RFQ longitudinal coordinate.

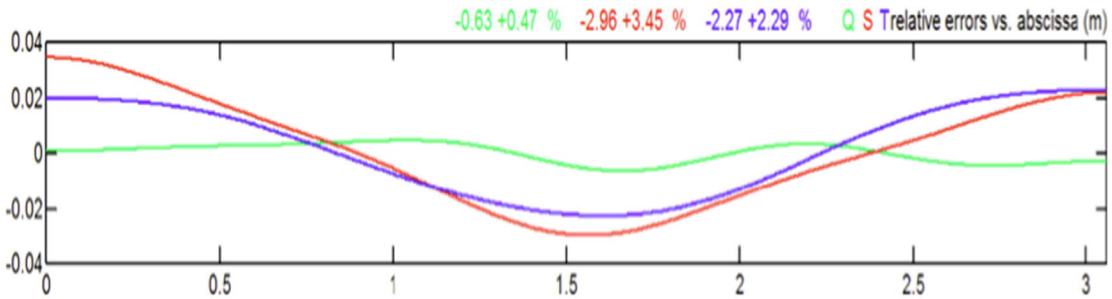

Fig. 2.5: Quadrupole (Q) and dipole (S and T) deviation of the accelerating field (in percentage) from the design value.

The RF conditioning, performed on a test stand, progressed quickly up to the nominal accelerating field level. The nominal field was reached after about 80 hours of conditioning, while after 4 more hours of conditioning the RFQ was stable at 108% of the nominal voltage. The first beam tests are reported in Ref. [29]. Beam transmission measurements have been performed as a function of the RF power injected into the cavity both at the test stand and after installation in the Linac4 tunnel. The results shown in Fig. 2.6 are consistent with the simulations.

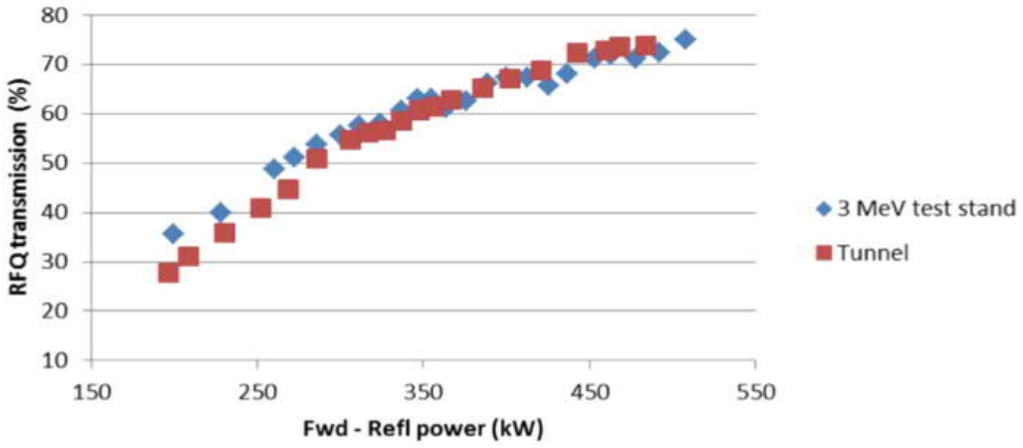

Fig. 2.6: Beam transmission measurements performed at the 3 MeV test stand and in the Linac4 tunnel.

2.3 Chopper line

The RFQ is followed by a 'chopper line', also called medium energy beam transport (MEBT). It contains the beam chopping system and the focusing elements required for matching of the beam from the RFQ to the DTL. The chopper consists of a fast travelling-wave electrostatic beam deflector followed by a dump, which is capable of stopping selected sequences of beam bunches (micro-pulses). The purpose of this operation is to avoid the losses at high energy that occur when injecting linac bunches at 352 MHz frequency into the PSB bucket at 1 MHz frequency; linac bunches that would fall in the unstable area at the edges of the ring bucket are removed at 3 MeV energy, where they do not produce radiation. Besides minimizing activation from capture losses in the PSB, the chopper system can be used to create a sharp edge at the beginning of the linac pulse, eliminating particles which might have incorrect emittance, and finally to create empty intervals in the pulse timed with the rise-time of the PSB distributor magnet that switches the linac beam between the four PSB rings.

The chopping system is located after the RFQ, where the bunch structure is already formed but energy is still low, thus minimizing the voltage and the length of the chopping structure. In addition to the chopping system, the line includes transverse and longitudinal optical elements, required to transport the beam through the small aperture of the chopper structure and to match the beam out of the RFQ and into the DTL, and a large number of diagnostics elements.

In order to minimize the amount of partially filled bunches, which could lead to losses at higher energy, the rise time of the chopper must be of the order of the time separation between two bunches, 2.84 ns. The chopping scheme envisaged for injection into the PSB consists of removing 133 linac bunches out of the 355 that would fall into one PSB bucket at the injection frequency of 0.99 MHz. The corresponding chopping factor (fraction of beam removed by the chopper) is 37.5%. Moreover, the chopper is also removing 1 μs of beam (357 bunches) every 100 μs to create a gap for the rise-time of the distributor to the 4 PSB rings. The chopping scheme is shown in Fig. 2.7.

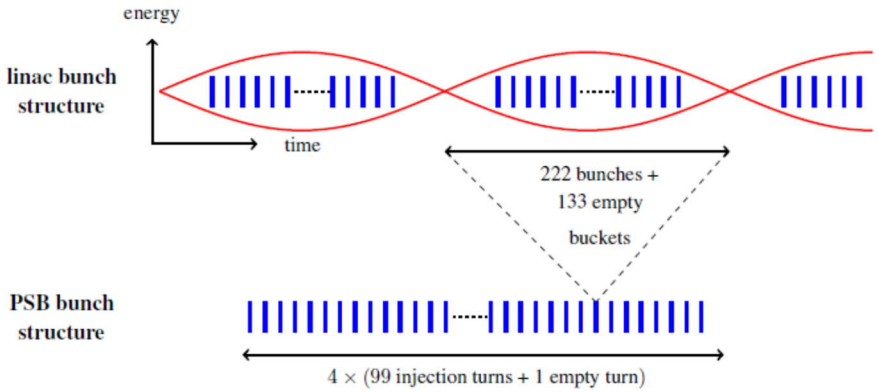

Fig. 2.7: Chopping scheme for injection into the PSB assuming a linac pulse length of 0.4 ms.

The main chopper deflection parameters (voltage, length, and deflection angle) are the result of a compromise between beam dynamics requirements (compact elements, large apertures, high voltage, sufficient separation between chopped, and un-chopped beams) and the driver limitations in achieving at the same time short rise time and high voltage. After a detailed analysis, the design has been based on a minimum effective voltage between the chopper plates of ± 400 V, which provides an effective kick of 5.7 mrad with an effective chopper length of 800 mm and a 20 mm gap between deflecting plates. The layout of the chopper line is shown in Fig. 2.8, while Fig. 2.9 shows the beam dynamics layout (elements and beam envelopes in the three planes) of the line.

The elements of the complete line are (from left to right, downstream) are:

- matching section (4 quadrupoles plus one bunching cavity);
- beam chopper (2 quadrupoles with chopper plates inside);
- transport of the chopped beam: bunching cavity, quadrupole, and beam dump;
- matching section (4 quadrupoles plus one bunching cavity).

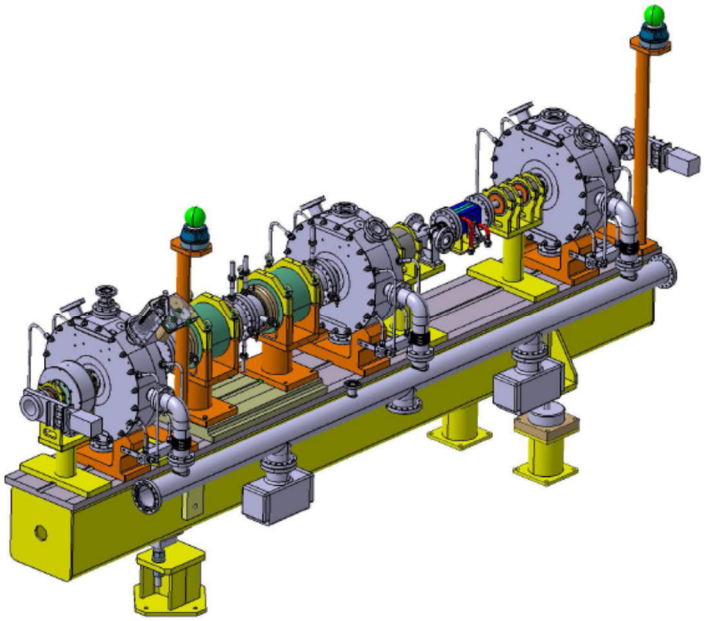

Fig. 2.8: Mechanical design of the chopper line on the supporting beam.

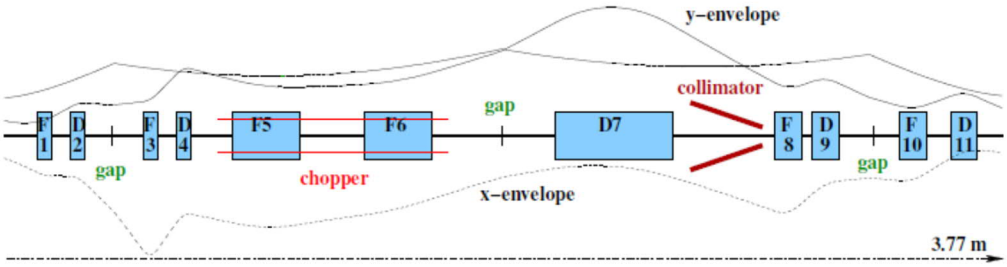

Fig. 2.9: Elements of the chopper line with beam envelopes in the *x*, *y*, and *z* axes.

The 11 quadrupoles are of the Linac2 type, each independently powered. Their parameters are given in Table 2.4.

Table 2.4: Magnetic elements in the chopper line.

Quadrupole type	Number	Length [mm]	Gradient [T/m]	Max. gradient [T/m]
VII	2	255	1.6	2.9[a]
III	6	56	16–32	60
IV	2	82	13–17	39
IX	1	155	4.5	9

[a] Chopper plates inside

The bunching cavities (bunchers), resonating at 352 MHz, provide a maximum voltage of 150 kV to the beam. Their main parameters are given in Table 2.5. Figure 2.10 shows one of the bunchers open before assembling.

Table 2.5: Main buncher parameters.

Buncher type	B30	B40
Number of units	2	1
Aperture diameter [mm]	30	40
Inner cavity diameter [mm]	490	467.2
Gap [mm]	12	12
Q value (computed)	23 600	22 300
Transit time factor	0.581	0.435
Shunt impedance (linac) [MΩ]	3.91	3.35
R/Q [Ω]	27.88	14.18
Nominal voltage [kV]	140	100
Peak dissipated power [kW]	16.0	16.1
Peak electric field on nose cones [MV/m]	25.4	23.8

The beam dynamics design of the line has been optimized to maximize the separation between chopped and unchopped beam at the dump position, keeping the minimum plate voltage. Optics design and the beam separation at the dump position have been presented in Section 1.3.

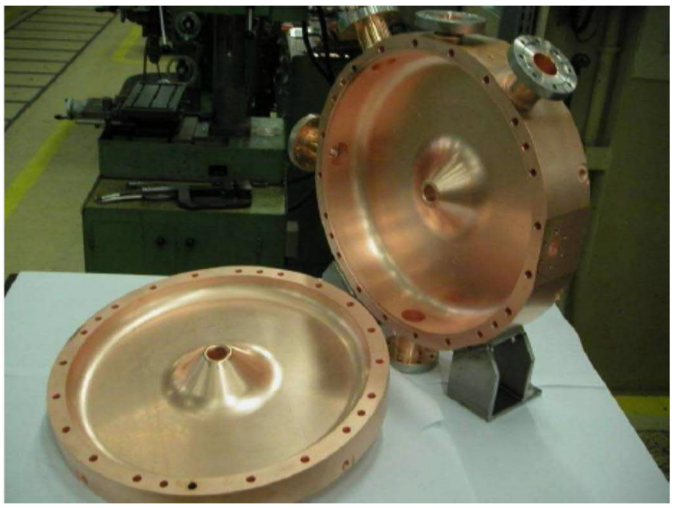

Fig. 2.10: Open buncher cavity.

2.3.1 Chopper structure

Short rise times in the nanosecond range are obtained by a travelling-wave strip line structure where the strip lines are meander-folded in order to match the speed of the travelling-wave to the beam velocity (Fig. 2.11). A section of 1.2 m accommodates two chopper units of 0.5 m, each housing two deflecting plates of 0.4 m length. To minimize the total length of the chopper line, the chopper units are designed to be installed into the bore of existing linac quadrupoles (Fig. 2.11). The water-cooled deflecting plates are driven simultaneously in opposite polarity. In Fig. 2.11 the connectors for RF and water input and output are visible.

The travelling-wave structure consists of a double-meander stripline matched to a beam velocity of $\beta = 0.08$. The structure is printed on an alumina substrate of 3 mm thickness. The design is similar to the SNS chopper structure, which is also a printed meander structure but uses notched micro strip lines with separating ridges in between. While the SNS structure is printed onto glass micro-fibre PTFE

composite material, the CERN chopper adopts an alumina substrate which is considered to be more stable against ionizing radiation and which has lower vacuum out-gassing rates as well as higher heat transfer coefficients.

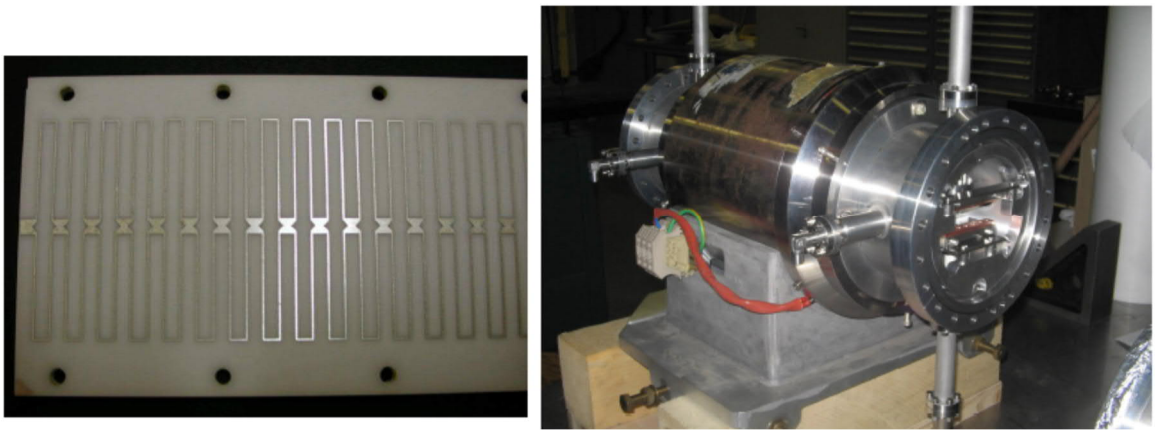

Fig. 2.11: Alumina ceramic plates with printed meander structure and the complete chopper structure inside the quadrupole.

Since the strip lines do not completely cover the deflector plates, the applied voltage has to be multiplied by an effective surface coverage factor of about 80% in order to obtain the actual voltage seen by the beam. For ± 500 V (1 kV in total) deflection voltage, the voltage available for the beam is therefore 800 V. The electrical length of the printed meander structures can be slightly tuned (i.e., made shorter) by cutting longitudinal grooves over the full length in the metallic support. The tuning range is between 0 and –5% in delay with rather minor and uncritical changes in characteristic impedance, and allows adjusting of the electrical delay of both meander plates, different due to production tolerances, to within ± 0.1ns. The plate base layer is a silk screen printed silver alloy, normally used for brazing ceramic-metal interfaces. This layer (a few micrometres thick) is fired at high temperature under vacuum and has an adhesion strength of 100 N/mm^2. Subsequently, by electrochemical deposition, the conductor (copper) thickness is increased up to 30 µm, followed by a flash of gold to avoid surface degradation due to contact with air.

2.3.2 Chopper pulse amplifier

The 800 V pulse amplifier adopts a four stage, Marx configuration. Each stage is composed of a switching unit, a pulser energy storage circuit, and a level and supplies shifter module. The main parameters are reported in Table 2.6.

Table 2.6: Pulse amplifier characteristics.

Parameter	Value
Output Voltage	Adjustable to 800 V
Maximum amplitude variation during the pulse	± 10%
Output polarity	Pos. or Neg.
Input/output impedance	50 Ω
Input signal	TTL (fronts < 2ns)
10–90% transient time	≤ 4.8 ns
Minimum pulse length	25 ns
Maximum pulse length	800 µs
Minimum off pulse	15 ns
Maximum repetition frequency	2 MHz
Maximum burst length	800 µs
Maximum burst repetition frequency	2 Hz

2.3.3 Chopper dump

The beam bunches deflected by the chopper structure are absorbed by an internal dump, placed about 1 m downstream from the second chopper plate. The dump has been designed to stand the high beam power of a high duty-cycle SPL beam, about 2.5 kW. For Linac4, the dump can operate with minimum or no cooling.

The dump (Fig. 2.12) is made of a conical element (the 'dump core') embedded into a thick brick-shaped jacket with 5 hypervapotron circular cooling loops. The inner conical surface of the core is inclined at an angle of 11° in order to spread the deposited power uniformly. The minimum bore aperture of the cone is 12 mm, thus limiting the flux of scattered particles at degraded energy as well as the main-beam particles at large radii. The dump jacket is made of stainless steel, while the core is made of alumina dispersion-strengthened copper Glidcop Al60. A 150 µm thick electrolytic nickel layer is deposited on the inner copper surface, in order to minimize radiation induced by the particle loss on the surfaces. Figure 2.13 shows the inner core and the assembled jacket.

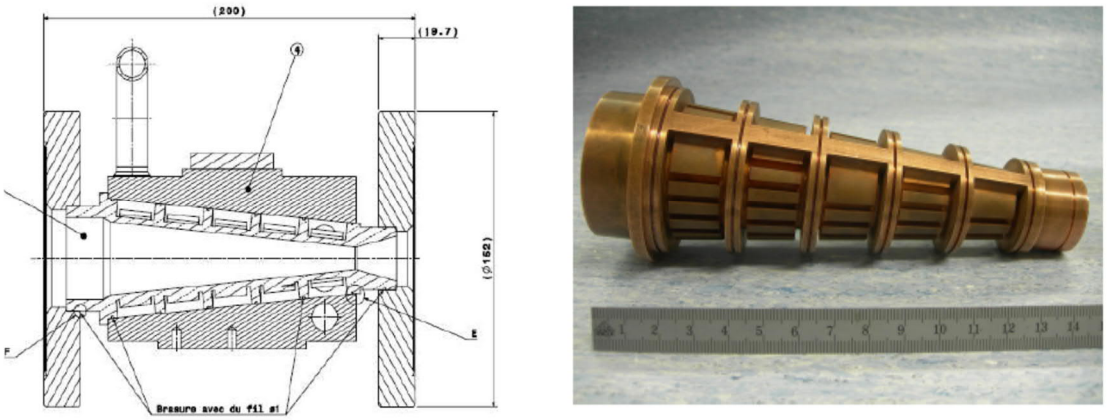

Fig. 2.12: Cross-section and inner core of the chopper dump.

2.4 General design choices for accelerating structures

The choice of accelerating structures is taken according to i) the effective shunt impedance (ZT^2) of structures, which represents their power efficiency and changes with the particle velocity β, ii) their applicable frequencies (e.g., some structures can only be built efficiently at higher frequencies), iii) the

necessary prototyping and tuning effort, which is required to make the structures work, and iv) their impact on beam dynamics.

Two initial studies were made to assess the suitability of superconducting (SC) cavities for the high-energy section of Linac4 [30,31]. While it is clear that the RF peak power can be reduced substantially in this section, the real estate accelerating gradient is not higher for a SC solution. In terms of beam dynamics, the expected beam performance is similar. It was concluded that the SC option between 90 and 160 MeV would be interesting, if the full SPL [32] would be built immediately. In that case the cryogenic infrastructure of the SPL could provide the cooling needs for a SC section of Linac4. Without the SPL, a cryo-plant for a Linac4 section of only 20 metres length would be needed with a strong impact on the construction and maintenance costs and only minor savings on the operational costs.

The common general guidelines for the design of the accelerating sections were [33,34]:

- The structures should be able to operate in both low duty cycle mode for Linac4 (2 Hz, 600 μs beam pulse length) and high duty cycle mode (50 Hz, 1.2 ms) for the SPL. The cooling circuitry is dimensioned for high duty, while in Linac4 most of the cooling pipes are not connected. Comfortably large beam apertures have been chosen (seven to eight times the rms beam size) to minimize beam losses in the SPL operation mode. Tuning is provided by movable pistons at low duty, while at high duty it will be provided by control of the cooling water temperature;
- The resonator lengths are optimized for a peak RF power (resonator and maximum beam loading) of 800 kW, to be provided either by a 1.3 MW klystron recuperated from LEP or by one branch of a new 2.8 MW klystron;
- The selection of mechanical and RF solutions was done considering the high reliability and simplified maintenance requirements of Linac4. In the vacuum and RF connections, only metallic gaskets are used;
- Relatively high accelerating gradients could be selected, because using recuperated klystrons and operating at low duty cycle moves the cost optimum towards higher fields, even considering operating costs. This choice allowed keeping the overall accelerator length to about 80 m and to fit in the area available on the CERN site;
- In the resonator design, a 20% safety margin has been kept with respect to the maximum klystron power, to account for waveguide losses and phase-amplitude control, and another 20% for additional cavity loss with respect to the simulated RF power.

The final choice of structures is listed in Table 2.7 and their shunt impedances together with the shunt impedance of a side coupled linac in the high-energy range are shown in Fig. 2.13.

Table 2.7: Accelerating structures in Linac4.

Structure	Energy range	Gradient	Composition
DTL	3–50 MeV	3.2 MV/m	3 tanks, 3 klystrons
CCDTL	50–102 MeV	4–4.3 MV/m	7 modules of 3 cavities, 7 klystrons
PIMS	102160 MeV	4 MV/m	12 cavities, 8 klystrons

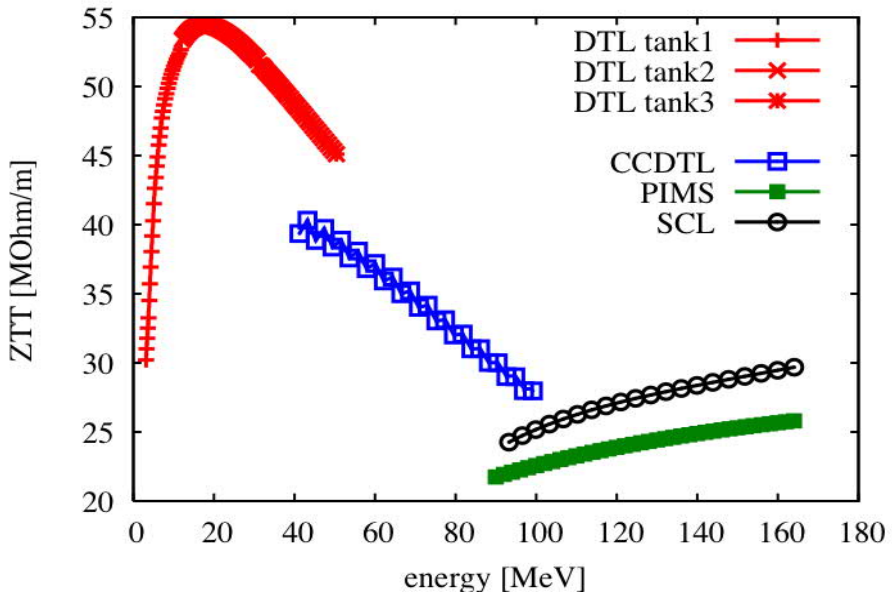

Fig. 2.13: Effective shunt impedance for the three acceleration sections of Linac4 and for a side coupled linac (SCL) at double frequency.

In the low-energy region a drift-tube linac (DTL) of the Alvarez type is the classic choice. Following the example of the spallation neutron source (SNS) [35] permanent magnetic quadrupoles (PMQs) are used in the drift tubes. Their use allows to: i) minimize the diameter of drift tubes, which results in a high shunt impedance, ii) simplify construction: no electric connections through the drift tube stems, and iii) minimize the cost: no power supplies and control electronics as required for electro-magnetic quadrupoles (EMQs). Traditionally EMQs are preferred in DTLs because they allow a fine tuning of the transverse focusing to the actual beam parameters. Simulations of the Linac4 DTL have shown that beams between 30 and 70 mA peak current can be transported without significant deterioration using the EMQs before and after the DTL to match the beam into the DTL and into the subsequent CCDTL.

From 50 MeV onwards, a cell coupled drift tube linac (CCDTL) is used for acceleration up to 102 MeV. This structure consists of short 3-gap DTL type tanks. Three of these tanks are connected via coupling cavities and form one CCDTL module, which is then fed by one klystron that feeds the centre cavity. The coupling cavities and accelerating cavities work in the $\pi/2$ mode, which means that in steady state there is no power lost in the coupling cells (zero field). Altogether 7 modules are used in Linac4. Since the quadrupoles are outside of the structures, EMQs can be used without degrading the shunt impedance.

The last structure called pi-mode structure (PIMS) is derived from the normal conducting LEP accelerating structure and replaces an originally planned SCL operating at 704 MHz [36]. The PIMS has the advantage of a simple and more economic construction as compared to the SCL, with only 84

accelerating cells compared to the 468 of the SCL design, and of standardizing the RF system to a single frequency for all Linac4, saving on klystron development costs and on spare parts. Furthermore, there is already construction and operating experience at CERN on this type of cavities, and thanks to their reduced number of cells the last two cavities of the PIMS can be used for energy painting into the PSB, which is possible because of the low number of coupled cells. These advantages outweigh the slightly lower shunt impedance of the PIMS when compared with the SCL (Fig. 2.14). A beam dynamics comparison showed that the beam quality out of both structures is comparable and a study on transient beam loading effects showed that voltage swings due the loading of the cavity are negligible [37].

2.5 Drift tube linac

Three DTL cavities operating at 352.2 MHz accelerate the beam from 3 to 50 MeV. A 1.3MW LEP klystron powers Tank1, while Tank2 and Tank3 take advantage of the higher output power of new 2.8 MW klystrons. PMQs were chosen for transverse focusing. Their small diameter leads to a cavity design with high shunt impedance and acceleration efficiency. As cabling is not required, the PMQs are placed in vacuum to simplify the drift tube design.

A constant accelerating gradient of 3.1 MV/m in Tank1 and of 3.3 MV/m in Tank2 and Tank3 has been found to be optimum in this respect. Keeping the gradient constant in Tank1 leads to a compact design [38] and makes tuning of the cavity easier. Peak fields are reduced by design in the first 10 cells of Tank1 in order to limit the risk of breakdown in the presence of magnetic fields [39,40]. In order to provide a margin for longitudinal matching from the chopper line, the synchronous phase starts at –35° in Tank1 and ramps linearly to –24° over the tank. A FFDD focusing scheme over all three tanks proved to be the least sensitive to alignment and gradient errors in the transverse acceptance [41]. The missing longitudinal focusing between the tanks is compensated by lowering the synchronous phase in the first and last accelerating gaps of each tank. The diagnostics and steering in the inter-tank areas fit within $3\beta\lambda$ between Tank1 and Tank2 and $2\beta\lambda$ between Tank2 and Tank3. The final design parameters are shown in Table 2.8.

Table 2.8: DTL cavity parameters.

Parameter	Cavity 1 / 2 / 3
Cells per cavity	39 / 42 / 30
Average accel. field	3.1 / 3.3 / 3.3 MV/m
Maximum surface field	1.49 / 1.40 / 1.44 Kilp
Synchronous phase	–35 to –24.5 / –24 / –24 deg
RF peak power per cavity	0.94 / 1.91 / 1.83 MW
RF beam power	0.36 / 0.78 / 0.75 MW
Focusing scheme	FFDD
Quadrupole length	45 / 80 / 80 mm
Number of segments	2 / 4 / 4
Length per cavity	3.896 / 7.341 / 7.255 m
Tuners per cavity	12 / 20 / 17
Post-couplers per cavity	12 / 20 /29

The individual DTL cells have been optimized using 2D electro-magnetic simulations, in terms of effective shunt impedance per unit length while maintaining consistency in synchronous phase and centre cell particle energy, and limiting the peak electric field. A consistent tank design is generated in a cell-by-cell loop on the cell optimization adding up the energy gain. Three-dimensional simulations have been used to estimate the influence of non-axis symmetric cylindrical features that cannot be simulated in two dimensions, like tuners, post-couplers, and the power coupler [42].

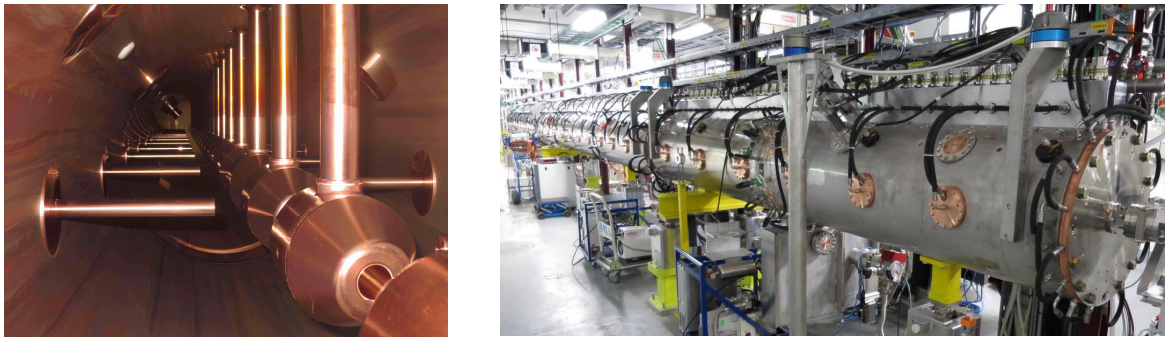

Fig. 2.14: DTL Tank3 on the inside (left) and Tank1-3 installed in the Linac4 (right).

A self-supporting structure using copper-plated ring- forged 304L stainless steel cylinders of 50 mm thickness serves as resonating cavity. As in Linac2, copper drift tubes are mounted on girders that are positioned on the steel tanks. The three DTL RF resonators (tanks) are assembled from 2, 4, and 4 segments, respectively (Fig. 2.14). Each segment is about 2 m long. These dimensions are compatible with tank splitting, raw material purchase, precision machining, assembly and copper plating. The tanks provide at the same time the vacuum and RF envelopes. EN AW-5083 aluminium girders with stainless steel bushings are placed flat on top of the tanks and 12 mm diameter cooling channels along the tanks provide cooling [43].

In order to reduce complexity and avoid using bellows or flexible rubber seals in the drift tube mounting and positioning, the bushings are precision machined and drift tubes are mounted to tolerances without adjustment mechanism. An industrial grade spring-loaded metal seal between drift tube and tank provides for vacuum tightness and RF continuity at once, making the design highly reliable. The principal functions of sealing and positioning are assigned to two separate work pieces, the tank and the girder, which can be manufactured in parallel at individual work-sites. Drift tubes are held in place by a mounting mechanism shown in Fig. 2.15 [44].

The three cavities are equipped with post couplers every third, every second, and every drift tube respectively on alternating sides for the stabilization of RF fields. Two movable tuners per cavity moving in parallel tune the cavities in operation. Post-couplers are water cooled while tuners are plain and transfer dissipation by heat conduction. Groups of three drift tubes are cooled in series and the water flow is interlocked by flow meters.

The DTL construction has taken place in industry and at CERN. The ESS-Bilbao Organisation provided some critical components including the drift tube parts as an in-kind contribution. Assembly of the drift tube parts by electron beam welding and the mechanical assembly of the DTL tanks has been undertaken at CERN [45,46].

The required mechanical tolerances in the DTL are mostly defined by beam dynamics [47]. The positioning of PMQs, transverse horizontally and vertically, and their roll angle are critical. While longitudinal PMQ positioning errors are non-critical for beam dynamics up to a millimetre, the positioning and orientation of drift tubes, affects the distribution of accelerating fields and the beam aperture respectively. The key to a successful DTL assembly is the careful definition of tolerances and their reference system in drawings, as well as the close follow-up of the manufacturing. The final alignment of the assembled segments and tanks is verified by laser tracker measurements on reference points in the drift tubes and tanks. All tanks have been verified to be in or very close to tolerances. The alignment of the drift tubes in Tanks 2 and 3 is presented in Fig. 2.16.

Great care has been taken to achieve smooth drift tube, stem, tank and end-cover surfaces. The inner surface of the tanks was finished on a lathe with a surface roughness of Ra = 0.6 µm on the 520 mm diameter. The manufacturer of the copper pieces achieved Ra = 0.4 µm on stem lathing and drift tube

body milling. This effort improved the quality factor Q by few per cent and thus reduced power losses, power consumption, heat dissipation and cooling needs in everyday operation.

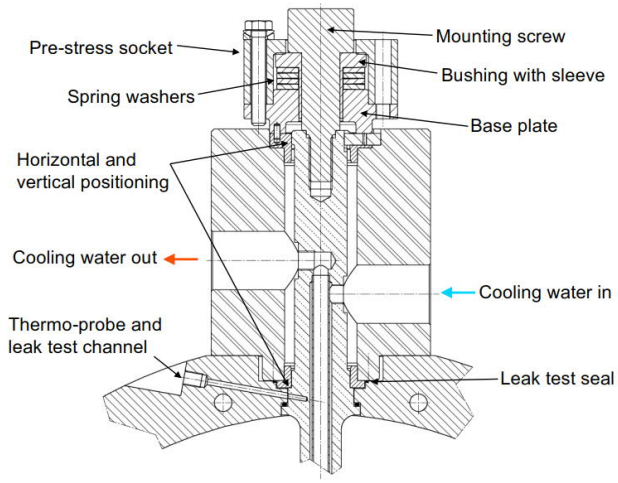

Fig. 2.15: Drift tube mount assembly.

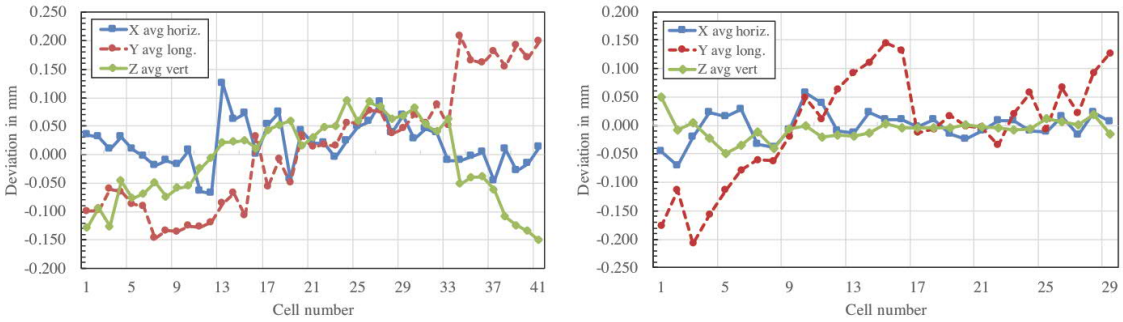

Fig. 2.16: Alignment of drift tubes in the Linac4 DTL Tank2 (left) and Tank3 (right) horizontally, vertically, and longitudinally.

After the assembly of the cavities with adjustable tuners and post-couplers, they needed to be tuned to the operation frequency and stabilized in tilt sensitivity. On Tank1 the work has been undertaken without a predefined procedure and with considerable effort the field variation could be brought within the limits of ± 1% [48]. Following this experience, a new technique for the stabilization of drift tube tanks which allows tuning and stabilization of a tank within a day has been developed and successfully applied to Tank2 and Tank3 (Fig. 2.17) [49,50]. All DTL tanks were conditioned steadily to nominal field levels plus 20% [51,52].

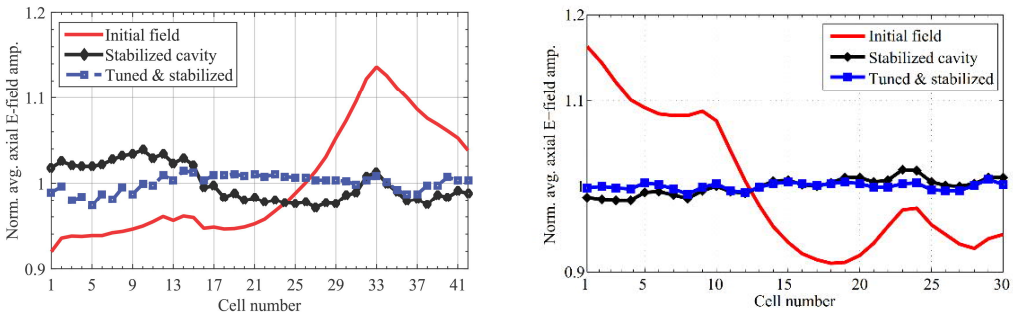

Fig. 2.17: Field flatness in the Linac4 DTL Tank2 (left) and Tank3 (right) before stabilization, after stabilization, and after tuning.

2.6 Cell coupled drift tube linac

The cost and mechanical complexity of a drift tube linac are driven by the required alignment precision of the quadrupoles, which are housed inside the drift tubes. At low beam energies, the high space charge forces within the beam require very short focusing periods, meaning that there are hardly any alternative structures to the DTL. At higher energies, the focusing periods can be lengthened and structures can be used with several accelerating cells between quadrupoles. In the Linac4 CCDTL, short DTL-type tanks, each containing two drift tubes, are connected to off-axis coupling cells, which transfer RF power from one tank to the next. Three accelerating cavities and two coupling cells form one Linac4 CCDTL module (see Fig. 2.18), operating in the $\pi/2$ mode [52].

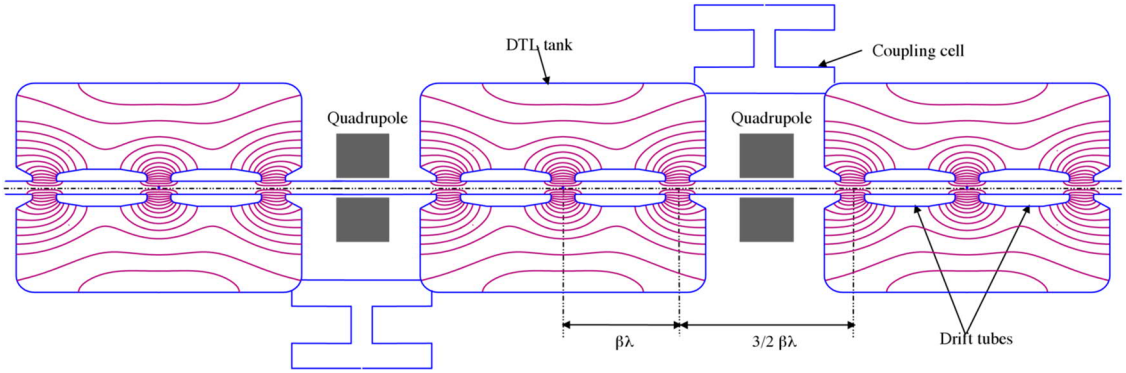

Fig. 2.18: Scheme of a CCDTL module, with electric field lines.

The accelerating tanks on their own operate in the usual 0 mode and RF power is supplied via iris coupling to the central cavity. Once the cavities have established their steady-state standing-wave pattern, the coupling cells are basically field free and therefore do not contribute to RF surface losses during operation. The coupling cells provide a distance of $(3/2)\beta\lambda$ between the centres of the last and first gaps of neighbouring tanks, which—from an energy of 40 MeV onwards—provides enough space to fit quadrupoles between adjacent tanks. The main parameters of the Linac4 CCDTL are summarized in Table 2.9.

Table 2.9: Main CCDTL parameters.

Input energy	50 MeV
Output energy	102 MeV
Frequency	352.2 MHz
Accelerating gradient E_0	4–4.3 MeV/m
Peak electric surface field	1.6–1.7 Kilpatrick
Peak RF power per module	1 MW
Average pulse current	40 mA
Design RF duty cycle	10%
Synchronous phase	–20°
Lattice	F0D0
No. of PMQs	14
No. of EMQs	7
Beam aperture (cavity)	28 mm
Cell diameter	0.52 m
No. of cells per cavity	3
No. of cavities per module	3
No. of modules	7
Length	25 m
RF peak power (CCDTL total)	9 MW

RF beam power (CCDTL total)	2 MW
Vacuum	10^{-7} mbar

The main advantage of the CCDTL with respect to the DTL is the separation of the quadrupoles from the drift tubes, which leads to (i) less demanding tolerances for the alignment of the drift tubes and (ii) easier alignment of the quadrupoles, which can be referenced and adjusted with respect to alignment targets outside the RF structure. In the case of Linac4, PMQs are used between the cavities of each module. Between modules, electromagnetic quadrupoles (EMQs) are employed to provide intermediate beam matching.

Each cavity consists of two half-cells, which were machined out of pre-shaped 3D-forged stainless steel. The half-cells were then copper plated (see Fig. 2.19) and connected with spring-loaded metallic gaskets, which close the vacuum and provide RF continuity. The fixation mechanism for the stems is similar to that used for the DTL [53].

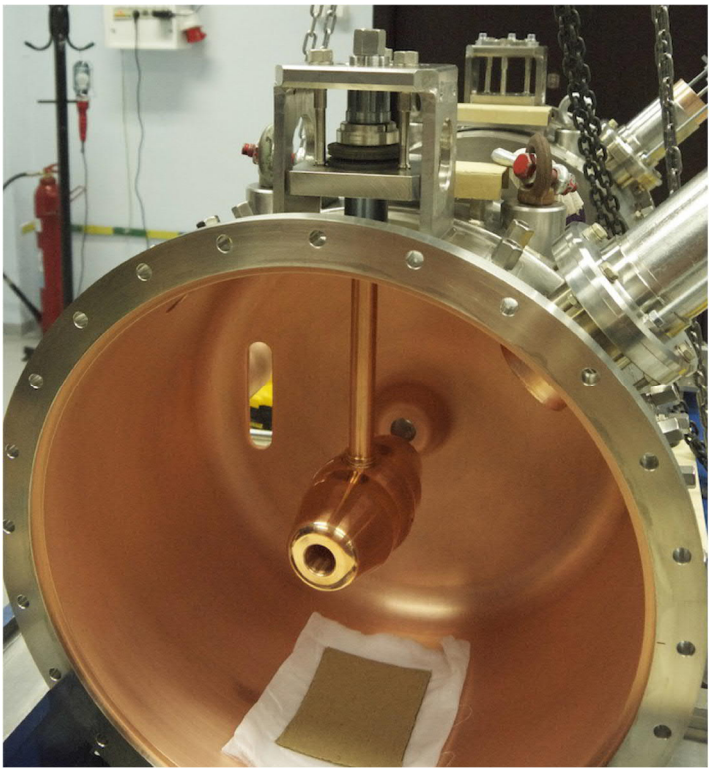

Fig. 2.19: Copper-plated CCDTL half-tank with coupling slot and installed drift tube.

The CCDTL construction was executed in the framework of a collaborative project between CERN and the Budker Institute for Nuclear Physics (BINP) of Novosibirsk, Russia, and the VNIITF Institute of Snezinsk, Russia. The project was managed and partially funded by the International Science and Technology Centre (ISTC) International Organisation. Based on the design and test of a prototype built at CERN, the mechanical design of the modules was developed at VNIITF, which fabricated all cavities. The design of the drift tubes and their construction were done at BINP. The modules were pre-assembled and pre-tuned at BINP, then disassembled and shipped to CERN. There, a BINP team assembled the 7 modules with the support of CERN. BINP then tuned the CCDTL modules to approximately +100 kHz, leaving to CERN the final tuning after verifying the impact of transport into the tunnel and temperature changes [54]. Figure 2.20 shows the installed modules in the Linac4 tunnel.

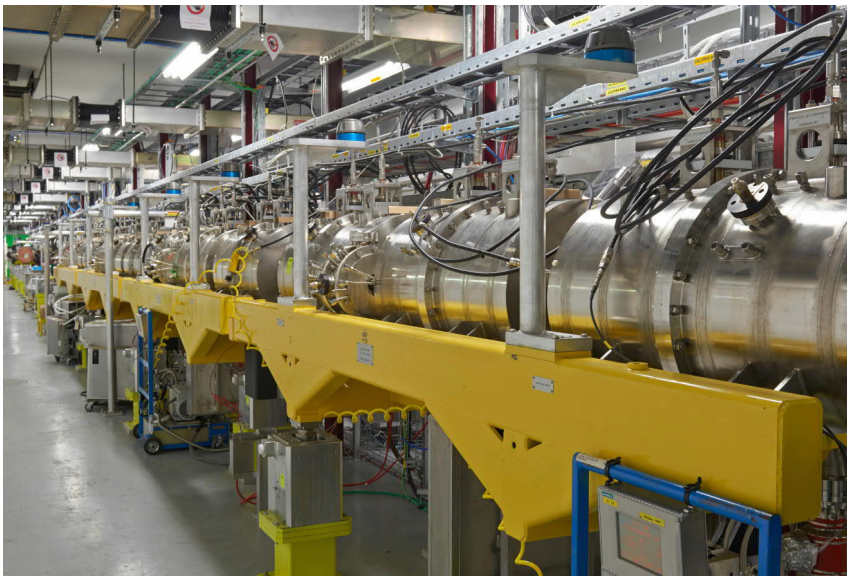

Fig. 2.20: The CCDTL in the Linac4 tunnel.

2.7 Pi-mode structure

The effective shunt impedance per length of the 0-mode structures DTL and CCDTL decreases continuously from an energy of 20 MeV onwards. Above approximately 100 MeV, $\pi/2$ and π-mode structures (the angles $\pi/2$ and π refer to the phase advance from cell to cell) can accelerate the beam more efficiently than 0-mode structures (Fig. 2.14).

The Pi-mode structure section consists of 12 cavities, at a frequency of 352.2 MHz. Cavities are made of seven cells of equal length. Each cavity is adapted to the particle velocity of its energy range, so that the RF design differs in cell length (gap distance) and gap length. The gap length between nose cones is used as a parameter for adjusting the resonance frequency, while the inside radius of all cells is kept constant (in contrast to the LEP design). This saves material and facilitates the machining. Table 2.10 lists the main parameters of the PIMS section.

Table 2.10: Main PIMS parameters.

Input energy	102 MeV
Output energy	160 MeV
Frequency	352.2 MHz
Accelerating gradient E_0	3.9–4 MV/m
Peak electric surface field	33 MV/m
Peak RF power per cavity	1 MW
Average pulse current	40 mA
Design RF duty cycle	10%
Synchronous phase	–20°
Lattice	FODO
No. of quadrupoles	12
Beam aperture	40 mm
Cell diameter	518.7 mm
No. of cells per cavity	7
No. of cavities	12
Length	21.5 m

RF peak power (PIMS total)	11.9 MW
RF beam power (PIMS total)	2.3 MW
Vacuum	10^{-7} mbar

The major changes to the LEP design are the coupling slots that connect adjacent cells and distribute the electromagnetic field along the cavity. As the group velocity in π-mode structures is zero, a strong coupling between cells is necessary to maintain the required electromagnetic field distribution, in particular when movable tuners and beam loading transients dynamically interfere, to maintain the field tilt within the ± 5% tolerated by the beam [55,56]. This leads to the choice of two relatively large coupling slots between cells, providing a cell-to-cell coupling factor of 5.4% for the first cavity and 4.7% for the last one. The electric field within a cavity is shown in Fig. 2.21.

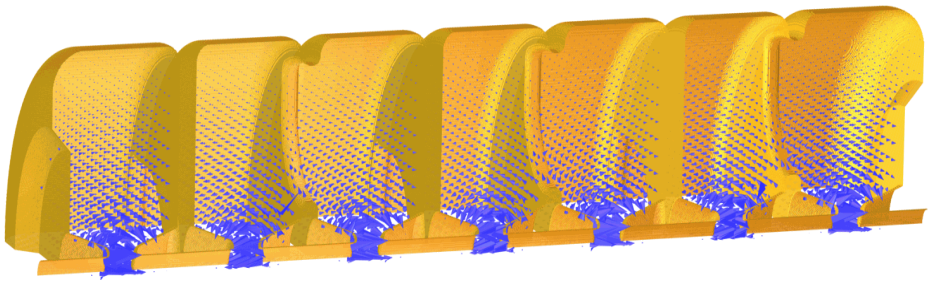

Fig. 2.21: The electric field in one quarter of a seven cell PIMS cavity.

The thermo-mechanical design has been done for a maximum duty cycle of 10%. The average dissipated power of about 80 kW (11.4 kW per intermediate wall) requires a good heat transfer and a high yield strength of the material. The PIMS components are therefore made from 3D forged OFE copper. In order to save material, cells are formed from discs and rings (compare Fig. 2.22), joined together by electron-beam welding. Brazing is avoided to preserve the material quality; only the central ring of each cavity needs to be brazed due to the waveguide connection. V-shaped cooling channels are drilled into the discs and are connected by flexible hoses from the outside. In this way, there are no brazed or welded joints between vacuum and water, as in the LEP cavities.

Fig. 2.22: Discs and rings before welding.

The PIMS cavities are tuned in two steps: Before welding discs and cylinders together to a cavity, tuning islands located on each disc are machined to an individual height to adjust the resonance frequency of each cell. After welding the cavity, piston tuners are employed in each cell to adjust the

resonance frequency and field distribution of the accelerating mode. This second tuning operation is necessary since the welding shortens cells partly unpredictably by 0.3 to 0.6 mm.

A prototype cavity has been built [57,58] and high power tested [59] at CERN (Fig. 2.23). The cavity conditioned very quickly, even without a prior bakeout. After 30 hours, the cavity could be fed by pulses of 800 μs length at the nominal 700 kW peak power. Thereafter, the cavity was conditioned within 24 hours to 1100 kW, the maximum power available from the klystron, and tested for 72 hours. After the successful tests of the prototype cavity, it was decided that this cavity be used as the first PIMS cavity for Linac4.

Fig. 2.23: PIMS prototype during the high average power test.

The remaining 12 PIMS cavities (11 accelerating and 1 debuncher cavity) have been produced in a collaboration between CERN, the National Centre for Nuclear Research (NCBJ) in Poland and Forschungszentrum Jülich (FZJ). The 96 discs and 84 rings were fabricated and tested in Poland [machining, brazing, metrology, vacuum leak testing] while 96 ports were electron-beam welded to the rings in Jülich. The cavities were finally assembled, electron-beam welded and tuned at CERN. The conditioning was straightforward for all cavities.

PIMS cavities are connected to the air waveguide system via a power coupler, which consists of a tuner-adjustable waveguide coupler and a short window [60,61].

2.8 Transfer line

The 160 MeV Linac4 beam is transported to the PS booster injection via a new 70 m long transfer line, L4T, joining the existing Linac2 transfer line (LT) at the LT.BHZ20 bending magnet. Including the existing LT and LTB lines, the total distance from the last PIMS cavity to the BI line (BHZ40 magnet) is 130 m. As shown in Fig. 2.24, the line is composed of four main straight sections separated by bending magnets. The first section links the last PIMS cavity and the first horizontal bending magnet. When the magnet is not pulsed, the beam goes straight to the measurement line L4Z (Section 2.9) and to the beam dump. When pulsed, the three horizontal dipoles bend the beam by 70° (23.3° each) toward LT.BHZ20. The second straight section houses various diagnostics, magnets and a debuncher cavity used to control and vary the beam energy spread. The tunnel being 2.5 m lower than the Linac2 level, the beam is deflected up by a first vertical bending magnet (by 15°) and the transfer line goes on a rising slope, over a metallic structure until the second vertical bending that steers it back on the horizontal plane. Among other devices, the last straight section houses a bunch shape monitor (BSM) [62] for longitudinal beam emittance measurements [63] and a 5 m long beam pipe going through the separation wall between the Linac4 and Linac2 buildings.

The beam is focused by air-cooled pulsed electromagnetic quadrupoles of two types: the L4 type quadrupoles (used in the inter-tank sections of the linac) with a 27 mm aperture radius and a maximum integrated gradient of 2.4 T, and the L4T type quadrupoles, 50 mm aperture, and 1.8 T max integrated gradient. The bending magnets are water cooled and have a 0.77 and 0.48 T·m nominal integrated field over an effective length of 870 mm. Horizontal and vertical bendings are independently coupled on the same power supplies.

Beam current transformers (BCT) located at the beginning of all straight sections measure the beam current, monitoring the transmission and the correct setting of the bending magnets. Four diagnostic tanks, each housing two SEM Grids (H&V) and one wire-scanner, are used to measure the beam profiles at different locations in addition to two other tanks installed in the L4Z line. A total of ten beam position monitors (BPM) measure the beam centre as well as the beam average energy with time of flight. The general parameters of the L4T line are given in Table 2.11.

An H^- ions stripping foil unit is permanently installed in the first straight section, before the first bending magnet. It will be used as a test stand to assess the properties of the carbon foils used at the PS booster injection.

Table 2.11: Main L4T parameters.

Total length (to LT.BHZ20)	70.36 m
Number of quadrupoles	17 (2 × L4 type – 15 × L4T type)
Number of bendings	5 (3 horizontal – 2 vertical)
Number of corrector magnets	26 (13 horizontal – 13 vertical)
Debuncher cavity	1 PIMS at 352.2 MHz
Number of beam current transformers (BCT)	5
Number of SEM Grids	8 (4 horizontal – 4 vertical)
Number of wire scanners	4
Number of beam position monitors (BPM)	10
Number of bunch shape monitor (BSM)	2

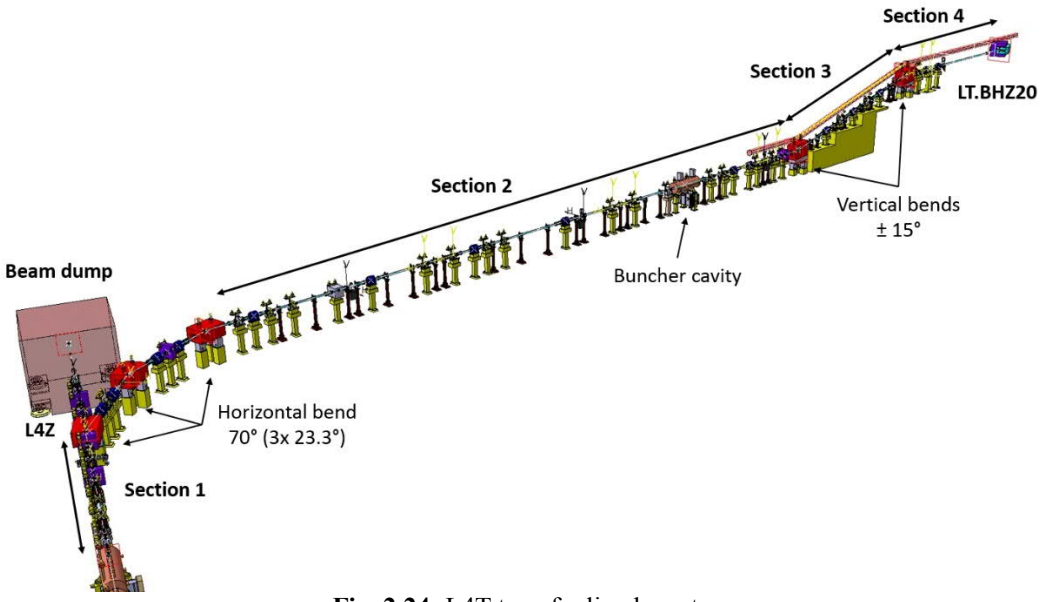

Fig. 2.24: L4T transfer line layout.

Most of the transfer line equipment is installed on individual supports. The devices are mounted on their supports with pins that insure the reproducibility of the alignment in case of re-assembly. The support tables come with a three-axis alignment system. The target arms, fixed to the tables, were carefully studied and optimized in order to limit the vibration and reach the rigidity needed for an accurate alignment. Some of these supports are shown in Fig. 2.25.

Fig. 2.25: L4T supports and survey target arms.

In order to maximize the beam aperture in the bending magnets, the vacuum chambers are based on a 'race-track' design and are made of 316 LN stainless steel to limit their influence on the magnetic field quality. We have a total of four different types of chambers (including LT.BHZ20):

- Horizontal (23.3°) Y shape in the first and second horizontal bending.
- Horizontal (23.3°) V shape in the third horizontal magnet.
- Vertical (15°) V shape in both vertical bending magnets.
- Horizontal (24°) V shape in LT.BHZ20 magnet.

As a mitigation measure of a possible vacuum leak during the future machine operation, three bending magnet vacuum chamber spares were produced: 1 vertical (15°), 1 for BHZ20 magnet, and one horizontal (23.3°) Y shape whose vacuum flanges would have to be chosen and welded depending on its destination.

2.9 Measurement lines

In addition to the permanent diagnostics installed along the linac and the transfer line, the 160 MeV beam transverse parameters can be measured offline in two dedicated measurement lines: the L4Z, between the last PIMS cavity and the main dump, and the LBE (linac beam emittance) located upstream of the PS booster injection, just after the LTB.BHZ40 magnet. The longitudinal parameters are not directly measured in a dedicated spectrometer line as was the case for the Linac2 LBS line. The longitudinal emittance is reconstructed with bunch length measurements taken for different RF parameters of the debuncher cavity located in the L4T line.

1.1.1 Transverse emittance

The 160 MeV beam transverse emittance is reconstructed with an indirect process, the forward method [63], which consists of the classical three profile reconstruction technique combined with an extra step allowing for the space charge effects to be taken into account. The beam profile is measured at three (or more) different monitors separated by drifts (no active elements in between). The upstream quadrupole

settings are chosen such as to get a beam waist in the middle measurement location and therefore increase the resolution. The resulting emittance ellipse does not include the space charge effects, but is used as a starting point for an iterative process of multiparticle simulation runs taking the particle charges interaction into account. At every run, the emittance ellipse parameters are varied and the resulting beam profiles compared to the measured one. The process converges and the emittance is reconstructed once the simulations match the measurements. During normal operation, the multiparticle simulation iterative step will not be needed as long as the routine measurements match the reference beam profiles.

2.9.1 L4Z line

After the beam is accelerated at 160 MeV by the last PIMS cavity, it can be sent towards the PSB or towards the L4Z line, going straight to the main beam dump, by keeping the first horizontal bending magnet off. Besides dumping the Linac4 beam safely, the line is used to measure the beam transverse emittances. The L4Z line is a relatively short beam line (5 m) and includes two diagnostic tanks housing horizontal and vertical beam profile monitors, and a beam current transformer to monitor the beam transmission. The two quadrupoles and two profile monitor tanks located in the first part of the L4T line complete the set-up for the transverse emittance reconstruction. The two quadrupoles modify the beam profiles at the measurement locations and generate a beam waist on one of the centre monitors, and four diagnostic tanks measure the beam profile in both horizontal and vertical planes with SEM Grids or wire scanners. The parameters of the measurement line are given in Table 2.12 and the layout of the L4T-L4Z line is shown in Fig. 2.26.

Table 2.12: Measurement line parameters.

Total length (PIMS to dump)	13.85 m	–
L4Z length (bending to dump)	4.98 m	–
Number of quadrupoles	2 × L4 type	in L4T
Number of corrector magnets	4 (2 horizontal – 2 vertical)	2 in L4Z
Number BCT	2	1 in L4Z
Number of SEM Grids	8 (4 horizontal – 4 vertical)	4 in L4Z
Number of wire scanners	4	2 in L4Z
Number of BPM	2	in L4T
Number of BSM	1	in L4T

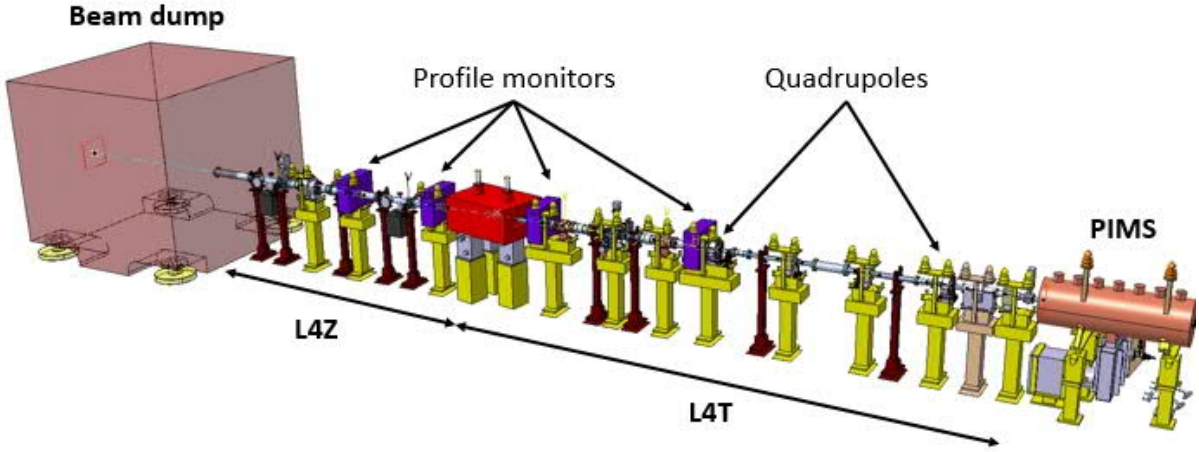

Fig. 2.26: L4T/L4Z measurement line layout.

2.9.2 LBE line

The 160 MeV Linac4 beam transverse emittance will also be measured at the end of the complete transfer-line (L4T-LT-LTB) 50 m upstream the PS booster injection. The LBE line, located after the LTB.BHZ.40 bending magnet is based on the same principle as the L4Z. It houses two quadrupoles (L4T type) and three diagnostic tanks with horizontal and vertical SEM grids and a wire scanner for the emittance measurement in addition to a corrector magnet and a beam current transformer. The line ends with a beam dump identical to the Linac4 main dump. The LBE main parameters are summarized in Table 2.13. Given the integration constraints in the area, the equipment is assembled on three support beams rather than individual feet. The LBE line layout is shown in Fig. 2.27.

Table 2.13: LBE main parameters.

Total length	13.8 m (BHZ40 centre to dump)
Number of quadrupoles	2 × L4 type
Number of corrector magnets	2 (1 horizontal – 1 vertical)
Number BCT	1
Number of SEM Grids	6 (3 horizontal – 3 vertical)
Number of wire scanners	3

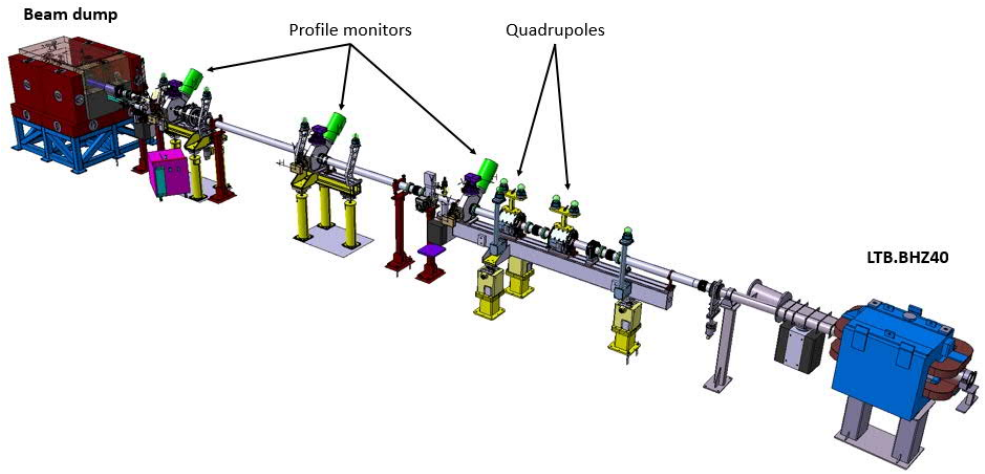

Fig. 2.27: LBE measurement line layout.

2.9.3 Longitudinal emittance

The 160 MeV longitudinal beam parameters are measured in the L4T line by reconstructing the emittance with the Forward method. The measurement principle is very similar to the one used in the transverse plane. Instead of measuring the transverse beam profile at three different locations, we measure the longitudinal micro bunch length with a bunch shape monitor (BSM) [3] for three (or more) different RF settings of the debuncher cavity (PIMS type) located upstream. In fact, by changing the amplitude and/or the phase of the cavity, the bunch length can be varied at the BSM location. By knowing the cavity parameters (its transfer matrix) we can reconstruct the longitudinal emittance applying the 'three gradients method' in the longitudinal plane [62]. As for the transverse plane, the space charge effects are included in the reconstruction process by having an iterative process of multiparticle simulations until we reach a convergence between measured and simulated bunch length. This method was validated during the Linac4 commissioning at 3, 12, and 50 MeV, energies at which the space charge influences the beam dynamics much more than at 160 MeV. By reconstructing the longitudinal emittance, this measurement technique brings us more information than a conventional spectrometer line, where we can only access the beam energy spread. The reconstructed beam can therefore be simulated and tracked with multiparticle codes until the PS booster injection region, giving an accurate estimate of both the beam phase and energy spread at that location. The layout of the L4T line part where the measurement takes place is shown in Fig. 2.28.

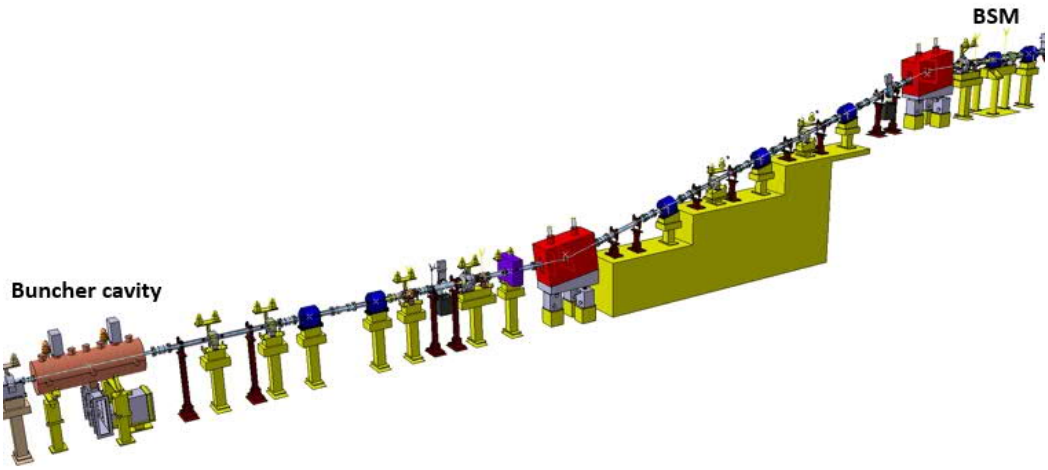

Fig. 2.28: Layout of the longitudinal emittance measurement set-up.

References

[1] J. Lettry *et al.*, *AIP Conference Proceedings* **2052** (2018) 050008, doi:10.1063/1.5083762.
[2] M. Stockli *et al.*, *Rev. Sci. Instrum.* **83** (2012) 02A732, doi:10.1063/1.3681921.
[3] M. Kronberger *et al.*, *AIP Conf. Proc.* **1390** (2011) 255, doi:10.1063/1.3637395.
[4] M. Paoluzzi *et al.*, *AIP Conf. Proc.* **1390** (2011) 265, doi:10.1063/1.3637396.
[5] RF-matching network,EDMS 1585312.
[6] A. Butterworth *et al.*, *AIP Conf. Proc.* **1655** (2015) 030007, doi:10.1063/1.4916434.

[7] R. Guida, *et al*., The new gas injection system for the LINAC4 accelerator at CERN, 2013 IEEE Nuclear Science Symposium and Medical Imaging Conference (2013 NSS/MIC), Seoul, 2013, pp. 1-5, doi:10.1109/NSSMIC.2013.6829817.
[8] D. Aguglia, Design of a system of high voltage pulsed power converters for CERN's Linac4 H^- ion source, 2013 19th IEEE Pulsed Power Conference (PPC), San Francisco, CA, 2013, pp. 1-6, doi:10.1109/PPC.2013.6627655.
[9] A. Grudiev *et al*., *Rev. Sci. Instrum.,* **85** (2014) 02B134, doi:10.1063/1.4842317.
[10] K. Nishida *et al*., *Rev. Sci. Instrum.,* **85** (2014) 02B117, doi:10.1063/1.4832060.
[11] S. Mattei *et al*., *AIP Conf. Proc.* **1515** (2013) 386, doi:10.1063/1.4792807.
[12] S. Mattei *et al*., *Rev. Sci. Instrum.,* **85** (2014) 02B115, doi:10.1063/1.4833919.
[13] S. Mattei *et al*., *Plasma Sources Sci. Technol*. **25** (2016) 065001, doi:10.1088/0963-0252/25/6/065001.
[14] S. Mattei *et al.,* J. *Comput. Phys*. **350** (2017) 891, doi:10.1016/j.jcp.2017.09.015.
[15] M. Ohta *et al.,Rev. Sci. Instrum.,* **85** (2014) 02B113, doi:10.1063/1.4833920.
[16] C. Schmitzer *et al.*, *Rev. Sci. Instrum.* **83** (2012) 02A715, doi:10.1063/1.3672109.
[17] Ø. Midttun *et al.*, *Rev. Sci. Instrum*. **83** (2012) 02B710, doi:10.1063/1.3670344.
[18] Ø. Midttun *et al.*, *AIP Conf. Proc.* **1515** (2013) 481, doi:10.1063/1.4792819.
[19] Ø. Midttun, J. Lettry and R. Scrivens, *Rev. Sci. Instrum.,* **85** (2014) 02A701, doi:10.1063/1.4824814.
[20] D. A. Fink *et al.*, *Nucl. Instrum. Methods Phys. Res*., A **904** (2018) 179, doi:10.1016/j.nima.2018.07.046.
[21] G. Voulgarakis *et al.*, *AIP Conf. Proc.* **1869** (2017) 030012, doi:10.1063/1.4995732.
[22] C.A. Valerio-Lizarraga *et al*., *Rev. Sci. Instrum.,* **85** (2014) 02A505, doi:10.1063/1.4847196.
[23] C.A. Valerio-Lizarraga, R. Scrivens, N. Chauvin, Space charge compensation in the Linac4 LEBT for three injected gas types, LINAC14, Geneva, Switzerland, pp. 510–512.
[24] C.A. Valerio-Lizarraga, I. Leon-Monzon and R. Scrivens, *Phys. Rev. Special Topics Accel. Beams,* **18** (2015) 080101, doi:10.1103/PhysRevSTAB.18.080101.
[25] A.M. Lombardi, C. Rossi and M. Vretenar, Design of an RFQ accelerator optimised for Linac4 and SPL, CERN-AB-Note-2007-027 (2007).
[26] C. Rossi *et al*., The radiofrequency quadrupole accelerator for the Linac4, LINAC08, Victoria BC, Canada (2008), pp.157–159.
[27] S.J. Mathot *et al*., Mechanical design, brazing and assembly of the Linac4 RFQ, IPAC10, Kyoto, Japan (2010), pp. 807–809.
[28] O. Piquet *et al*., RF tuning of the Linac4 RFQ, IPAC13, Shanghai, China (2013), pp. 3761–3763.
[29] C. Rossi *et al*., Commissioning of the Linac4 RFQ at the 3 MeV test stand, IPAC13, Shanghai, China (2013), pp. 3951–3953.
[30] J-L. Biarotte and G. Olry, A 90 – 160/180 MeV Spoke Linac as an option for the CERN Linac4/SPL, CARE-Note-2006-008-HIPPI (2006).
[31] E. Sargsyan and A. Lombardi, Superconducting Spoke Linac design as an alternative option for the CERN Linac4 high-energy part, AB-Note-2006-019-ABP (2006).
[32] F. Gerigk (ed.), Conceptual design of the SPL II, a high-power superconducting H^- linac at CERN, CERN-2006-006 (2006), doi:10.5170/CERN-2006-006.
[33] F. Gerigk *et al*., RF structures for Linac4, PAC07, Albuquerque NM, USA, pp. 3821–23, doi:10.1109/PAC.2007.4439920.
[34] M. Vretenar *et al*., Design and development of RF structures for Linac4, LINAC06, Knoxville TN, USA, 2006, pp. 679–81.
[35] J. Billen *et al*., Room temperature linac structures for the spallation neutron source, PAC01, Chicago IL, USA, 2001, pp. 1104–6, doi:10.1109/PAC.2001.986594.

[36] E. Benedico Mora and M. Vretenar, Design of a side-coupled linear accelerator structure for Linac4, CERN-AB-Note-2005-044 (2005).

[37] E. Sargsyan and A. Lombardi, PI-mode 352 MHz scaled LEP cavities as an alternative accelerating structure for the energy range of 90 to 160 MeV in the CERN Linac4/SPL, CARE-Note-2007-003-HIPPI (2007).

[38] A. M. Lombardi *et al.*, End-to-end beam dynamics for CERN LINAC4, CERN-AB- 2007-001 / CARE-Conf-06-039-HIPPI (2006).

[39] S. Ramberger *et al.*, Drift tube linac design and prototyping for the CERN Linac4, LINAC08, Victoria BC, Canada, 2008, pp. 184–186.

[40] J. Stovall, S. Ramberger and R. Lown, RF breakdown in drift tube linacs, CERN- sLHC-Project-Note-0007 (2009).

[41] G. Bellodi et al., Beams dynamics optimisation of LINAC4 structures for increased operational flexibility, LINAC10, Tsukuba, Japan, 2010, pp. 764–766.

[42] G. De Michele, F. Grespan and S. Ramberger, Power coupler simulations for the Linac4 drift tube linac, CERN-ATS-Note-2012-002 (2012).

[43] S. Ramberger *et al.*, Production design of the drift tube Linac for the CERN Linac4, LINAC10, Tsukuba, Japan, 2010, pp. 560–562.

[44] T. Ilg *et al.*, Mechanical design of the drift tube linac DTL for the spallation neutron source, PAC03, Portland OR, USA, 2003, pp. 2841–2843, doi:10.1109/PAC.2003.1289739.

[45] R. Garoby, SPL at CERN, CERN-sLHC-PROJECT-Report-0015 (2009).

[46] F. Grespan *et al.*, Linac4 DTL prototype: theoretical model, simulation and low energy measurements, sLHC-PROJECT-Report-0028 (2009).

[47] G. De Michele *et al.*, The Linac4 DTL prototype: low and high power measurements, CERN-ATS-Note-2012-003 (2012).

[48] S. Ramberger *et al.*, CERN Linac4 drift tube linac manufacturing and assembly, LINAC14, Geneva, Switzerland, 2014, pp. 923-925.

[49] I. Sexton *et al.*, The drift tube welding assembly for the Linac4 drift tube linac at CERN, LINAC14, Geneva, Switzerland, 2014, pp. 929–931.

[50] G. Bellodi *et al.*, Alignment and field error tolerance in Linac4, CERN-ATS-Note- 2011-021 (2011).

[51] M. R. Khalvati and S. Ramberger, Tuning and field stabilization of the Linac4 drift tube linac, LINAC14, Geneva, Switzerland, 2014, pp. 631–633.

[52] Y. Cuvet *et al.*, Development of a 352 MHz cell-coupled drift tube linac prototype, LINAC04, Lübeck, Gemany, 2004, pp. 288–290.

[53] Y. Cuvet *et al.*, Development of a cell-coupled drift tube linac (CCDTL) for Linac4, LINAC08, Victoria BC, Canada, 2008.

[54] A. Tribendis *et al.*, Construction and RF conditioning of the cell-coupled drift tube linac (CCDTL) for Linac4 at CERN, LINAC14, Geneva, Switzerland, pp. 746–750.

[55] G. Bellodi *et al.*, Alignment and field error tolerance in Linac4, CERN-ATS-Note-2011-021.

[56] R. Wegner and F Gerigk, *Nucl. Instrum. Methods Phys. Res. A* **606** (3) (2009) 257–70, doi:10.1016/j.physletb.2003.10.071.

[57] G. Favre *et al.*, Manufacturing the Linac4 PI-mode structure prototype at CERN, IPAC11, San Sebastián, Spain, 2011, pp 1774–1776.

[58] F. Gerigk *et al.,* The hot prototype of the PI-mode structure for Linac4, LINAC10, Tsukuba, Japan, 2010, pp. 220–222.

[59] F. Gerigk *et al.*, High power test of the first PIMS cavity for Linac4, IPAC11, San Sebastián, Spain, 2011, pp. 205–207.

[60] F. Gerigk *et al*., The Linac4 power coupler, IPAC11, San Sebastián, Spain, 2011, pp. 208–210.

[61] R. Wegner *et al*., Tuner-adjustable waveguide coupler (TaCo), CERN-ATS-Note-2011-085 TECH (2011).

[62] A.V. Feshenko, Method and instrumentation for bunch shape monitor, PAC01, Chicago IL, USA, 2001, pp. 517–521, doi:10.1109/PAC.2001.987557.

[63] J.-B. Lallement *et al.,* Linac4 transverse and longitudinal emittance reconstruction in the presence of space charge, LINAC14, Geneva, Switzerland, pp. 913–915.

3 Linac4 systems

3.1 Beam instrumentation

The Linac4 beam diagnostic systems include instrumentation to be permanently installed in the machine capable of measuring all parameters needed for routine operation as well as temporary measurement benches used only during commissioning. Three test benches for source and low energy beam transport (LEBT) commissioning, medium energy (3 and 12 MeV) commissioning, and beam commissioning at 50 MeV and 100 MeV were assembled and used for measuring the beam parameters.

The permanent instruments allow measurement of:

- **Beam intensity** through a Faraday Cup in the LEBT and a series of beam current transformers (BCT) along the linac and its transfer lines. Measuring beam intensities at different locations also allow determining the transmission through the accelerating structures or transferring lines.
- **Beam position** using strip line beam position monitors (BPM). These devices also measure beam intensity when being cross-calibrated to BCTs.
- **Beam energy** through time of flight (ToF) measurements made with BPMs working as phase probes.
- **Transverse profiles** through wire grids and wire scanners. A Laser wire provides similar but non-invasive measurements by stripping some of the H^- ions and either collecting the stripped electrons or the neutral H^0.
- **Transverse emittance** with the 3-profile method using wire scanners of wire grids and as well with the laser-wire emittance scanner.
- **Longitudinal bunch shape** with a dedicated bunch shape monitor (BSM).

- The instrumentation provided along the linac consists of:
- **Ion source and LEBT:** a Faraday Cup to (destructively) measure the total beam current, a BCT to measure beam current non-destructively, and a sandwich of 2 wire grid planes to measure the horizontal and vertical beam profiles.
- **RFQ and chopper line (MEBT)**: the MEBT is equipped with a BCT for intensity measurement and 2 L-shaped wire scanners to measure the transverse profiles.
- **DTL and CCDTL**: in the limited space between the end of the DTL and the first CCDTL tank 2 wire grid planes, a BCT and a BPM are installed. Special versions with smaller dimension had to be designed to fit in the available space. In the CCDTL, two wire scanners are installed after modules 1 and 4, and two wire grids are installed after modules 3 and 7. Each inter-module section features a BPM in addition.
- **PIMS**: between the CCDTL and the PIMS there is another inter-tank region with a BCT, a BPM, and a wire grid.
- **Transfer lines**: the transfer line L4Z contains one BCT, 2 tanks with wire grids and wire scanners, and a laser emittance meter, while the line L4T has five BCTs, ten BPMs, and four tanks with wire grids and wire scanners and a laser emittance meter.

3.1.1 Beam current transformer

The current transformer (Fig. 3.1) consists of a magnetic core with a secondary winding (the beam replacing the primary winding) and a calibration winding. It is designed for the rather long Linac4 pulses of 600 μs making sure that the droop during the maximum pulse length does not exceed 1%. In order to make the transformer as insensitive to external magnetic fields as possible, three layers of mu-metal and one layer of Armco magnetic shielding are employed. For the transformer in the DTL-CCDTL inter-tank region a single mu-metal layer is implemented because of space restrictions.

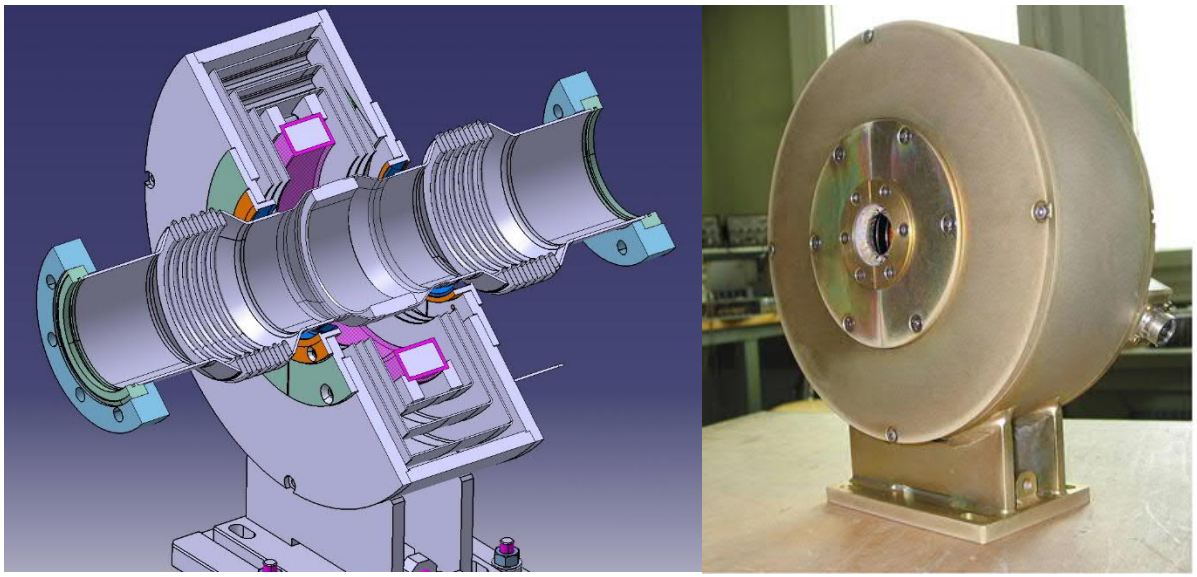

Fig. 3.1: Beam current transformer drawing.

Table 3.1 below lists all transformers of Linac4. There are four types of transformers at Linac4 which essentially only differ in the aperture needed for the vacuum chamber. The transformers in the inter-tank regions are smaller in size and have less performant shielding.

Table 3.1: Linac4 transformers.

Transformer	Position	Internal diam. VC	N winding	BW core + amplifier
L4L.BCT.1213	LEBT line	100 mm	50	0.6 Hz–3.8 MHz
L4L.BCT.3113	MEBT line	27 mm	50	0.6 Hz–3.8 MHz
L4L.BCT.4013	MEBT line	27 mm	20	2 Hz–16 MHz
L4C.BCT.0117	DTL-CCDTL	40 mm	20	2 Hz–16 MHz
L4P.BCT.0117	CCDTL-PIMS	40 mm	20	2 Hz–16 MHz
L4T.BCT.0107	L4T line	67 mm	20	2 Hz–16 MHz
L4T.BCT.0673	L4T line	100 mm	20	2 Hz–16 MHz
L4T.BCT.1043	L4T line	67 mm	20	2 Hz–16 MHz
L4T.BCT.1243	L4T line	100 mm	20	2 Hz–16 MHz
L4T.BCT.1553	L4T line	100 mm	20	2 Hz–16 MHz
L4Z.BCT.0273	L4Z line	100 mm	20	2 Hz–16 MHz

A dedicated VME module (TRIC: transformer integration card) was developed controlling every aspect of BCT data treatment. The signal from the secondary winding is amplified by a pre-amplifier with 2 different gains, installed very close to the monitor, and digitized by two 200 MHz ADC channels in the TRIC card. The samples are then averaged with a user defined time base between 10 ns (2 samples) and several µs (several hundred samples). By changing the time base, either the full beam pulse can be seen or one can zoom into a small part of the pulse. With this technique, the rise and fall times of the fast chopper can be observed to a precision of 10 ns (Fig. 3.2).

After every beam pulse a precise calibration pulse is sent into the transformer's calibration winding. Comparing the beam pulse to the calibration pulse, taking into account the signal and calibration offset, allows determining the beam current to a precision of 1%.

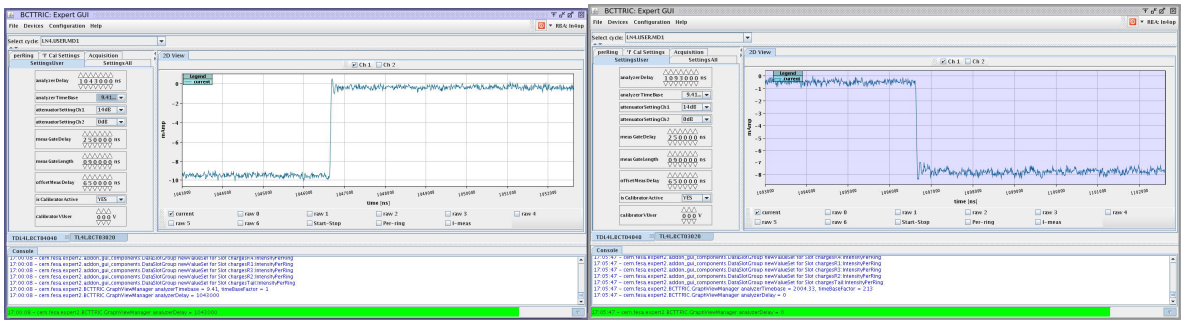

Fig. 3.2: Bunch rise and fall time, highest BCT time resolution of 10 ns.

3.1.2 Beam position monitor

Shorted stripline pick-ups are used for their versatility to match the limited space constraints, and for their good linearity and sensitivity (Fig. 3.3). Fifteen BPMs are integrated into the Linac between the DTL and the PIMS modules while another 27 are spread along the transfer line to the booster. Different BPM types are needed due to a large variety of vacuum chamber diameters: 34 mm and 39 mm for the linac, 100 mm for the transfer line, and 67 mm on the movable test bench.

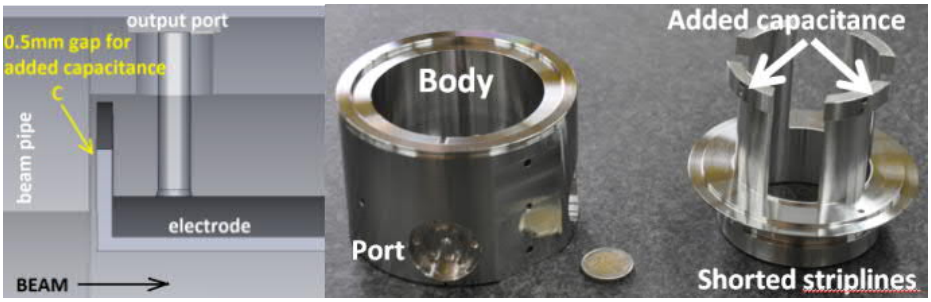

Fig. 3.3: Beam position monitor assembly.

The BPMs measure beam position, relative intensity, and average beam energy through time of flight measurements when using the devices as phase probes.

The signal coming from the BPM electrodes is down-mixed with a local oscillator. The intermediate frequency (IF) is sampled at four times the IF to acquire the I/Q data 90° apart, giving the relative phase φ and intensity. The position is calculated taking the difference between opposite electrodes divided by their sum. The beam intensity is proportional to the sum of all signal intensities.

3.1.3 Wire grids

Wire grids are used for transverse profile measurements and were also employed in the slit/grid emittance meter or the spectrometer used for commissioning (Fig. 3.4). At low energy (up to 50 MeV) 40 µm carbon wires are used while at higher energy 30 µm tungsten wires were chosen. This is due to signal creation, which is a combination of two physical effects: charge collection, mainly at low energy where the particle gets stopped by the material, and secondary emission, mainly at high energy where the particle traverses the material.

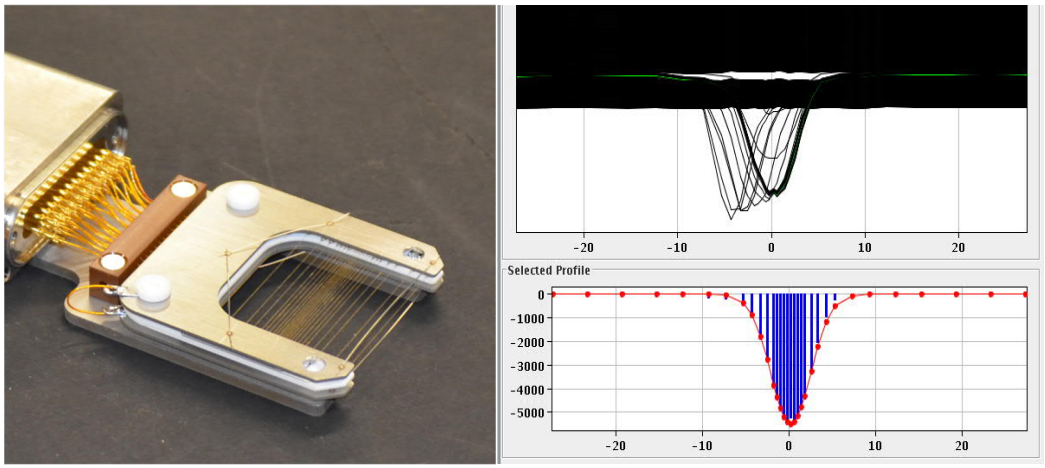

Fig. 3.4: Profile grid with variable wire spacing and measurement.

Except for the LEBT, where a sandwich of horizontal and vertical plane is employed and a single pneumatic in/out mechanism is used, all other locations have separate horizontal and vertical planes with their associated pneumatic mechanism. The wire spacing depends on the expected beam width, and is generally denser in the centre, and has a larger spacing at the outer positions. Like this, the profile can be measured with high precision in the beam centre while the beam halo is still covered by the outer wires. Details about wire material and wire spacing can be found in the appendix.

Since a wire inserted into the beam will produce stripping of the H^- electron, it is not possible to measure profiles when inserting several grids at the same time. The stripped electrons will disturb the measurement at the following grid. It was also feared that these stripped electrons produce cross-talk between wires, but comparison between profiles, measured with wire scanners and those measured with wire grids, show differences of less than 1%. By using L-shaped wire scanners in contrast to X-shaped ones, the cross-talk between the horizontal and vertical wire can be clearly seen.

A VME card, implementing 36 channels of 250 kHz sampling ADCs, digitizes the wire signals, which are linearly amplified. All profiles are therefore time resolved to a resolution of 4 µs. A wire scanner control card, which is accessed through a serial connection from the VME interface, is used for in/out control as well as HV control for the wire frame and/or wire polarization. This card can also send a test signal onto the wires allowing the full electronics chain as well as the wire resistance to be checked, and can therefore also be used to detect broken wires.

3.1.4 Wire scanners

Wire scanners can measure beam profiles to a higher precision than wire grids (typically some 100 µm) but need several beam pulses to accomplish a measurement; they use 40 µm carbon wires (Fig. 3.5). The electronics is the same as for the wire grids except of the PLC based stepping motor control, which is employed instead of the pneumatic in/out system of the wire grids. Two channels from the same 36 channel ADC are used to convert the wire scanner signal giving a time resolution of 4 us as in the wire grid case.

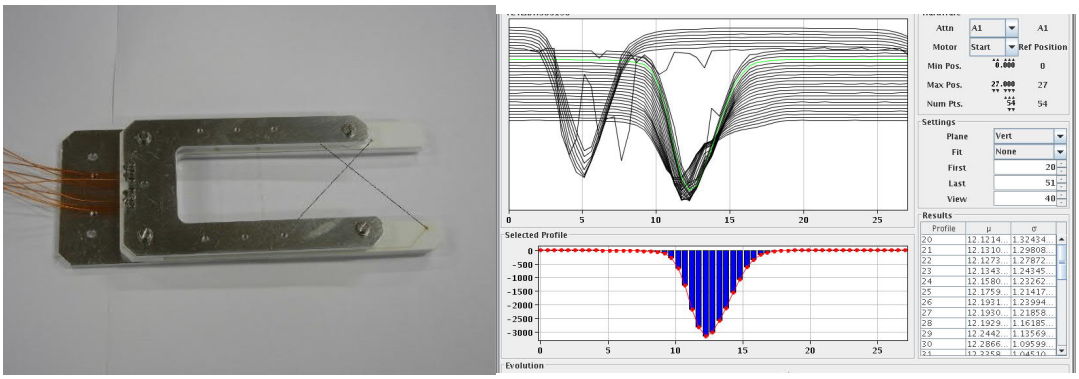

Fig. 3.5: The L-shaped wire scanner and chopping as seen by the vertical wire scanner in the MEBT.

3.1.5 Bunch shape monitor

The bunch shape monitor was built by INR Troitsk and is designed to measure the longitudinal intensity distribution in a micro bunch (Fig. 3.6). The detector uses a 100 µm Tungsten wire which is inserted into the beam. The wire is polarized with $U_{targ} = -9$ kV, accelerating secondary electrons, created through the interaction of the primary beam with the wire, radially away from the originating wire. A fraction of the electrons passes through a slit and enters a deflector combined with an electro-static lens. The deflector is supplied with an RF voltage of the same frequency as the accelerating frequency, whose phase with respect to the accelerating RF may be modified in steps of 1 degree.

The electro-static lens combined with a steering magnet focuses the beam onto a second slit behind which an electron multiplier is used to amplify the electron signal. An additional spectrometer magnet in front of the electron multiplier has been installed allowing the separation of electrons created through secondary emission from those stemming from H^- dissociation having a higher energy.

Since the created secondary electrons are virtually instantaneous and the high electric field around the target wire accelerates the electrons very quickly to their final energy, the time structure of the secondary electrons is identical to the time structure of the primary beam. Changing the phase delays therefore allows scanning through the longitudinal beam pulse and measuring the bunch shape.

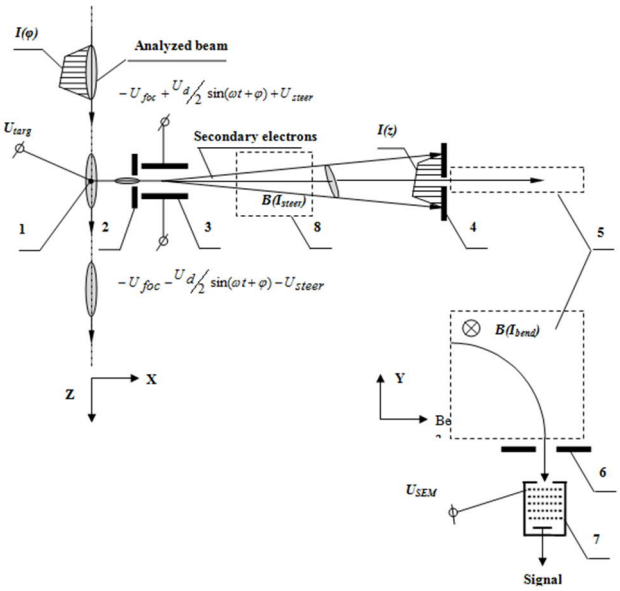

Fig. 3.6: Schematic of the bunch shape monitor.

The BSM parameters like the target position, the high voltage on the target wire, the focusing and steering voltages, the steering magnet current etc., can be locally controlled on an electronics box

provided by INR. This box can be switched to remote control and a PC with a LabView program then remotely controls all parameters. The HV voltages are controlled through analogue voltage levels created through DACs and switched on and off through digital I/O levels. All control voltages are read back with ADCs. A PLC provides movement control for the target wire. Part of the LabView program is dedicated to this remote control of individual BSM parameters. A typical measurement is shown in Fig. 3.7.

Before operating the BSM for bunch shape measurements, the correct focusing and steering of the secondary electron beam onto the second slit must be found. The LabView program provides a scanning section, stepping through steering settings for a given focusing voltage. The settings are correct at the peak of the smallest curve obtained. The scanning is done with the deflecting RF switched off.

The BSM is triggered ~2 ms before arrival of the beam. The RF deflection signal is switched on and once stable the beam arrives and the secondary electrons are deflected in front of the second slit thus transforming the longitudinal distribution into a transverse distribution in front of the slit. A small slice of the distribution passes through the slit and is detected by an electron multiplier after passing through the spectrometer magnet and the third slit. Changing the RF phase with respect to the accelerating RF one can step through the longitudinal intensity distribution. The signal from the electron multiplier is sampled at a frequency of 1 MHz and changes of the longitudinal distribution along the 400 µs beam pulse can be observed at 1 µs time resolution.

The BSM was first installed on the 3/12 MeV measurement bench, then moved to the 50/100 MeV measurement bench and will finally be installed in the transfer line between PIMS and the 160 MeV dump. The LabView program provided by INR is going to be replaced by a standard CERN application.

A second BSM with a larger opening for the vacuum chamber will be installed just before the wall of the L4T transfer line and will be used for longitudinal plan measurement before transfer of the beam to the PSB.

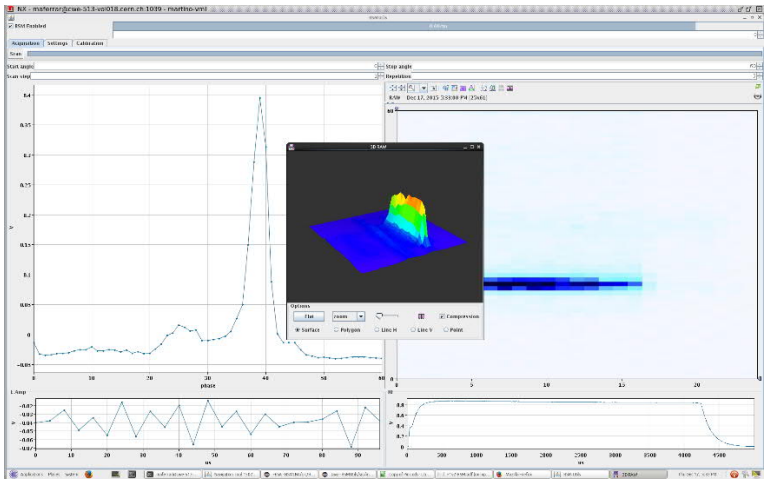

Fig. 3.7: Bunch shape measurement.

3.1.6 Beam loss monitors

Ionization chambers of LHC type are used as beam loss detectors with a readout system adapted to the requirements of a linac. The system has a very high dynamic range detecting currents from 10 pA to 200 mA. The processing part keeps track of several integration windows ranging from 2 µs to 1.2 s. As well as collecting loss data and storing it in a database, the system continuously compares the losses to

user defined thresholds both in hardware and software. When a threshold is exceeded the system stops further beam through the beam interlock system (BIS).

Double shielded cables are used to transport the analogue signal from the detectors to the front-end electronics. The analogue electronics is controlled by an FPGA, which can automatically switch between two acquisition modes. For currents between 10 pA and 30 mA a fully differential current to frequency converter assisted by an ADC for fine interval sampling is employed. Currents above 20.3 µA are measured via directs sampling by a second ADC.

3.1.7 Laser-wire scanner

The laser-wire scanner is used to measure transverse beam profile and emittance in a non-destructive manner. The instrument is based on the principle of photo-detachment; its conceptual design is illustrated in Fig. 3.8.

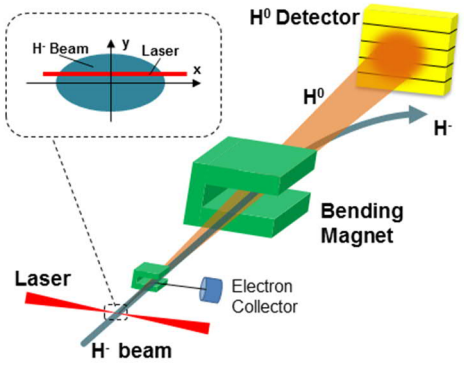

Fig. 3.8: Schematic principle of a laserwire scanner.

Prototype laserwire scanners were tested during commissioning at 3, 12, and 50 MeV. The difference between laser-based measurements and SEM Grid ones was within 1%. Two laser-wire scanners will be permanently installed in the transfer line.

3.1.8 Slit/grid emittance meter

The beam commissioning at low energy (45 keV, 3 MeV, and 12 MeV) relied on a specially built slit/grid emittance meter (Fig. 3.9).

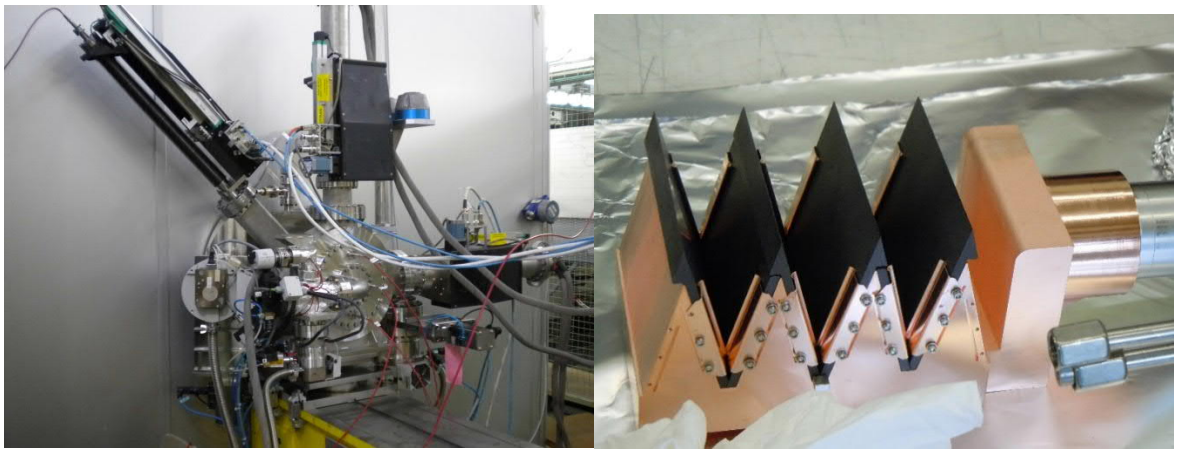

Fig. 3.9: The LEBT slit/grid emittance meter and the slit of the 3/12 MeV emittance meter.

While the 45 keV version used an L-shaped slit of 200 µm thickness, moved under 45° and implemented on a 1 mm steel plate, the slit at 3/12 MeV consisted of a harmonica shaped carbon

material mounted on a copper support. Separated slits for horizontal and vertical emittance measurements were needed.

The material and the geometry were chosen such that the energy deposition on the slit material provoked by the beam could be spread over a wide area and carbon was used because of its high resistivity to heat. In both cases, a horizontal and vertical wire grid with 48 wires of 0.75 mm wire distance was used. Both, slit and wire grid could be moved with stepping motors with a position resolution of 50 µm.

The stepping motors were PLC controlled and a LabView program provided automatic stepping through user-defined positions for slit and grid, readout of the grid signals as well as display of the measured phase space. The measurement parameters as well as the raw data read from the wire grid were written to data files for later offline evaluation. Since the grid data was converted with the same sampling ADC as used for the other wire grids and the wire scanners, emittance measurements with a time resolution of 4 µs along the beam pulse could be made. A typical measurement is presented in Fig. 3.10.

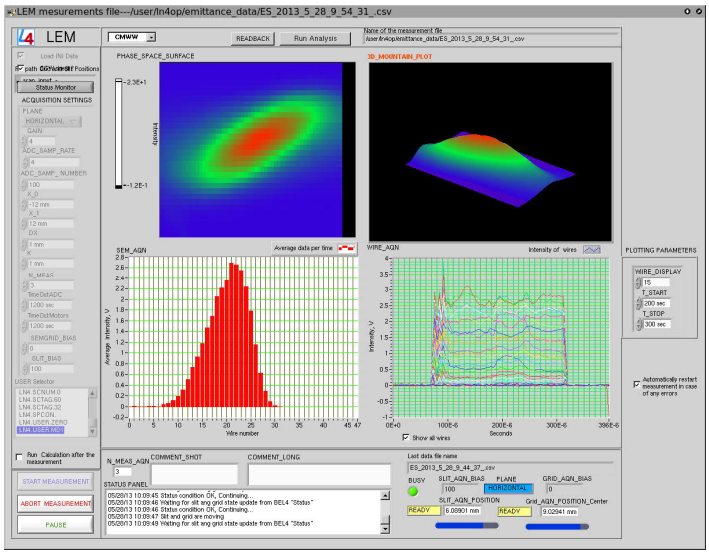

Fig. 3.10: Results from the slit/grid emittance meter.

3.2 Beam intercepting devices

The beam intercepting devices (BID) installed at Linac4, between the ion source and the PS booster injection, include the *beam stopper (ion) source,* the *main dump,* the *beam stopper* in the L4T transfer line, the *half-sector test dump,* and the *LBE* and *LBS dump.*

3.2.1 Beam stopper (ion) source

Two identical beam intercepting devices acting both as a beam stopper and as a beam dump are installed in the low energy beam transport (LEBT) line between the ion source and the RFQ (Fig. 3.11). The low beam energy of 45 keV results in a low continuous load of only 2.88 W, which allowed using the same design as for the Linac2 stopper. This consists in a stopping plate made of pure Tantalum (30 mm distance along beam axis) without water cooling nor shielding. An actuation system puts the Ta plate in beam position whenever requested by beam operation.

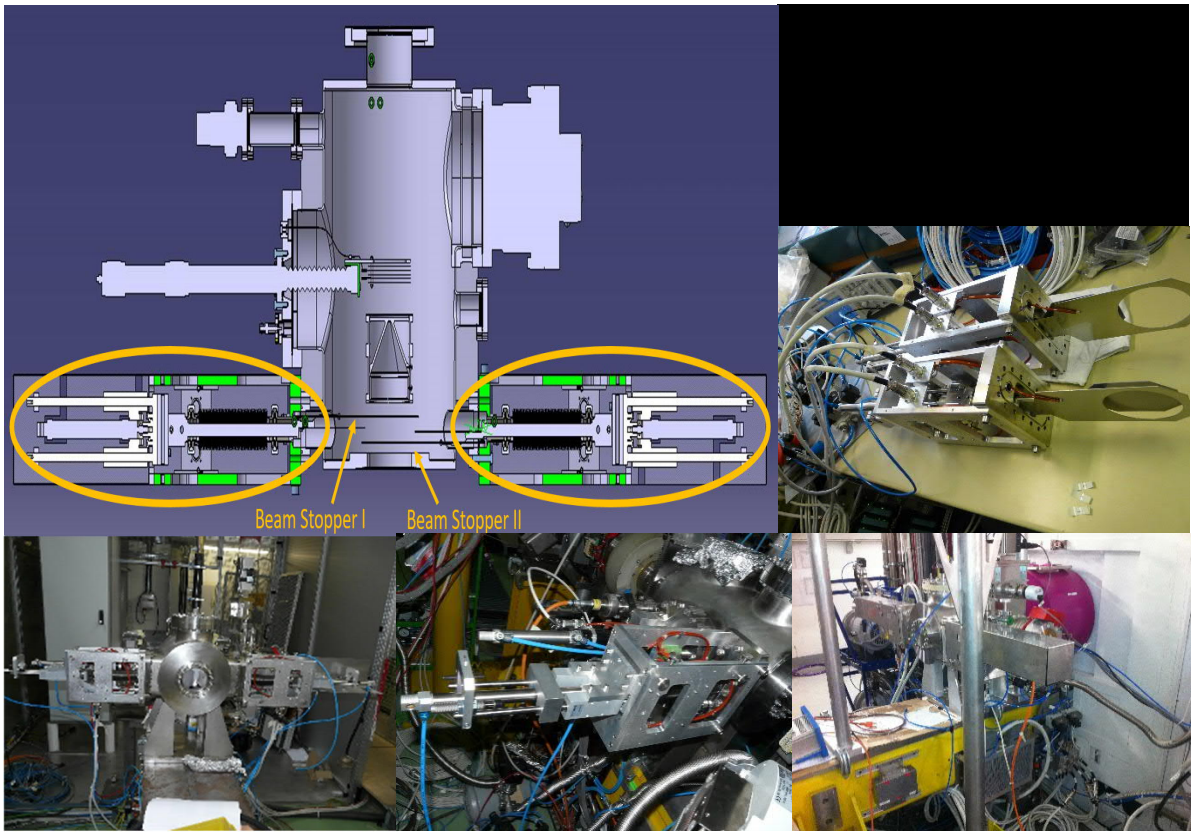

Fig. 3.11: Different views of the beam stopper source.

3.2.2 Main dump L4

The main dump is located 13 m behind the last RF structure right next to the transfer line to the PS booster. It is used for commissioning at 160 MeV, and during normal operation to intercept pulses not sent to the PS booster. It is designed for a continuous and time-unlimited absorption of the nominal beam. For this purpose, the dump consists of a graphite core (R4550), shrink fitted onto a stainless steel (304L) vessel with embedded helicoidally rectangular water channels. The flange, cap and beam pipe in front of the dump are made of stainless steel (316LN) to assure vacuum tightness. The total weight of the dump is around 350 kg with a length and diameter of 900 mm and 322 mm, respectively. The layout of the dump is shown in Fig. 3.12 and its assembly in Fig. 3.13.

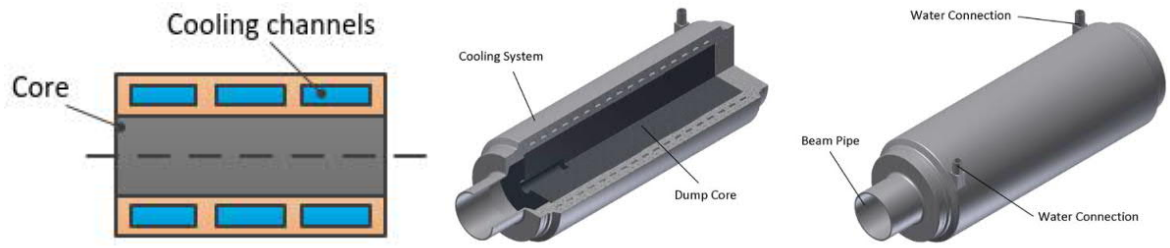

Fig. 3.12: Main dump layout.

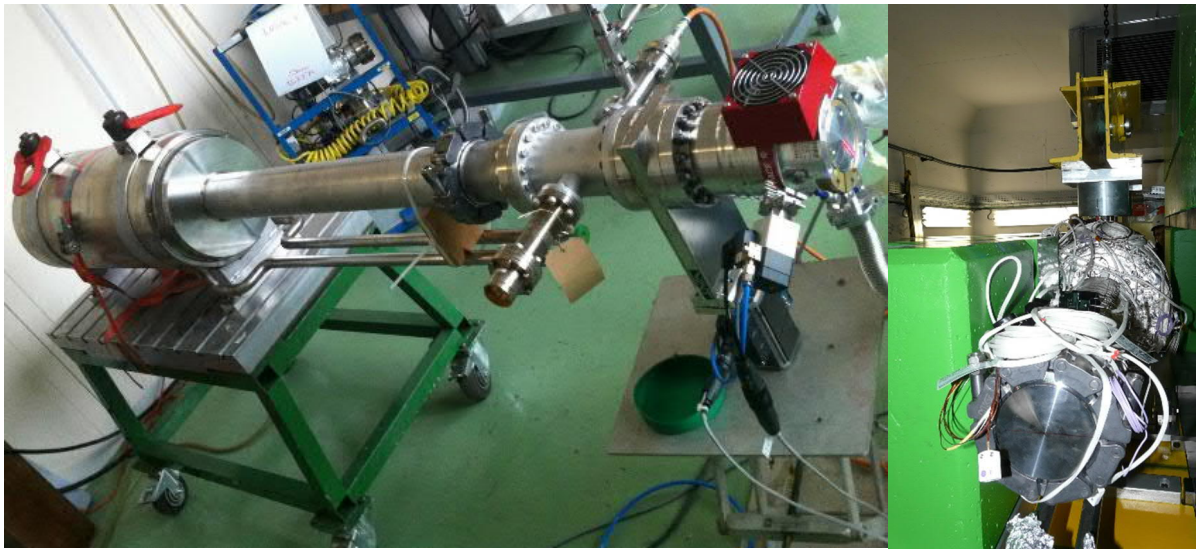

Fig. 3.13: Main dump assembly.

The main dump is shielded to protect personnel accessing the Linac4 tunnel and limit the activation of surrounding structures, air, and environment to a relatively safe level. The shielding consists of iron blocks around the dump and borated concrete blocks around them. The shielding can be opened on one side (movable drawer) and the internal part (part of the iron shielding if needed and the dump) removed, if the replacement of the dump is needed. The shielding is shown in Figs. 3.14 and 3.15.

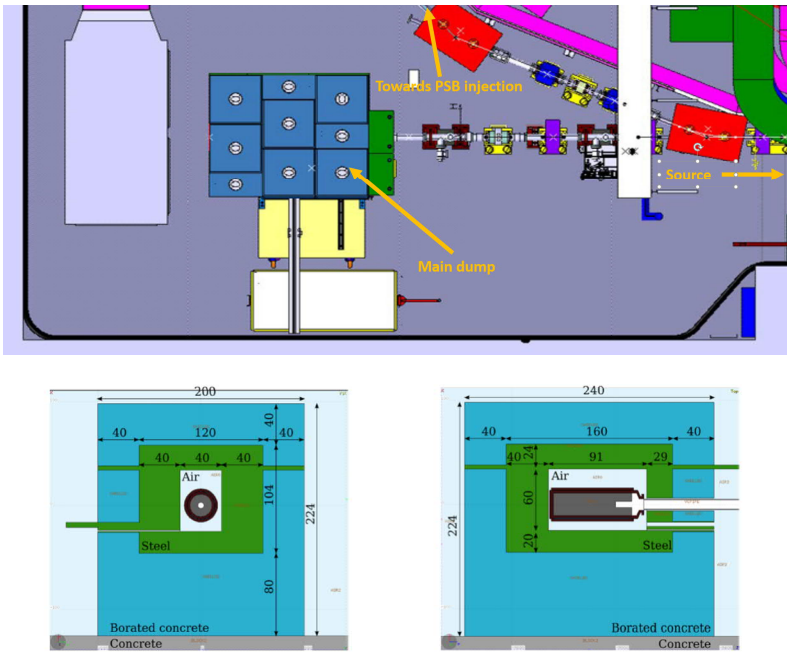

Fig. 3.14: Layout and dimensions of the main dump with shielding.

Fig. 3.15: Main dump shielding open for accessing the dump (left) and closed (right).

3.2.3 Beam stopper L4T

A beam stopper—as an important safety element for the machine (EIS)—was installed in the L4T transfer line after the main bending towards the PS booster. The stopper (Figs. 3.16 and 3.17) is designed to withstand one full Linac4 beam pulse in case other safety mechanisms fail. It consists of a primary graphite core (R 4550; min. length: 120 mm, diameter: 80 mm) and a secondary stainless-steel core (AISI 304L; min. length: 100 mm). No cooling system is needed. The graphite is shrink fitted onto the external stainless-steel core.

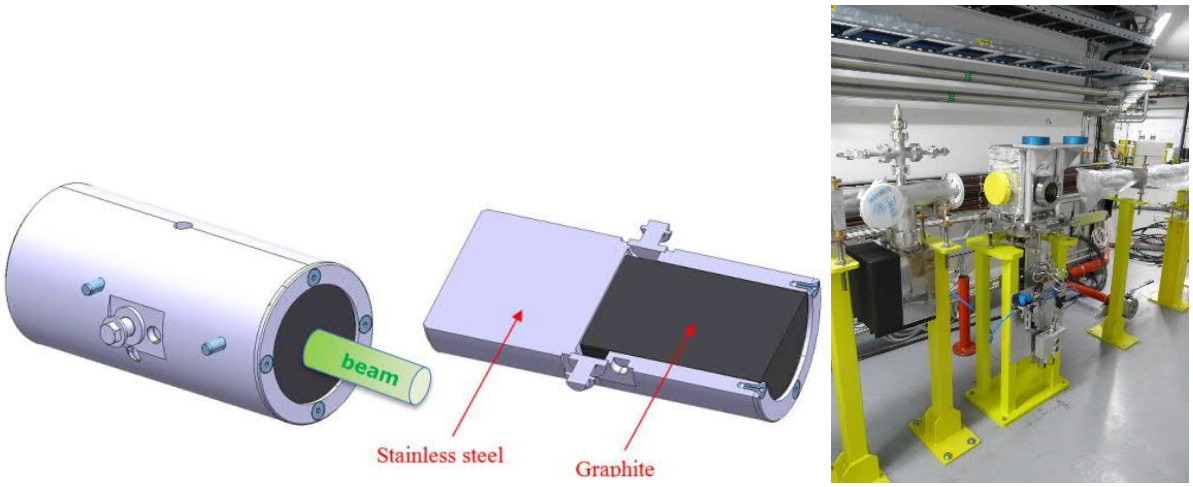

Fig. 3.16: Scheme and photograph of the L4T beam stopper.

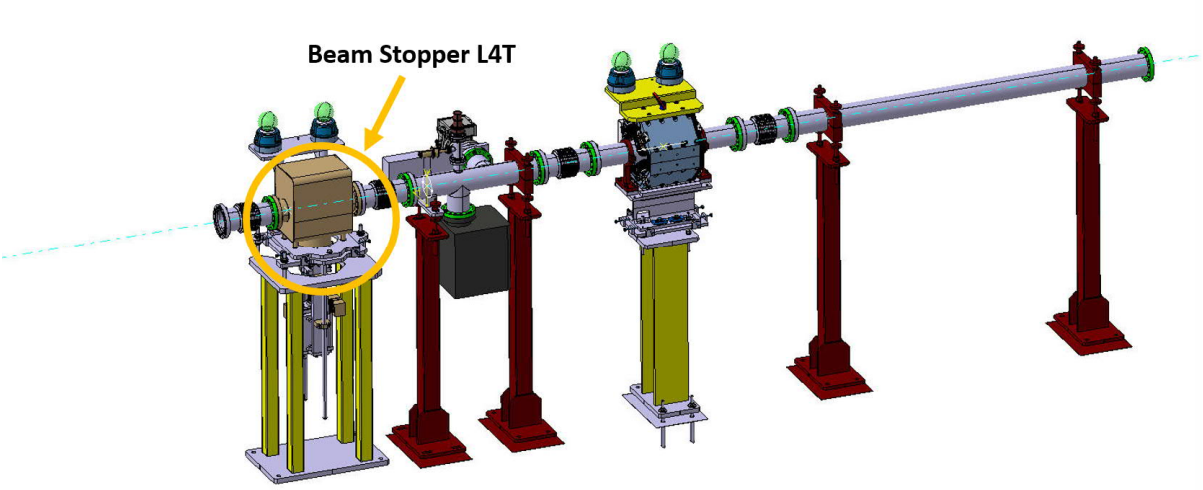

Fig. 3.17: Position of the beam stopper in the L4T line.

3.2.4 LBE dump

The LBE line used to measure transverse emittance before injection in the PS booster has been refurbished to be used with the 160 MeV beam. A 'main dump' assembly has been installed to terminate the line and intercept the beam after the measurement. The beam is comparable with the beam on the main dump thus the same design is used. Indeed, the working conditions for the LBE dump are worse than for the main dump because of the smaller beam spot (3×3 mm^2 compared to 3×6 mm^2 for a 1σ beam size) hence both main dumps were designed for the higher energy densities corresponding to the LBE location. The layout and a photo of the LBE dump are presented in Fig. 3.18.

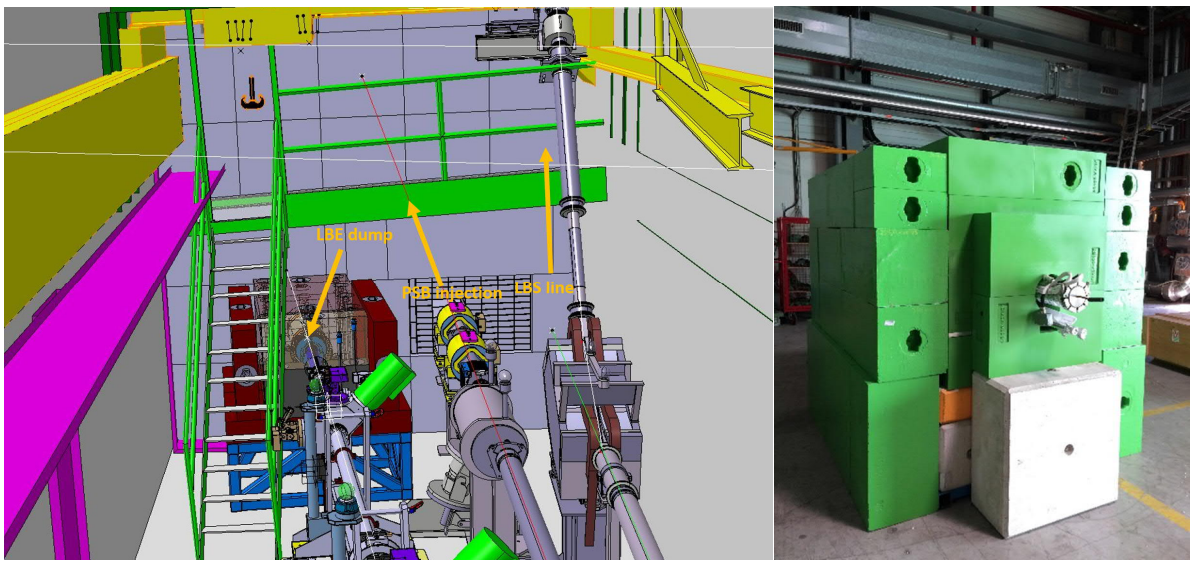

Fig. 3.18: Layout of the LBE area showing the position of the dump and a photograph of the dump in place.

3.3 Low-level RF

The goal of the Linac4 low-level radio-frequency (LLRF) system is to maintain a flat voltage for all cavities except the last two PIMS (triangular voltage modulation, constant phase) and the debuncher (constant voltage, triangular phase modulation). The LLRF consists in a slow **tuning system** that keeps

the cavity at the tune that minimizes the required power (function of voltage, beam current, and stable phase), and a **fast cavity field regulation** (cavity loops) that modifies the generator drive to keep the cavity field at the desired value.

3.3.1 Tuning systems

The required power is minimized when the cavity is detuned so that generator current and cavity voltage are in phase. During each pulse, the cavity voltage (V) and the forward signal from a coupler at the cavity entrance ($I_{c,fwd}$) are demodulated to generate baseband I-Q pairs at 44.025 M-samples per second (MSps). They are then filtered and decimated (CIC decimators [1]) reducing the rate to 2.75 MSps. The cross-product is computed and, after further filtering and decimation, the error data is divided by the square modulus of the cavity voltage. This generates a tuning correction, independent of the amplitude of cavity voltage. At the end of the RF pulse the normalized correction is sent to the motor(s) piloting plunger(s), except for the RFQ that is tuned by regulating the cooling water flow.

3.3.2 Field regulation

The loop delay from LLRF drive to the Antenna signal (measured by the LLRF), is around 1 μs. That includes generator and circulator group delay, waveguide to cavity, and cable delay in the antenna signal path. Allowing 200 ns for processing in the LLRF, the close-loop delay amounts to 1.2 μs. Figure 3.19 shows the regulation loops. We have four main sub-systems (shaded areas on Fig. 3.19).

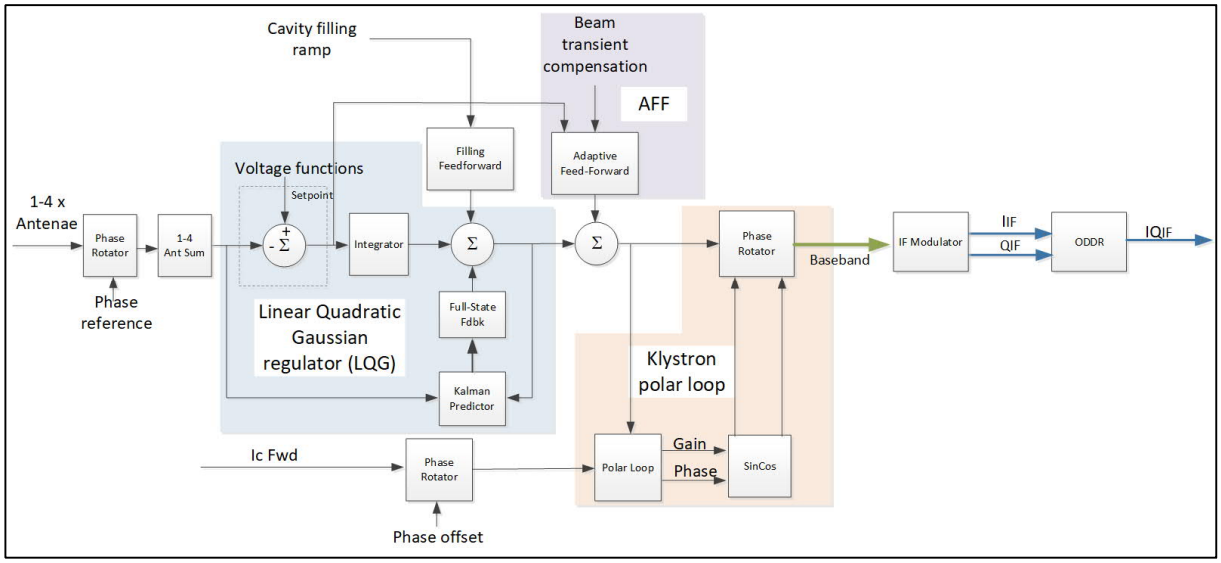

Fig. 3.19: Field regulation loops (cavity loops module).

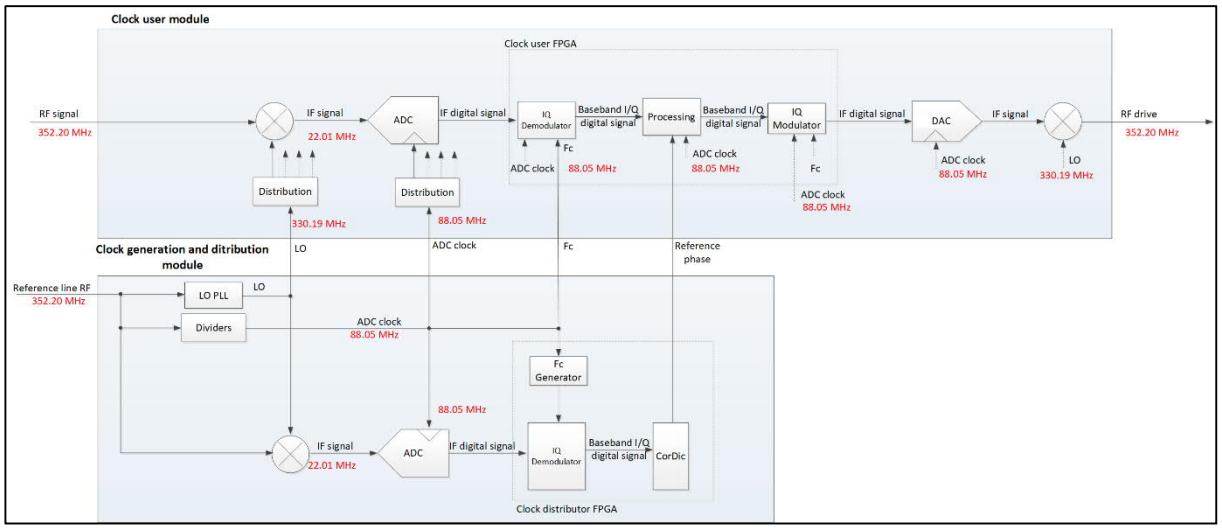

Fig. 3.20: Demodulation, processing, and modulation.

The RF is switched on 150 µs minimum before injection. The **cavity filling ramp** raises the generator drive in 100 µs.

The **linear quadratic Gaussian regulator** (LQG [2]) is then switched on and stabilizes the field in the remaining 50 µs until the beam batch is injected. Although we cannot measure the *present* cavity voltage, we can estimate it because the cavity response is well known and the generator drive is generated by the LLRF, and therefore known as well (except for the generator noise). The *optimal* estimator is the Kalman predictor [2], a model of the cavity response with delay, driven by the same drive as the generator. The (delayed) cavity voltage measurements are used to update the predictor's estimates, and correct for the inexact model and the unknown noise sources such as beam loading. The measurement noise is caused by the imperfect demodulation. The process noise is mainly caused by the generator and beam loading.

The predictor generates an accurate estimate of the inaccessible present cavity voltage value, that can be used to implement a full-state feedback. In order to track the reference input (desired cavity voltage set point), an integral feedback is added, using the difference between the measured cavity voltage and the set point. The integrator and full-state feedback gains are optimized using linear quadratic regulator theory.

To compensate for the beam loading transient at the head of the beam batch (hopefully fairly reproducible from pulse to pulse, as long as source intensity remains constant) an **adaptive feed-forward** (AFF) correction is added to the generator drive (Fig. 3.19). It is updated before every pulse, from measurements on past pulses (cavity voltage minus set point). It takes about five pulses for the AFF to reach 90% of the optimal correction.

Klystrons transform the ripples present on their high voltage (HV) supply into RF amplitude and phase noise. Similarly, their gain and phase shift are drifting, as a consequence of the HV droop during the RF pulse. This can cause much problem with the LQG: as the open loop phase rotates, the phase margin decreases and the loop can go unstable. The effect of DC fluctuations on the RF parameters is multiplicative noise (modulation of gain and phase), and it is best compensated by a polar feedback acting on the overall gain and phase shift (**klystron polar loop**, Fig. 3.19). The forward current measured with a coupler at the cavity input is compared to the klystron drive, generating a gain and phase shift data. After subtraction of set values, the error signals are integrated and control a vector modulator. A similar klystron polar loop is in operation in the LHC [3].

When we drive two cavities with a single klystron, the regulation loops receive the antenna signals from both cavities. A slow mechanical phase shifter is inserted in one of the two waveguides and is controlled to adjust the relative phases. The common drive will be regulated by the fast loops, LQG, and AFF (Fig. 3.19). The fast perturbations being common to both cavities (klystron noise and transient beam loading), the overall performances should not be degraded much. Mechanical vibrations could however be problematic.

3.3.3 Hardware implementation

We use the classic I-Q Digital demodulation scheme first proposed in 1995 (Fig. 3.20) [4]. The RF signal (antenna, coupler, or reference line) at f_{RF} (352.2 MHz) is first mixed down to an IF at 1/16 f_{RF} (22.01 MHz) by mixing with an LO at 15/16 f_{RF} (330.2 MHz). The analog IF signal is sampled by an ADC whose clock runs at 1/4 f_{RF} (88.05 MHz). After time de-multiplexing and sign inversion, a stream of baseband (I, Q) pairs is generated at 44.025 MSps. The stability and precision of the harmonically related clocks (LO and ADC clock) are critical for the overall performance. Linac4 has a coaxial reference line, powered with a 100 W signal, and running in the tunnel, with –30 dB coupler adjacent to each cavity. The signal from these couplers are routed to the LLRF on cables (~100 m long) running together with the corresponding antenna signals. This layout is intended to minimize phase variations caused by temperature changes; to guarantee a similar thermal behaviour, the antenna and reference signal cables came from the same cable roll, for a given cavity. On the surface, the reference line signal is used to generate the demodulations clocks (LO and ADC clock). This is realized in the clock distribution module (lower block in Fig. 3.20). A reference phase is measured from the demodulation of the reference signal. The reference phase is subtracted from the antenna demodulation, so that the scheme is not sensitive to drift in the generation of the LO and ADC clocks. After processing in baseband (field regulation loops shown in Fig. 3.19, implemented in an FPGA clocked at 88.05 MHz), the output is mixed to the 22.01 MHz IF frequency, converted to analog, and mixed up to generate a 352.2 MHz generator drive. The same LO is used for demodulation and modulation so that the open-loop transfer function is not sensitive to LO phase drift.

3.3.4 Beam loading compensation

The specifications called for a field regulation within 1% (amplitude) and 1° (phase) over the 40 mA DC beam pulse. The dominant source of field perturbation is beam loading. Thanks to the chopper the beam pulse is perfectly rectangular in intensity. So far, the machine has been operated with 25 mA DC maximum. The following figures show the performances of the field regulation in a typical cavity (CCDTL1). The stable phase is –20° so that the beam induced perturbation appears mainly in the voltage amplitude. Figure 3.21 (left trace) shows the amplitude of the measured cavity voltage without any regulation. At the beginning of the linac pulse the klystron drive is gently ramped to approach the demanded voltage (8.2 MV) after ~100 μs. The 100 μs long beam batch is clearly visible from time 302 μs to 402 μs: without any compensation the beam loading reduces the cavity voltage by about 800 kV. Figure 3.21 (right trace) shows the performance of the LLRF: after ramping the klystron drive, the feedback (LQG) is closed at time 100 μs resulting in a fast stabilization of the voltage at the precise demanded 8.2 MV. The 150 μs long beam batch is injected at time 302 μs resulting in a barely visible transient as it is further compensated by the AFF. A stronger transient appears after the batch tail (452 μs) that is not compensated by the AFF (see below).

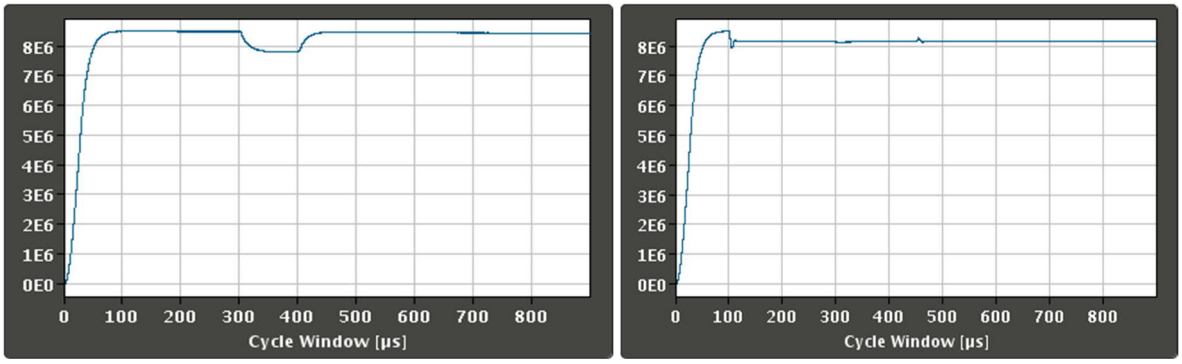

Fig. 3.21: Amplitude of CCDTL1 field (V). Left: no regulation, 100 µs long beam batch, 25 mA DC. Right: LQG and AFF ON, 150 µs long beam batch.

Figure 3.22 shows an enlargement of the amplitude trace during the beam segment. On the left trace the LQG regulator is active but the AFF is disabled. The field stabilization is excellent during the batch but shows an uncompensated transient in the head. This is unavoidable, caused by the finite response time of the LQG (around 5 µs). On the right-hand side the AFF is active during the beam segment. It very effectively reduces the head transient by a factor five linear. It is not active (and need not be active) on the tail transient as this appears after the batch has crossed the cavity. With both regulations active the field perturbation is reduced to 30 kV peak to peak, to be compared to the nominal 8.2 MV (0.4 % peak to peak). The above plots were taken during the 2019 run, while the klystron polar loop was not implemented yet. This additional regulation will be deployed on all cavities in 2020, adding robustness against klystron high voltage drifts and droop.

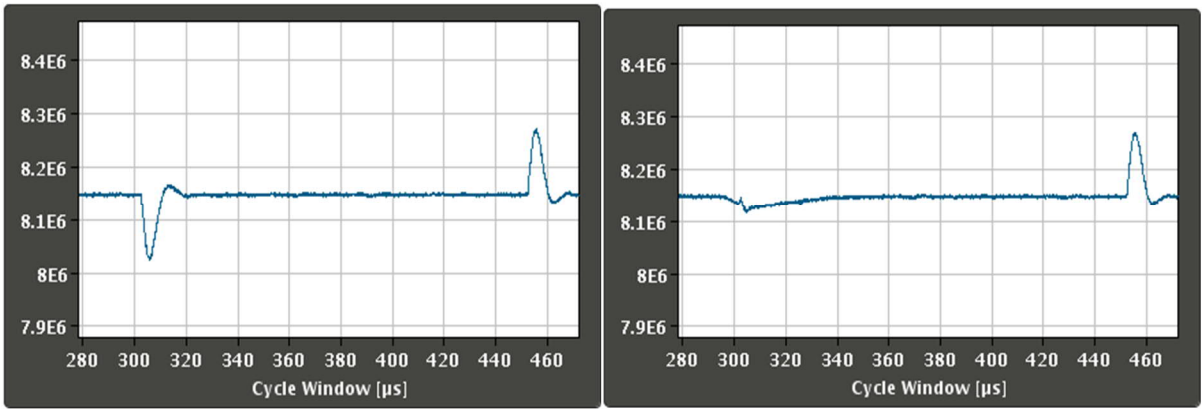

Fig. 3.22: Amplitude of CCDTL1 field (V). Zoom during the beam segment. Left: LQG only. Right: LQG and AFF.

3.4 High-power RF

The RF power for the Linac4 accelerating structures is generated by a combination of nine klystrons recuperated from the large positron electron collider (LEP) machine (output power 1 MW and 1.3 MW, frequency 352 MHz) and eight new state-of-the-art klystrons at 352 MHz and 2.8 MW peak output power.

This system is subjected to the following constrains: optimum re-use of the existing equipment of LEP, space limitation between the cavity windows at high beam energies, and stringent phase and amplitude requirements for the (H^-)-beam.

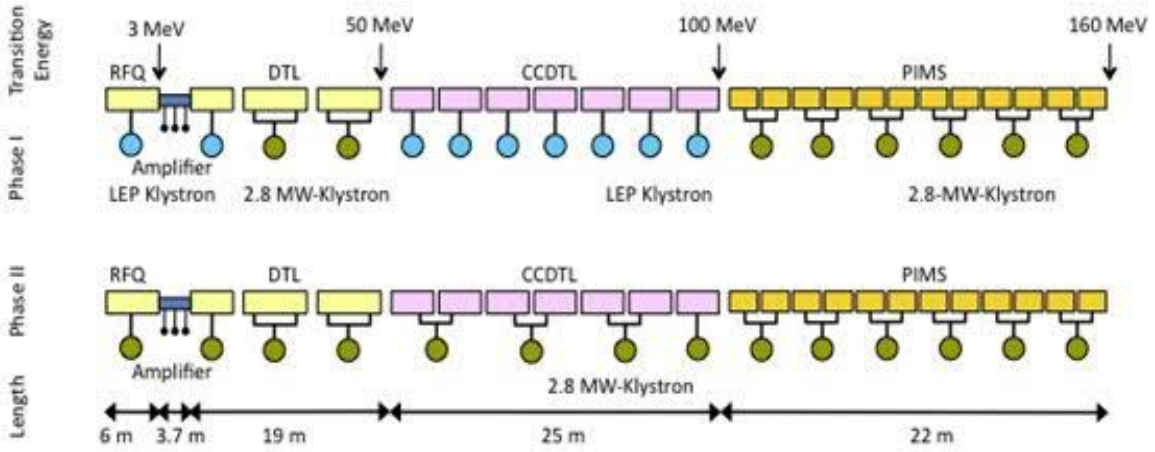

Fig. 3.23: Linac4 RF power schemes, initial (top) and final (bottom).

3.4.1 Power distribution

The high-power RF distribution schemes of Linac4 are presented in Fig. 3.23, initial (top) and final (bottom). In the initial phase of Linac4 operation most of the accelerating structures are powered by klystrons at 1.3 MW nominal peak power, recuperated from the stock of the old LEP collider ('LEP klystrons'). New 2.8 MW klystrons will be used only in two locations, for the last two DTL tanks and for the PIMS modules. In the first case, the maximum power per RF window of less than 1 MW requires feeding the structure through two windows with the inherent strong constrains on the RF phase that can be respected only by having a single power source. In the latter case, the short distance between two adjacent PIMS does not leave enough space in the equipment hall for the installation of two klystrons – the equipment hall has the same length as the linac.

In the installation, we distinguish three different powering schemes:

- single klystron powering a single structure;
- pairs of LEP klystrons connected to the same modulator powering one structure each; and
- new 2.8 MW klystron powering two structures (or one DTL through two apertures).

Over the course of operation, once the LEP klystrons reach the end of their lifetime, they will be replaced with new klystrons—one new for every two old. This exchange is justified by the high fabrication cost of the original LEP klystron that were designed for CW operation; modern pulsed klystrons have a much lower cost per unit power. Pairs of LEP klystrons connected to the same modulator will then be replaced by new klystrons, to come to the final configuration of Fig. 3.24 bottom. Integration of the equipment in the klystron gallery is made such as to minimize the work when changing from the two types of klystrons.

While the first two powering schemes consist of the usual amplifier, isolator (circulator and RF-load) and waveguide system, the design of the third layout is somewhat more challenging. As shown in Fig. 3.23, the RF power is split directly at the amplifier's output by means of a custom-made magic-tee and then fed to two circulators. The sum port of the magic-tee is matched with a high power RF-load. The two circulators connect to the accelerating structures and to an RF-load, each.

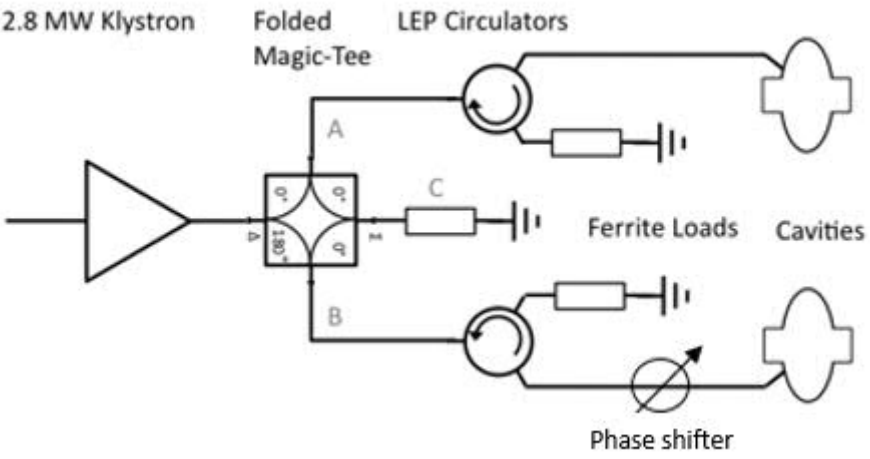

Fig. 3.24: Power scheme for a 2.8 MW klystron powering two structures.

The phase and amplitude in the two paths (labelled A and B in Fig. 3.24) depend on the symmetry of the magic-tee, the working point of the circulators and the electrical lengths of the waveguide systems. The waveguide system is designed and assembled such to reduce static differences to about 20° between the two branches. The residual error and dynamic effects, e.g., thermal drift, is compensated by 3-stub phase shifters installed on the longer branches. The overall RF signal is controlled by the LLRF system.

Different powering schemes were analysed based on measured or specified S-parameters of the different components allowing to roughly predict phase and amplitude differences. The power splitting between the two cavities (A and B) as well as the amount of power disposed in the load (C) was studied by means of Mason's rule [5]. This allowed for investigations of the phase and amplitude difference between the different branches depending on the circulator working point as well as production tolerances of the magic-tee and defined the phase shifters specification parameters. The solution for the power splitting has been validated at the dedicated high power RF Linac4 test stand.

3.4.2 Components

3.4.2.1 Klystrons

The Linac4 accelerator in its initial configuration is powered by both eight new, state-of-the-art klystrons and nine former LEP klystrons. Klystrons are consumables that, eventually, have to be replaced at the end of their cathode lifetime. Once all the LEP klystrons reach the end of their lifetime, they will be replaced with new klystrons; one new for every two old. Fourteen, 2.5 MW, 1.8 ms, 2 Hz modulators will power either one new or two old klystrons.

LEP klystrons

More than twenty old klystrons from three different manufacturers were recuperated from LEP. The main parameters of the LEP-type klystrons are shown in Table 3.2.

Table 3.2: Main parameters of the LEP-type klystrons.

Output power	1.3 MW
Operating frequency	352 MHz
DC to RF conversion efficiency	62 %
Operating voltage	100 kV
Maximum beam current	20 A
Gain	40 dB

Two major modifications of these klystrons are necessary to cope with the operational mode of Linac4:

- In order to optimize the HV cabling, and therefore to minimize the stored energy, the original HV tank of the klystron must be replaced. The new design integrates the klystron filament heating transformer, the mode anode voltage divider as well as measurement test points. Only one 4 m high voltage cable is necessary to connect the klystron to the modulator. The mode anode voltage divider will be individually adjusted as a function of the klystron's perveance and performance. The final L4 modulator will be equipped with a specially developed system, which will allow trimming of the klystron cathode current over a large range [6].
- The LEP klystrons were originally designed and tuned for high efficiency (i.e., above >62%). An unfortunate but inevitable consequence is that the tubes are fairly unstable below saturation. This known phenomenon is due to backscattered electrons and is a common feature of high efficiency klystrons developed in the eighties. Opposite to the LEP machine, the Linac4 machine requires a very good stability of the RF output signal over the range of 0.7–1.0 of maximum saturation power. This was achievable by properly retuning the klystron cavities as well as operating the klystron about 10% above nominal (i.e., at 109 kV). However, the associated impact on the klystrons performance is important and the efficiency loss is large. The impact on the lifetime is, however, not known. In the case of Linac4, which has a fairly low duty cycle, the impact on operation is negligible. After modifications, each klystron undergoes a series of tests prior to installation in the Linac4 machine. These tests consist in measuring and verifying all klystron parameters during long reliability runs.

Retuning carried out on more than ten EEV and PHILIPS klystron was successful: 1.1 MW peak output power (@ 109 kV, 22 A), group delay 250 ns at 1.5 dB below the saturated output power, stable under all operating conditions. THOMSON klystrons however are more prone to oscillations and demonstrated somewhat lower performances. It was decided to use these tubes where less power is required (e.g., RFQ).

The new, state-of-the-art, 2.8MW klystrons

Eight power stations must be equipped with more powerful RF amplifiers. For this purpose, new 352 MHz 2.8 MW klystrons have been developed by two different companies, according to CERN specifications. The main parameters are shown in Table 3.3. As for the modified LEP klystrons, stability along the saturation curve and short 250 ns group delay are amongst the main constraints imposed by the fast RF feedback requirements. The eight new klystrons in operation have shown very good performance, contributing to an excellent RF system availability during the commissioning period.

Table 3.3: Main parameters of the new 2.8 MW klystrons.

Output power	2.8 MW
Operating frequency	352 MHz
DC to RF conversion efficiency	55 %
Operating voltage	110 kV
Maximum beam current	50 A
Gain	40 dB

3.4.2.2 Waveguide

The waveguide components used for Linac4 are of the EIA standard type WR 2300 (non-pressurized). For the surface installation (klystron hall) full-height (two-to-one aspect ratio) and for the down link and the installation in the tunnel half-height waveguides are used.

3.4.2.3 Circulators and RF loads

Due to the limited space in the klystron hall it was decided to mount pairs of circulators onto one support structure (see Fig. 3.25). Each circulator is equipped with sensors for the permanent magnet and the cooling water temperature. These values serve as input for the temperature compensation unit (TCU) implemented in a PLC reducing the effect of thermal drift. In a later stage the TCU will be used to reduce the reflection of the input and output port. Circulator and ferrite load parameters are presented in Tables 3.4 and 3.5.

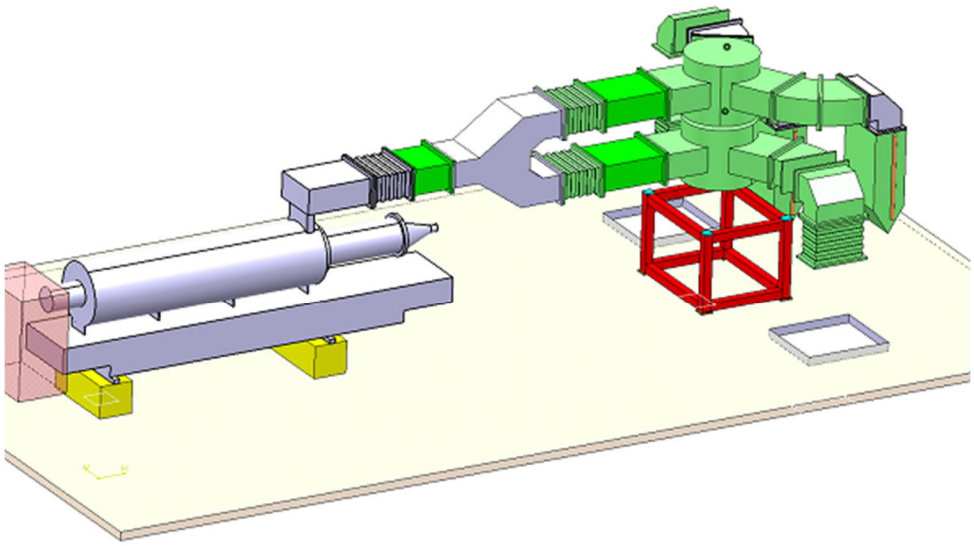

Fig. 3.25: Pairs of circulators mounted onto one support structure.

Table 3.4: Main parameters of the circulators.

Peak forward power	1.5 MW
Operating frequency	352 MHz
Average forward power	120 kW
Insertion loss	≤ 0.1 dB
Isolation	≥ 28 dB
Group delay	≤ 50 ns

Table 3.5: Main parameters of the dry ferrite loads.

Peak input power	2.8 MW
Operating frequency	352 MHz
Continuous dissipation capability	10 kW
Isolation	≥ 28dB

3.4.2.4 Phase shifters

When two cavities are fed by the same klystron the phases are adjusted by three-stub phase shifters that are able to provide up to a 60° phase shift installed in one of the two branches (Figs. 3.23 and 3.26).

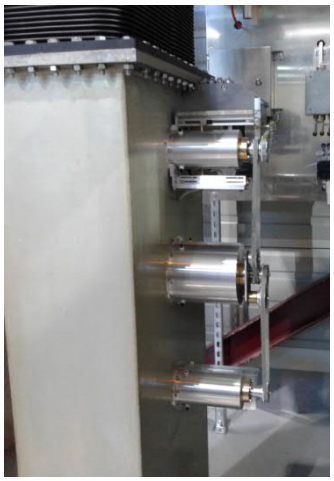

Fig. 3.26: Three-stub phase as install in Linac4.

3.4.2.5 Protection and interlocks

The circulators must be protected against high reflected cavity power that may result under certain fault conditions and would cause arcing between the ferrite plates. This is done using fast interlocks on cavity reflected power and arc detection in the waveguides, to switch off RF power within several microseconds. Short transients with reflected power peaks considerably higher than the installed power but less than a few microseconds long will however occur during injection damping. These would not result in circulator arcing and must be tolerated by the interlock system. There are also fast interlocks on klystron reflected power to act in the event of circulator malfunction. Klystrons and high-voltage equipment are protected by the slower PLC based interlock system that acts on the power converter.

3.5 Magnets

More than 220 new permanent- and electro-magnets of different types were required for the different sections of the Linac4 project. In order to limit the number of different types, magnets with the same design as well as identical electrical, mechanical and magnetic characteristics have been grouped into families. Linac4 comprises 11 of these families as listed in Table 3.6:

- The 3 MeV front end has been equipped with four low-energy correctors and two solenoids in addition to several existing quadrupole families, which have been recuperated from the former Linac2 (the recuperated magnets will not be discussed here).
- The first part of the DTL requires special attention: due to the limited available space, a low-energy corrector and a short version of a standard linac corrector (corrector type 2) have been used together with an electro-magnetic quadrupole (EMQ) in the DTL inter-tank regions. The drift tubes of the DTL are equipped with permanent magnet quadrupoles (PMQ) of different types: PMQ DTL 45-1 (4), PMQ DTL 45-2 (39), and PMQ DTL 80 (70).
- Several permanent- and electro-magnets are installed in the inter-tank regions of the CCDTL: EMQs (7), Correctors type 1 (4), and PMQ CCDTL (14).
- The inter-tank regions of the PIMS comprise 6 correctors type 1 and 12 EMQs.
- For the new transfer line L4T, 2 EMQs, 15 TL-quadrupoles, 5 TL-bending magnets, and 13 two-plane TL-correctors type 1 have been built.

Table 3.6: Linac4 sections and their magnets.

Position	Magnet type	Qty.
3 MeV front end (L4L)	Low-energy corrector	4
	Solenoid	2
DTL (L4D)	Low-energy corrector	1
	Corrector type 2	1
	EMQ	1
	PMQ DTL 45-1	4
	PMQ DTL 45-2	39
	PMQ DTL 80	70
CCDTL (L4C)	Corrector type 1	4
	EMQ	7
	PMQ CCDTL	14
PIMS (L4P)	Corrector type 1	6
	EMQ	12
Transfer line (L4T)	EMQ	2
	TL bending (horizontal)	3
	TL bending (vertical)	2
	TL quadrupole	15
	TL corrector type 1	13

3.5.1 Design and manufacturing aspects

Together with the classical requirements and constraints like the magnet aperture, the integrated magnetic field, the integrated magnet gradient and the required field quality which are defined by the beam optics, the driving parameters for the Linac4 magnet design were the mechanical boundary conditions, strictly defined by the layout of the accelerating structures and the dimensions of the new Linac4 building. The limited space available between the tanks imposed tight restrictions both on the longitudinal and the transversal dimensions of the final assembly of the inter-tank magnets, which called for a very compact and efficient design.

To benefit from power converters of the same type as already used at CERN, it was decided to operate the magnets in the accelerating sections in pulsed mode with the repetition frequency of 2 Hz. This decision minimizes the rms power consumption and allowed the building of a convection-cooled magnet without water cooling (except for the TL-bending magnets) resulting in reduced investment and operation costs for cooling, power converters, and magnets. Furthermore, an air-cooled magnet design allows a reduction in the overall magnet dimensions and helps to cope with the difficulty of limited available space. For the drift tubes of the DTL and part of the CCDTL inter-tank regions, permanent magnet quadrupoles with adjustable gradient have been chosen.

The electro-magnetic design work has been performed using the finite element program OPERA 2D or OPERA 3D/TOSCA from Vectorfields/Cobham [7]. The 2D code was used to design the pole profile and the yoke cross-section, the magnet ends were optimized with the 3D code, and all simulations used measured $B(H)$ curves representing the material intended to be used for the yoke manufacturing [8]. Complementary studies like dynamic effects, magnetic cross talk and the influence of magnetic materials on the field quality have been performed when required [9].

All magnets have been manufactured in industry according to the design and the technical specifications prepared by CERN. Intensive contract follow-up together with a stringent quality assurance at the supplier guaranteed high quality standards. After the delivery to CERN, each magnet had to pass a certification process to assure that it has been manufactured according to specification and meets the defined tolerances. The magnets are equipped with alignment target supports to permit a proper adjustment in the machine. Before installation, magnetic measurements were performed systematically to validate the magnetic design and to characterize the magnetic performance.

3.5.2 Magnetic measurements

The compliance of a magnet to its specification has been validated by specific magnetic acceptance tests. These tests were aiming at (i) validating the magnet design and manufacturing process; (ii) ensuring that the delivered units remain within the specified tolerances; (iii) running summaries and statistics to identify production trends; and (iv) characterizing the magnet performances in view of the operation in the machine.

Part of the new Linac4 magnets, especially those in the transfer lines, have conventional designs with apertures in the range of between 40 and 124 mm and can therefore be measured easily with well-established instrumentation. However, the PMQs and EMQs for the accelerating structures are characterized by a small aperture diameter between 20 and 40 mm, which makes it rather difficult to measure them precisely. While the available stretched wire system provides integral gradient measurements even inside such small bores with good accuracy, a dedicated rotating coil system was not available in order to measure all other field parameters. In the case of the EMQs, the difficulty is additionally augmented by the fast cycling rate, typically 2.4 ms which corresponds to a field ramp rate of more than 700 T/s.

For these reasons, a new measurement bench to test the series of Linac4 PMQ and EMQ magnets became indispensable. Apart from the compliance with small apertures, the following requirements, arising from beam optics, had to be fulfilled:

- determine the main magnetic field polarity;
- measure the integral field strength and direction (vs. excitation current where applicable);
- measure the field quality in terms of both integral harmonics and position of the magnetic axis;
- carry out a complete harmonic analysis for small-aperture magnets.

Specifically, for pulsed measurements it is necessary to:

- specify the field repeatability (history dependence and power supply stability);
- measure the eddy current effects;
- analyse quadrupoles with a high angular accuracy.

Furthermore, the entire system should have a polyvalent harmonic coil concept to measure permanent and pulsed quadrupoles in continuous or stepwise rotation mode, interchangeable magnet supports and optimized dipole and quadrupole-compensated harmonic coils able to measure the field quality up to the requested order. For the pulsed mode, a high-resolution positioning system is required in order to reach the same harmonic resolution within a few µrad.

The new Linac4 measurement bench [10,11], shown in Fig. 3.27, is mechanically adaptable to a large range of small-aperture magnets, including all Linac4 elements. Harmonic measurements can be done in two basic modes, the standard continuously rotating coil, optimized for quasi-static fields and the stepwise rotating coil, which may be used for fast-cycling electro-magnets. The crucial component is a dual-mode incremental/absolute angular encoder which allows precise coil positioning within 50 µrad.

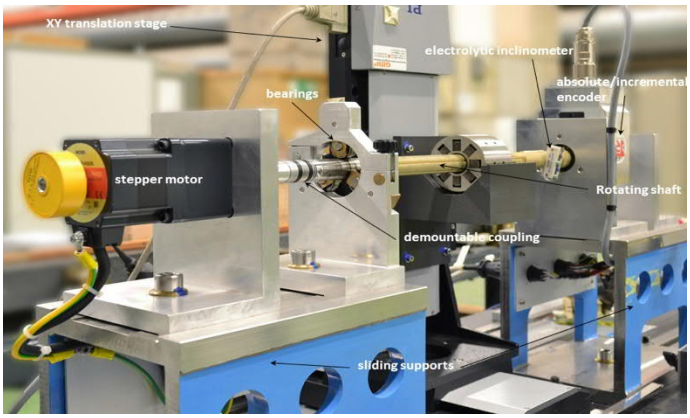

Fig. 3.27: New Linac4 magnetic measurement bench.

3.5.3 Low-energy correctors

The low-energy correctors needed for the low-energy beam transfer line (LEBT) and the chopper line are combined horizontal/vertical corrector magnets. They have an effective length of 170 mm and a mechanical aperture of 108 mm × 108 mm, providing an integrated field strength of 1.28×10^{-3} T·m. The yokes are made of 0.5 mm thick laminated electrical steel and the coils are wound from solid copper wire and are air cooled by natural convection. The magnetic measurements of the integrated field strength are in good coherence with the outcome of the 3D simulations. The transfer function shows that the iron yoke operates in the linear range far from saturation. As expected, the field quality is affected by very large allowed multi-poles due to the low aspect ratio (length to aperture).

Due to the limited space in the first DTL inter-tank region, an additional low-energy corrector is installed in this region instead of a corrector type 2.

3.5.4 Solenoids

Low energy solenoids with an aperture radius of 75 mm have been specified for the MedAustron accelerator, in collaboration with CERN. These DC-operated solenoids entirely fulfil the Linac4 requirements and feature an effective length of 303 mm and an integrated axial field $\int B_z^2 dz$ of 1.68×10^{-2} T^2m. The same design has been adopted for Linac4.

The design work included a comprehensive study on the impact of the conductor configuration onto the field homogeneity. The complete conductor geometry including layer transitions and connection leads have been modelled in OPERA 3D and several layouts have been tested in order to optimize the final design. The four water-cooled coils are mounted into a magnetic steel barrel to confine the fringe fields (see Fig. 3.28). The field quality has been intensively cross-checked using the ray-tracing feature of OPERA 3D. A dedicated simulation could provide certainty that the close-by corrector

magnet does not distort the solenoid field quality in a significant way and the magnetic coupling remains negligible.

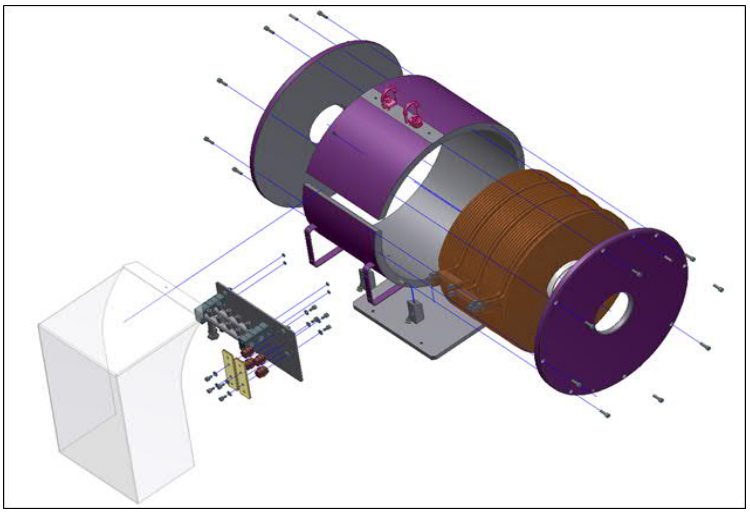

Fig. 3.28: Exploded view of the new Linac4 solenoid.

3.5.5 Electro-magnetic quadrupoles (EMQ)

A common EMQ type has been used for inter-tank sections of DTL, CCDTL, and PIMS. The quadrupoles have an aperture radius of 27 mm and provide a maximum integrated gradient of 2.4 T. They are designed to operate with a repetition rate of up to 2 Hz and a flat top length of 2 ms keeping the rms current and the power consumption low enough to allow air cooling. In addition, an air-cooled magnet design permits a reduction of the overall magnet dimensions, helping to meet the stringent geometric boundary conditions in the inter-tank regions.

The yokes are made of 0.5 mm thick laminated electrical steel glued together, cut by electro discharge machining (EDM) and pressed into a stainless-steel ring; the coils are wound from solid copper cast in resin after the final magnet assembly (see Fig. 3.29). Apart from a very compact design (overall length less than 106 mm), this layout brings the advantage to keep the mechanical tolerance on the poles and in the magnet assembly narrow and assures that the requirements on the field homogeneity are met.

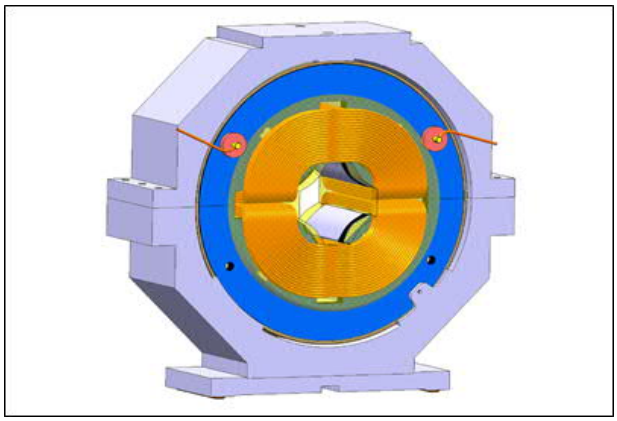

Fig. 3.29: Layout of the electro-magnetic inter-tank quadrupoles (EMQ).

The integrated field quality was fine-tuned by trimming the pole ends (chamfering) with the help of 3D simulations. The field quality was assessed through harmonic analysis on the boundary of the good field region. The multipole content b_n (for $n = 3,4,\ldots,10$) of the final design is well below the required $\pm\ 1 \times 10^{-2}$ (100 units).

Field errors due to eddy currents in the magnet and in the vacuum chamber have been computed and compared with measurements on a prototype of similar design. The time constant of the 1.5 mm thick vacuum chamber (50 μs) was found to be small compared to the time constant of the magnet itself (200 μs) and can therefore be ignored [12].

The magnetic measurements on the prototype magnet have been performed with rotating coils at 15 A (corresponding to 18% of the nominal current), which is compatible with the air-cooled coils powered for very short periods. The results have been averaged over measurements at opposite current levels in order to eliminate the offset due to remanent field. The values of the measured multipole components correspond well with the ones of the simulated components. It can be seen that the measured harmonic content is more than one order of magnitude below the tolerance of 100 units. In addition, the effect of eddy currents has been tested and a stabilization time of 1 ms was obtained. The results of the series measurement campaign, which included the measurements of integrated gradient, field direction, field homogeneity, magnetic axis, and eddy current effects, have been summarized in Ref. [13].

3.5.6 Permanent magnet quadrupoles (PMQ) type DTL 45/80

Transverse focusing in all the DTL sections is provided by PMQs, which have been chosen as the best practical way to provide the required high gradients within the small volume available inside the drift tubes of the accelerating structures. Additional advantages include simple fixed-optics operation, no heat losses in the RF-tanks and no need for cable connections towards the drift tubes. Samarium cobalt ($Sm_2 Co_{17}$) is chosen as magnetic material for its high maximum B_r of 1.2 T and the best long-term stability against neutron-induced degradation. In addition, it presents a good temperature stability with a dB_r/dT of -3×10^{-4} K^{-1} at room temperature.

In total, 109 PMQs are housed in the drift tubes of the three tanks of the DTL section. There are two types of PMQs: 39 short PMQs (45 mm) in Tank 1, which have been produced by Aster Enterprises Inc. Acton, MA, US and 70 long PMQs (80 mm) for Tank 2 and Tank 3, manufactured by Elytt Energy, Madrid, Spain. In addition to the 109 drift tube PMQs, 4 short units have been produced by CERN to be installed in the DTL inter-tank regions.

The final design of the PMQ is based on a modified Halbach array. The PMQs must be tuned in focusing/defocusing pairs to the same integrated gradient, generally decreasing along the linac as the energy increases. The field is generated by either 16 permanent magnet in case of the PMQ DTL 45-2 or eight permanent blocks in case of the PMQ DTL 45-1 and the PMQ DTL 80, all magnetized to the same remnant magnetization B_r along the appropriate direction, housed in slots cut at different radial positions to adjust coarsely the gradient. The gradient can be fine-tuned over a 0.5% range by adding up to 25 μm of stainless steel shims at the inboard. The housing for the samarium cobalt blocks is made of a special grade of austenitic steel 316LN with very low magnetic permeability ($\mu_r \leq 1.003$) as needed for the fields of the blocks to superpose linearly. Stainless steel also matches well copper of the drift tubes in terms of thermal expansion and galvanic potential, and its low thermal conductivity protects the magnets against accidental overheating during welding.

The measurement method developed for the PMQs makes combined use of two instruments, a) a single stretched wire system and b) a rotating coil system based on a 200 mm long and 19 mm in diameter quadrupole-compensated coil array [14,15].

3.5.7 PMQs CCDTL type

The beam focusing in the CCDTL is provided by 14 permanent quadrupoles, all with a different but fixed gradient and by 7 EMQs to keep a certain amount of flexibility for beam tuning.

The final design [16] is an iron free PMQ based on a Halbach array with an aperture diameter of 45 mm. Each magnet yoke is made of a single piece of non-magnetic austenitic steel 316LN. The precisely machined yoke acts as an accurate frame to maintain the 8 samarium cobalt permanent magnet

blocks in their position. The exact radial position of the blocks is set with non-magnetic shims inserted between the austenitic steel yoke and the permanent magnet blocks. A radial displacement of 6 mm permits to adjust the integrated gradient from 1.1 to 1.6 T. The impact of magnetization and manufacturing errors on the field quality has been calculated with 3D finite-element models in order to define exactly the magnetic and mechanical tolerances on the permanent magnet blocks and the yoke. The maximum allowed deviation of easy axis orientation has been set to 2º, the remanence and coercivity variation in the whole production had to remain within 2% and the mechanical positioning error of the 8 magnet blocks was limited to 0.04 mm.

3.5.8 Corrector magnets

Several types of combined horizontal/vertical correctors with different mechanical apertures and field strengths were needed for the inter-tank regions and the new transfer line. In order to reduce the costs and the number of spare magnets, a common window-frame design with a free aperture of 100×100 mm^2 is used for all subsystems. The distance between the tanks has limited the maximum overall length of the corrector magnets to 120 mm (Type 1) respectively 80 mm (Type 2). The correctors can provide a maximum integrated field strength of 4.8×10^{-3} T·m, respectively 3.8×10^{-3} T·m at the nominal current of 10 A. Like the quadrupoles, these magnets are operated in pulsed mode with the repetition frequency of 2 Hz.

The mechanical layout is similar to the low-energy correctors: the yokes are made of 0.5 mm thick laminated electrical steel and the coils are wound from solid copper wire and are air cooled by natural convection.

3.5.9 Transfer line quadrupoles

While the first part of the new transfer line will make use of two linac-type quadrupoles, the remaining part involves quadrupoles with larger aperture. A series of 15 quadrupoles with an aperture radius of 50 mm providing an integrated gradient of 1.8 T have been built. Contrary to the accelerating section, there are no geometrical constraint in the transfer line, but a compact design has been proposed in order to reduce manufacturing costs and to improve the field quality. The propose design is a classical four-quadrant quadrupole with hyperbolic pole profile. The magnets are operated in pulsed mode at 1.1 Hz to reduce power consumption and avoid water cooling. The magnet yokes are laminated using low carbon steel sheets of 0.5 mm thickness glued together. The coils have been made of solid enamelled copper wire.

The selection of commercially available pulsed power converters restricted the choice of some electrical characteristics (i.e. the pulse rise time and the maximum current) and set further constraints for the magnet and coil design. One of the main challenges in the design was to match the magnet inductance and resistance to an existing power converter design. Since neither the aperture nor the effective length could be reduced significantly, the beam optics had to be modified instead to lower the field gradient. In parallel it was necessary to increase the stored energy delivered by the capacitor-discharge power converter to converge to a satisfactory solution [17].

The fact that the TL quadrupoles are fast cycled makes accurate magnetic measurements challenging. Rotating and fixed search coils had to be used in a complementary way to derive information on different aspects of the magnetic behaviour of these quadrupoles, such as the impact of hysteresis and dynamic eddy current effects. The series measurement campaign included the measurements of the integrated field gradient and direction, harmonic components and the offset of the magnetic axis. All the quadrupoles have been accepted and only three out of 21 required an adjustment of the transversal axis offset. The impact of eddy currents on the integrated field has been measured to be negligible.

3.5.10 Transfer line bending magnets

The horizontal 70 turn right after the linac will be achieved by three bending magnets connected in series, each deflecting the beam by 23.3º. Since Linac4 and the PS booster are not on the same level two vertical bending magnets are needed, providing a beam deflection of 14.5º each. For economic reasons it was decided to aim for a common design. To avoid Lorentz stripping on the H^- beam, the maximum field strength is limited to 0.9 T. The pulsed magnets provide a maximum integrated field strength of 0.78 T·m in an aperture gap of 60 mm at a repetition frequency of 1.1 Hz. Since the beam will travel through the transfer line with a constant energy, the required field homogeneity of $\pm 5 \times 10^{-4}$ has to be achieved only for two given field levels of 0.89 and 0.55 T, respectively.

The straight H-type magnets are made of two identical laminated half-yokes. To reinforce the laminated structure, non-magnetic austenitic steel end plates have been mounted on each end of the yoke. To improve the field homogeneity and to reduce saturation effects on the pole edges, longitudinal shims have been added to the pole profile of the 1-mm thick laminations. The two race-track coils are wound from hollow copper conductor and will be water-cooled. Magnetic measurements have been performed on each magnet to validate the transfer function, the field direction, the field homogeneity and the dynamic behaviour.

3.6 Power converters

The general parameters used to dimension the Linac4 pulsed power converters are given in Table 3.7. A maximum pulse length of 1.2 ms has been specified to make possible a future operation of Linac4 as injector to a low power superconducting proton linac (LP-SPL).

Table 3.7: Main parameters of power converters and klystron modulators.

Beam pulse length	1.2 ms[a]
Pulse repetition rate	2 Hz
Cooling	Natural air[b]
Remote controller	FGC3

[a]Does not apply to the 3-MeV front-end converters for which the flat top is limited to 600 μs.

[b]Except the power converters for the bending magnets of the new transfer line to booster, which are water-cooled.

The requirements in power converters and klystron modulators for each of the three main sections of Linac4 are summarized in Table 3.8. In total, including the new converters installed in the existing LT and LTB lines, 148 power converters, and 14 klystron modulators were built and installed.

Table 3.8: Summary of converter/modulator types and quantities[a] per sector.

3-MeV Front End power converters *(re-used from 3-MeV Test Stand)*		**Linac4 machine power converters**		**Transfer Lines to PSB (L4T + LT, LTB,LBE)**	
Type	***Qty***	***Type***	***Qty***	***Type***	***Qty***
- Pulsed HV, for H^- source	4				
- Klystron modulator for RFQ	1	- Klystron modulators	13	- Cycled, for bending magnets	2 + 3[b]
- Pulsed, for quadrupole magnets	11	- Pulsed, for quadrupole magnets	20	- Pulsed, for quadrupole magnets	17+14[b]
- DC for steering magnets and solenoids	10	- Pulsed, for steering magnets	24	- Pulsed, for steering magnets	26+14[b]

[a]Quantities indicated are without spares.

[b]Quantities indicated are the L4T line, followed by the LT, LTB, LBE lines.

3.6.1 Klystron modulators

Some of the remaining LEP klystrons are reused for LINAC4, each of which has a electrical power rating of 2 MW. Additionally, new klystrons designed for pulsed operation with nominal electrical power around 5 MW are used.

There are three possible configurations to feed these klystrons (see Fig. 3.30):

1. ***Single for LEP klystrons***: one modulator feeds one LEP klystron. One filament heater power converter and one 'anode mode' power supply system are required;
2. ***Double for LEP klystrons***: one modulator feeds two LEP klystrons in parallel. Each klystron will have its own filament heater power converter and 'anode mode' power supply system;
3. ***Single for "new" klystrons***: one modulator feeds one 'new' type klystron. One filament power converter will be required. No 'anode mode' power supply system is required since this terminal is not present in the klystron.

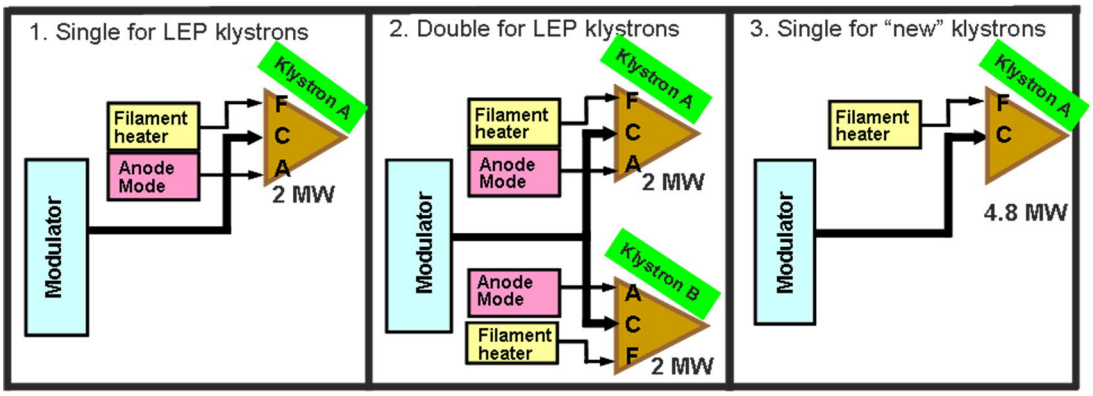

Fig. 3.30: The three possible klystron supply configurations.

In order to improve spare parts availability and facilitate maintenance, only one type of modulator has been developed. Its rated peak electrical power is 5.5 MW. It has two high voltage output connections, allowing to feed two LEP klystrons in parallel. In case a single klystron will be supplied (configurations 1 and 3) the second HV output connection can be safely deactivated (HV cap system inserted). The filament heater power converter and 'anode mode' power supply systems are all identical and independent of the other sub-systems. They may be inserted or not, depending on whether they are required or not by each configuration (see Fig. 3.30).

The main parameters of the klystron modulators and auxiliary supply systems are given in Table 3.9.

The LINAC4 strategy is to gradually replace the LEP klystrons with new 2.8 MW RF power klystrons (5.5 MW electrical power). Thus, eventually the anode mode control and parallel klystron operation will not be required.

Table 3.9: Parameters of the klystron modulators and auxiliary supply systems.

Cathodes power supply (modulator)	
Pulse width:	1.8 ms
Flat-top duration:	1.5 ms
Precision at flat top:	1%
HF ripple at flat top:	< 0.1%
Repetition rate:	2 Hz
Nominal voltage:	110kV
Nominal current:	2 × 25 A
Rise/fall times:	~300 µs
Cooling:	Air (natural or forced)
Maximum energy in case of arc:	< 20 J
Anode mode polarization power supplies	
Stability at flat-top:	1%
HF ripple at flat-top:	< 0.1%
Nominal voltage anode to cathode :	60 kV
Nominal current:	5 mA
Filament heater power supplies	
Stability and ripple:	< 1%
Nominal voltage:	30 V
Nominal current:	30 A
Floating withstand voltage to ground:	180 kVdc for 1 min

The simplified schematic of the modulators and the connection circuit to the klystrons oil tank (LEP type) is shown in Fig. 3.31. One AC electrical departure is required per modulator (400 V, 3-ph, 50 Hz, 50 A). Figure 3.32 shows a modulator unit.

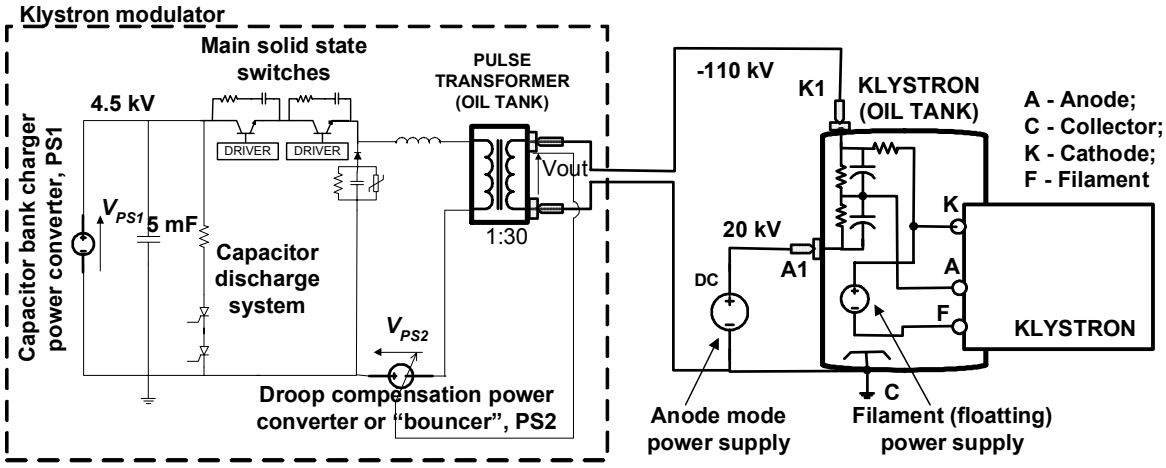

Fig. 3.31: Electrical schematic of the klystron modulators. Interconnection with a LEP klystron oil tank.

Fig. 3.32: Photo of a Modulator power converter for pulsed RF klystrons.

3.6.2 Power converters for the steering magnets

3.6.2.1 Pulsed steerers of the transfer line

The power converters for the pulsed steering magnets required a new development based on the existing Minidiscap design developed in the late 1990s. Some updates were implemented to harmonize components with other power converters and to implement an electronics control with the FGC3 control electronics.

The main magnet electrical parameters for operation are given in Table 3.10.

Table 3.10: Specification parameters for the pulsed corrector magnet power converters.

Parameter	Type 1	Type 2
Peak current	10 A	
Operating mode	Pulsed	
Flat-top length	2 ms	
Maximum repetition frequency	2 Hz	
Load inductance	6.55 mH	5.25 mH
Load resistance (without cables)	240 mΩ	160 mΩ
Precision (uncertainty)	1000 (1×10^{-3}) of nominal	
Mechanical dimensions	One rack per six converters	

The mechanical size of the converters is 19" width by 3U height. Up to six independent converters can be installed into a standard 19" rack. Only one AC electrical departure is needed per rack (400 V, 3-ph, 50 Hz, 16 A). A power distribution system is implemented internal to the rack.

3.6.2.2 Pulsed steerers of the LT and LTB transfer line

In total 12 power converters need to be replaced to ensure all correctors in these transfer lines are using the same power and controls technology. The Mididiscap capacitor discharge power converter is used for all other steerers in this area and would be the most appropriate technical solution. See Table 3.11 for the specification parameters.

Table 3.11: Specification parameters for the consolidation of the LT line Steerer (DHZ and DVT [40, 50]) and LTB line Steerer (DHZ and DVT [10, 20, 30, 40]) power converters.

Parameter	Value
Peak current	35 A
Operating mode	Pulsed
Flat-top length	2 ms max
Maximum repetition frequency	2 Hz
Load inductance	42 mH
Load resistance (without cables)	1500 mΩ
Precision (uncertainty)	1000 (1×10^{-3}) of nominal
Mechanical dimensions	One rack per six converters

3.6.2.3 Pulsed steerers of the LBE line

Two pulsed steerers are required. These are the same as the steerers in the L4T transfer line (also summarized in Table 3.12). As such two Mididiscap pulsed power converters will be used to power the circuit.

Table 3.12: Specification parameters for the LBE line Steerer power converters.

Parameter	Value
Peak current	14.5 A
Operating mode	Pulsed
Flat-top length	2 ms max
Maximum repetition frequency	2 Hz
Load inductance	6.5 mH
Load resistance (without cables)	240 mΩ
Precision (uncertainty)	1000 (1×10^{-3}) of nominal
Mechanical dimensions	One rack per six converters

3.6.2.4 DC steerers for LEBT and chopper line

The main magnet electrical parameters for operation are given in Tables 3.13 and 3.14. The power converters are commercial off-the-shelf systems, with the addition of a CERN designed polarity switch to delivery bipolar current and voltage (2Q), and controlled using CERN FGC3 electronics.

Table 3.13: Specification parameters for the DC corrector magnet power converters.

Parameter	DC steerer
Peak current	10 A
Operating mode	DC
Load inductance	7.6 mH
Load resistance (without cables)	177 mΩ
Precision (uncertainty)	1000 (1×10^{-3}) of nominal
Mechanical dimensions	One rack per four converters

Table 3.14: Parameters of the power converters for DC steering magnets.

Output peak voltage	+/- 70V
Output peak current	+/- 20A

3.6.3 Power converters for DC solenoids (LEBT)

The DC solenoid magnet parameters of the LEBT are summarized in Table 3.15. The power converters are commercial off-the-shelf systems, delivering unipolar current and voltage (1Q), and controlled using CERN FGC3 electronics.

Table 3.15: Specification parameters for the DC solenoid magnet power converters.

Parameter	DC solenoid
Peak current	200 A
Operating mode	DC
Load inductance	56 mH
Load resistance (without cables)	215 mΩ
Precision (uncertainty)	1000 (1×10^{-3}) of nominal
Mechanical dimensions	One rack per converter

3.6.4 Power converters for the pulsed quadrupole magnets

The power converters for the pulsed quadrupole magnets require a new development based on the existing Maxidiscap design which was developed in the late 1990s (of which many units have been installed Linac2, Linac3, LEIR, and 3 MeV test stand). The new design will in particular implement an electronics control with the FGC3 control electronics, and make some modifications to cope with the moderately high pulsed magnet inductance.

3.6.4.1 Pulsed quadrupoles of linac and transfer line

The main magnet electrical parameters for operation are given in Tables 3.16 and 3.17.

Table 3.16: Specification parameters for the quadrupole magnet power converters.

Parameter	Value	Value
Peak current	90 A	120 A
Operating mode	Pulsed	Pulsed
Flat-top length	2 ms	2 ms
Maximum repetition frequency	2 Hz	2 Hz
Load inductance	16.1 mH	26 mH
Load resistance (without cables)	549 mΩ	279 mΩ

Precision (uncertainty)	1000 (1×10^{-3}) of nominal
Mechanical dimensions	One rack per six converters

Table 3.17: Parameters of the power converters for pulsed quadrupole magnets.

Output peak voltage	± 1 kV
Output current	+ 300 A

Four quadrupole circuits permit bipolar currents for beam measurements. As the pulsed quadrupole power converters are unipolar, the bipolar operation could be achieved with the addition of polarity inversion units at their output.

Each converter is formed by one power crate with mechanical size of 19" width by 6U height and by one control crate with mechanical size of 19" width by 3U height. Up to three independent converters can be installed into a standard 19" rack. Only one AC electrical departure is needed per rack (400 V, 3-ph, 50 Hz, 16 A). A power distribution system, internal to the rack, is implemented by TE/EPC with a distribution of one converter, maximum, per phase.

Three of the quadrupoles circuits are connected to the beam interlock system (BIS) to prevent excessive beam loss at injection to the PS booster.

3.6.4.2 Power converters for the bending magnets

The power converters for the bending magnets of the transfer line are based on the design for the PS auxiliary magnets, but updated for the FGC3 electronics control platform. They belong to the power converter family, termed APOLO. The APOLO converters are all continuously current regulated and able to follow an arbitrary current function. The converters can supply up to 900 V peak voltage, and up to 900 A peak current, depending on the configuration. For this application, the reference function will be of trapezoidal shape, with a slow rise time and maximum flat-top time to minimize magnet eddy currents while complying with the maximum rms current available from the power converter. The main electrical parameters of operation are given in Tables 3.18 and 3.19.

Table 3.18: Specification parameters for the bending magnet power converters.

Parameter	L4T.RBH	L4T.RBV	LT.BHZ20	LT.BHZ30	LTB.BHZ40
Peak current	612 A[a]	372 A	590 A[b]	487 A[b]	174 A
Load inductance	96.9 mH	64.6 mH	95 mH	95 mH	70 mH
Load resistance (without cables)	549 mΩ	279 mΩ	62 mΩ	62 mΩ	43 mΩ
Operating mode	Cycled				
Flat-top length	150 ms				
Maximum repetition frequency	1.11 Hz				
Precision (uncertainty)	100 (1×10^{-4}) of nominal				
Mechanical dimensions, (w × d × h)	1800 × 900 × 2300 mm^3				1200 × 900 × 2300 mm^3

[a] The design current of this magnet was 590 A at nominal bending strength, however the measured current of the constructed magnet is higher.

[b]The originally estimated peak current for the bending magnet circuits did not account for heavy saturation. Following beam commissioning the actual setpoint was found to be –620 A for the LT.BHZ20 and LT.BHZ30 magnets.

Table 3.19: Parameters table of the power converters for bending magnets of new TL.

Output voltage	± 450 V
Output current	± 900 A
Pulse repetition rate	1.11 Hz
Flat-top duration	150 ms
Ramp-up time	250 ms
Ramp-down time	170 ms
Rms output current	< 400 A
Flat-top precision	~100 ppm

Each converter is housed in a special cabinet with dimensions 1800 mm (width) × 900 mm (depth) × 2300 mm (height). One AC electrical departure is needed per rack (400 V, 3-ph, 50 Hz, 250 A).

3.6.5 H-source power converters

A pulsed HV system was developed for the H^- ion source, to mitigate initial problems due to destructive arc breakdowns with its original DC power converters. The design is based on similar transformer technology as used for the klystron modulators, and similar power electronics technology as used for the Maxidiscap (termed H-Discap). The transformer is however a special design to allow bipolar operation (to allow protons to be accelerated if required). An important difference is the operation as a voltage source, and not as a current source as required by the pulsed magnetic circuits.

Three different pulse transformers are required to generate 10 kV, 25 kV, and 50 SkV respectively. These are all powered from a common 700 V pulsed power source based on the Maxidiscap module design. The power converter modules are installed on the surface, and the HV transformers integrated into the source Faraday cage. This is mandatory for generating high voltage distances and minimizes the distance where HV isolation is required.

In addition to the pulsed HV systems, a DC 35 kV system is required to polarize the source einzel lens. This system required a low current, high voltage system, with adequate capacitor decoupling close to the lens to compensate for the beam induced perturbations. Adequate safety precautions are also implemented to ensure the capacitor energy is discharged when entering the Faraday cage. Both the pulsed and DC HV systems require a dedicated control electronics, developed using FGC3 electronics.

The electrode configuration and voltages of the ion source is shown in Fig. 3.33. The general pulsed HV configuration is presented in Fig. 3.34.

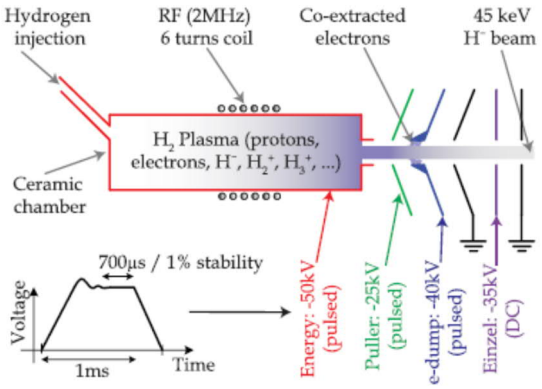

Fig. 3.33: H-source simplified cross-section.

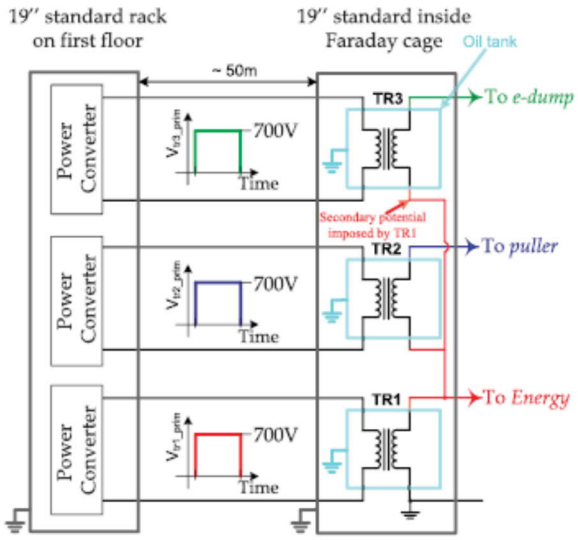

Fig. 3.34: General H-source pulsed HV converter configuration.

3.7 Vacuum system

3.7.1 Overview

The vacuum system of Linac4 has an overall length of about 152 m, divided into 11 vacuum sectors as depicted in Fig. 3.35. The required residual-gas pressure is less than 10^{-5} mbar until the LEBT, less than 5×10^{-7} mbar in the RFQ, and less than 10^{-7} mbar for the rest of the linac. The pressure thresholds are defined so that electrical breakdown is avoided and beam losses are minimized.

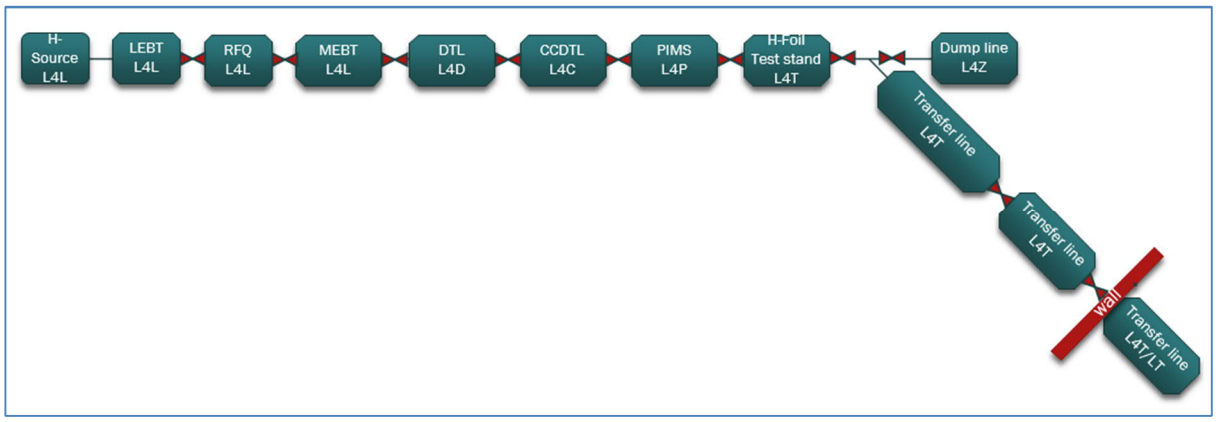

Fig. 3.35: Vacuum sectorization of Linac4.

3.7.2 Description of vacuum system

The 11 vacuum sectors (Table 3.20) are separated from each other by electro-pneumatic gate valves. Each sector can be pumped down to 10^{-6} mbar separately by turbomolecular pumping (TMP) groups. Lower pressures are attained by sputter ion pumps (SIP) and non-evaporable getter (NEG) pumps. Backing pumps are needed for the TMP: dry scroll pumps are used on the Source and RFQ vacuum sectors to eliminate any risk of hydrocarbon contamination while rotary vane oil-sealed pumps are installed in the TMP groups of the downstream sectors.

The first vacuum sector (source and LEBT) requires the permanent action of TMP groups due to a high hydrogen gas load from the source and gas injection in the LEBT. Due to the high hydrogen gas flow from the preceding sector, the RFQ requires high pumping speed. It is obtained by TMP, SIP and NEG pumps. The DTL is pumped by SIP and NEG pumps due to the heavy gas load from the permanent quadrupole magnets inside the vessels.

All subsequent sectors, except the L4Z line, have one fixed TMP group per sector used only during rough vacuum pumping down to 10^{-6} mbar; then, the pumping is ensured by SIP. In case of venting during the operation period, an addition mobile turbomolecular groups is temporary installed to accelerate the pump down process.

In total of 46 SIP, 14 TMP groups, and 7 NEG pumps are installed in the Linac4 and transfer line. The pressure in each sector is monitored by Pirani–Penning cold cathode gauges. ISO-CF flanges made of 316LN austenitic stainless steel with standard CF flat copper seals are the typical flange connection in Linac4. C-spring loaded metallic seals are used in locations when the standard ISO-CF does not offer the required dimension, or where strict tolerances on the total length of the RF cavities are important. The C-spring loaded seals are used with different surface liner (Al, Cu, and indium) depending on the application. Traditional indium sealing was not foreseen in the baseline design, but used in places where Al and Cu liners did not allow for a correct vacuum sealing.

All vacuum chambers installed inside magnets are made of 316LN. The drift chambers are made of 304L or 316L to CERN material specification. All bellows compensator ends are in 316LN. The thin undulated part of the bellows always has a bigger inner diameter than the beam tubes to avoid beam scraping, and the consequent energy deposition and vacuum leak generation.

Table 3.20: Overview of vacuum equipment installed in the Linac4 tunnel.

Vacuum sector	**L4L10**	**L4L20**	**L4L30**	**L4D40**	**L4C50**	**L4P60**	**L4T70/80/100**	**L4Z90**
	Source	**RFQ**	**MEBT**	**DTL**	**CCDTL**	**PIMS**	**Lines**	**Dump**
Length [m]	1.79	3.23	3.73	19.05	25	22.87	80.56	2.12
Sector valves	1	1	1	1	1	1	4	–
TMP groups	3/1	4	1	1	1	1	4	–
SIP pumps	–	5	2	5	14	12	1/4/2	1
NEG pumps	–	4	3	–	–	–	–	–
Gauges	3/1	3	3	3	4	4	1/2/1	1

3.7.3 Pumping system

The TMP groups (Fig. 3.36) are in general used only for rough pumping from atmospheric pressure to 10^{-6} mbar, but they can also be started remotely in case extra pumping speed is required for unforeseen gas loads for a short period.

The NEG pumps are installed directly on the RFQ cavity and on the wave guide pumping ports of the DTL. NEG pumps are passive devices, which need to be reactivated by heating at 450 °C for about 1 h, approximately twice a year, to recover full pumping capacity and release part of the dissolved hydrogen. The NEG pumps installed in Linac4 have a nominal pumping speed of 2000 l/s for H2 and 373 l/s for H2O; the effective pumping speed for H2 is about 1000 l/s due to a reduction of aperture at the cavity pumping port. The maximum quantity of hydrogen that can be absorbed between two regenerations is defined by the embrittlement limit, i.e., about 20 mbar l g^{-1}.

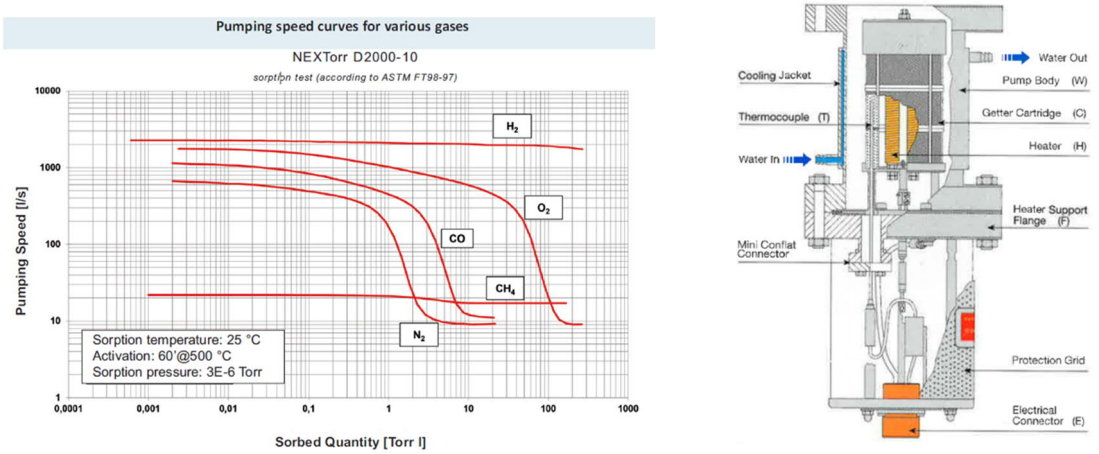

Fig. 3.36: Pumping speed for a SAES Getters D2000 NEG pump and sketch of pumping unit.

The pumping speed of the SIP (Fig. 3.37) depends on the gas pressure at the inlet of the pump, the nature of the gas, and the quantity of gas already pumped. The StarCell elements used inside the SIP are made of Ti. When the concentration of H_2 in the cathodes is higher than the solubility limit in Ti, hydride solid-state precipitation is formed. Consequently, the cathodes expand and become brittle generating anomalous field emission and short circuit. A typical hydrogen concentration limit is 10^4 mbar for commercial 500 s^{-1} SIP. The vacuum pumping system on the RFQ has to pump a high gas load of H_2. The three types of pump (TMP, SIP, and NEG) are placed in a way to reduce the risk of hydrogen embrittlement while optimizing the pressure profile as defined by simulations.

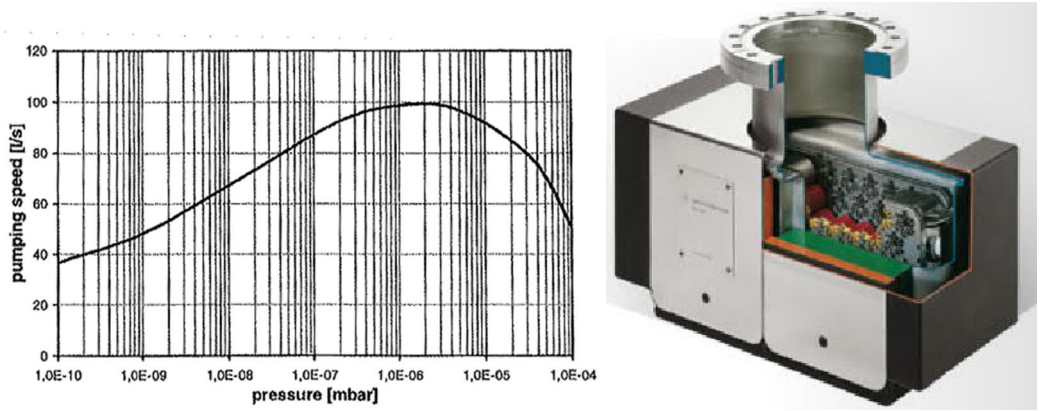

Fig. 3.37: Pumping speed for a AGILENT 100l/s STARCELL SIP and a pumping unit.

TMP pumps, primary pumps and NEG pumps are powered at low voltage (230 V) while SIP are powered at high voltage (6 kV). Pirani gauges are also operated at low voltage (230 V) and Penning gauges are operated at high voltage (3 kV).

All vacuum sectors are connected to a nitrogen venting line. The N_2 buffer battery of 120 m^3, initially at 200 bars, is located outside the Linac4 building. The distribution line in the tunnel has a working pressure of 5–10 bar. Each sector valve and TMP group are connected to the compressed air system in the tunnel with pressure buffer vessel and non-return valves between the valve and the air line. The non-return valve is to ensure all valves can be closed even if there is a problem on the main compressed air system in the building.

3.7.4 Controls

The vacuum control is provided for the vacuum equipment of Linac4 with the scope of ensuring a reliable and safe operation, and providing user alarms where needed. All interlocks are hard wired between the control equipment in the equipment room. Supervision is ensured by SCADA, an industrial controls software. One PLC master manages the whole machine, with Profibus as a field bus for real-time distributed controls. SIP, fixed TMP groups, gauges, and valves are connected to individual or grouped controllers, located in the racks of the equipment floor, themselves communicating with the PLC via the field bus. Start up of the SIP is directly interlocked to the gauge controller of the Penning gauges on the same sector. The vacuum controls layout is shown in Fig. 3.38.

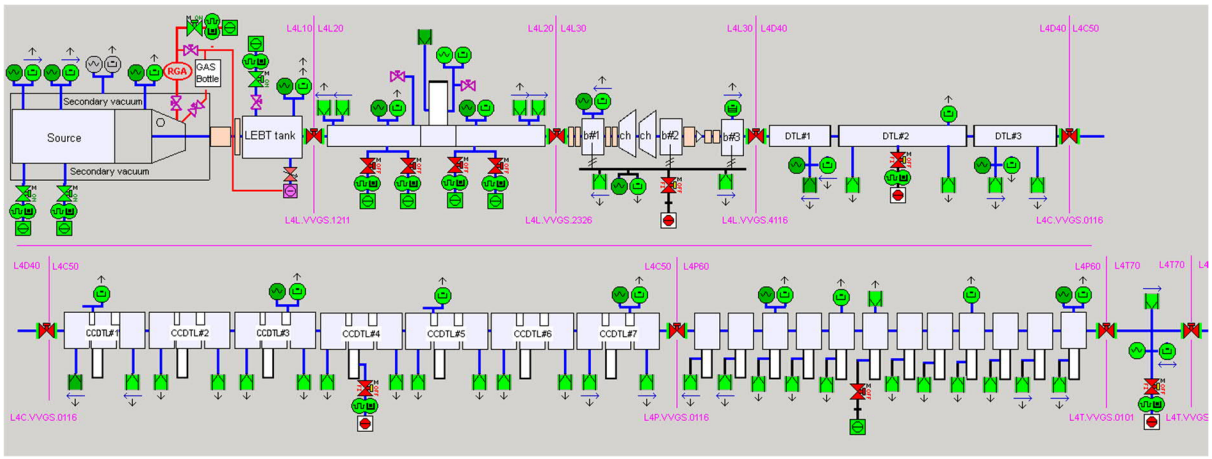

Fig. 3.38: Vacuum controls layout for Linac4 accelerating part.

Sector valves are closed upon a pressure increase in either of the two vacuum sectors they are delimiting. Pressure interlock is provided by the simultaneous increase of the current on several SIP of the sector.

3.8 Controls

The control system architecture for Linac4 is based on that used for the LHC and its injector chain. Figure 3.39 shows the different blocks involved to service all controls requirements. A given application will only use a subset of these services.

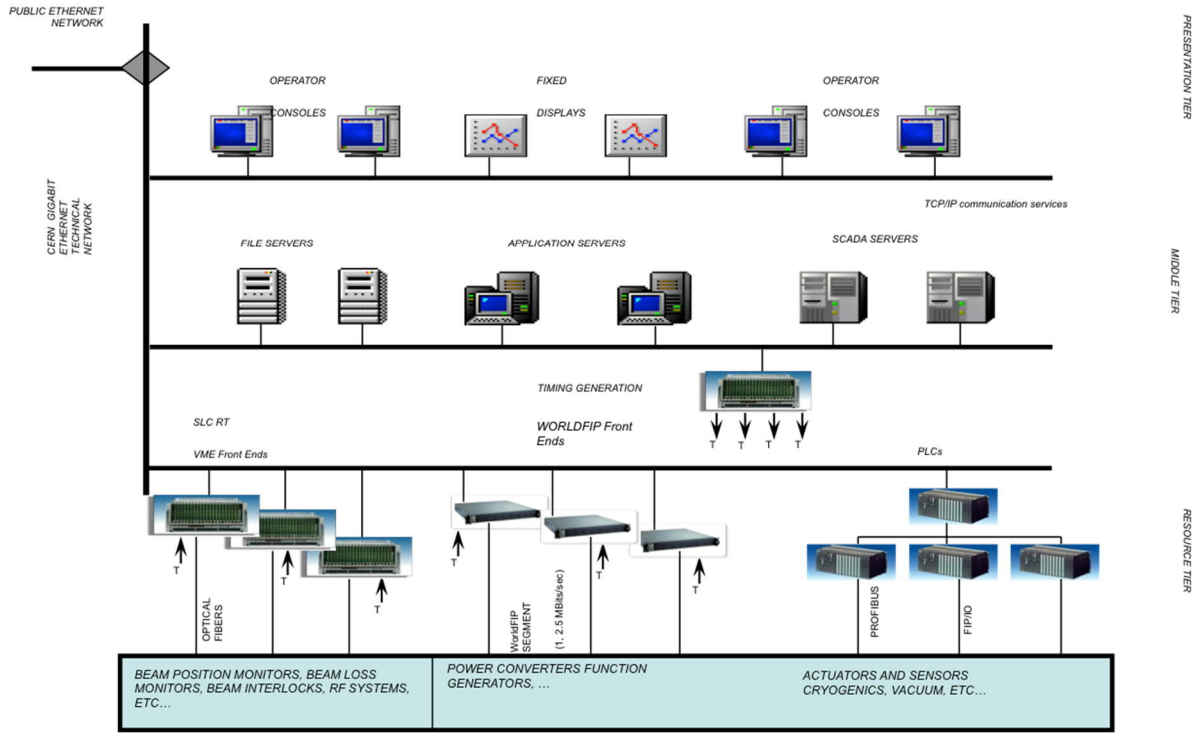

Fig. 3.39: Overall control system architecture for Linac4.

Graphical application programs run on operator consoles (Linux or Windows PCs) on what is called the presentation tier. Typically, applications based on the injector controls architecture (InCA [18]), a classic 3-tier model, send control values and receive status information to/from the front-end computers sitting in the resource tier, such as the WorkingSet and Knobs used daily. InCA also provides services such as access to databases, data logging for off-line analysis and arbitration for competing requests to access hardware.

Another example of a three-tier system is the open analog signals information system (OASIS [19]), which lets users view analog signals from front ends in virtual oscilloscope screens on an operator console. The signals can be very distant geographically, but OASIS handles network communication and trigger synchronization all over CERN to give the user the illusion of having local access to hundreds of signals.

Front-end computers can be programmable logic controllers (PLCs), PCs, or VME MEN A20 (Intel) processors running Scientific Linux CERN (SLC). Front ends typically use CERN's front-end software architecture (FESA [20]) framework, which provides a set of basic functionalities such as persistence of data, synchronization with the timing system, communication with the upper layers using controls middleware (CMW [21]), and a rapid application development environment for real-time tasks. Front-end computers also act as gateways between the ethernet-based technical network and field buses such as MIL1553, Worldfip, and Profibus.

Databases using Oracle technology are extensively used to document hardware and software installed in the front ends and to automatically generate generic software from this information. Other uses of databases in the control system include asset management, physical layout descriptions, logging for off-line analysis, and persistence for settings management.

CERN's general machine timing (GMT [22]) system is used for the coordination in time among different pieces of equipment (in the same or different accelerators), as well as for real-time tasks synchronization. This system consists of a master module (per accelerator) driving an RS-485 multi-drop network with messages signalling different events. At the receiving side, electronic modules in VME, PCI, and PMC formats can be installed in front-end computers and programmed to react to a

given event by producing either a TTL pulse (for hardware synchronization) or an interrupt to the front-end processor (for real-time software tasks). The GMT master's clock is driven by a rubidium-based GPS receiver and all the events generated on the timing cable are UTC-related. To synchronize with the beam, there are external clock inputs in the timing receiver cards. All pulses output by these cards are UTC time tagged with a precision of around 25 ns, a very useful feature for diagnostics.

3.9 Machine protection

3.9.1 The beam interlock system

The beam interlock system (BIS) was originally conceived and designed for the LHC, providing a fast, reliable, and dependable mechanism for safe operation of the accelerator. It is since many years deployed at the LHC (ring and injection), the SPS and the SPS-LHC transfer. It is now also deployed in Linac4, in the Linac4 transfer line and in the PS booster. The interlocking of the two accelerators has been considered together. Therefore, the BIS architecture takes into account that the PS booster is the (timing) master of Linac4 and that several destinations are possible for the beam: Linac4 DUMP, LBE line, and PSB.

In all instances, the same hardware solution (Fig. 3.40) is used with a central element called the *beam interlock controller (BIC)* and distant elements called the *beam interlock user interfaces (CIBU)*. The *BIC* and *CIBU* functionalities are realized by a set of CERN-made hardware boards.

The functionality of the BIC is to:

- Gather USER_PERMIT signals coming from the *CIBU* units installed in the rack of the *user systems*. The latter is the name given to any equipment interconnected to the BIS with the purpose of interlocking the beam operation.
- Perform an AND function of the received signals. According to the chosen BIS architecture, this result is produced either by one BIC or by several ones.
- The outcome, named BEAM_PERMIT flags, are transmitted to the so-called *actuator* system (like a kicker system to deviate the beam or an RF source to stop beam production).

A BIC has 14 hardware inputs together with one additional channel dedicated to the calculated output of a software process, commonly named software interlock system (SIS). A BIC is embedded in a VME based frond end computer. The latter is connected to the technical network and runs the Linux real-time operating system. Thanks to specific device drivers, and dedicated CERN software framework (FESA) class, the whole system can be remotely tested and monitored. The BICs are connected either in a ring architecture for circulating machines (like LHC and SPS) or in a tree architecture for the other cases (Linac4, SPS extraction…).

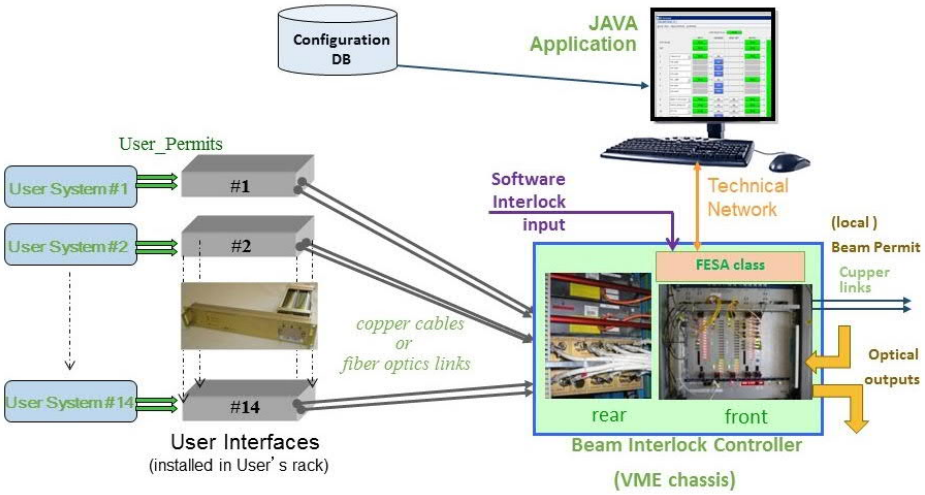

Fig. 3.40: Simplified layout of the beam interlock system.

To meet the stringent SIL 3[b] requirements of the BIS, derived from the requirement that CERN's accelerator complex is suitably protected against beam related damage, the beam interlock system is completely redundant. This redundancy is performed using two separate channels (named 'A' and 'B') from any of its inputs (USER_PERMIT signals) through to its output (BEAM_PERMIT flags).

Five controllers have been deployed for LINAC4 and its transfer line to the booster (Fig. 3.41), named 'RF Source', 'Choppers', 'Linac4', 'L4Z', and 'L4 Transfer'.

A tree architecture is used and only two out of the 5 BICs are connected to *actuators*:

- 'RF Source' BIC connected to both RF system of the H-source and the pre-chopper system.
- 'Choppers' BIC connected to both pre-chopper system and chopper system.

The redundant BEAM_PERMIT flags produced by a *BIC* are transmitted via copper cables as binary differential signals in using the RS-485 standard.

Around 30 CIBU units are deployed and connected the BIS to the user systems. They produce the different interlocking conditions provided by the following Linac4 systems: beam stoppers, power converters, vacuum, L4 source, L4 dump, RF, operator buttons, pre-chopper, chopper, WIC, beam instrumentation, beam loss monitors, and timing system.

The redundant USER_PERMIT signals are generated by two separate current loops from the *user system*, for each of the two current loops the following applies: the *user system* has to supply a voltage in order to set the signal USER_PERMIT=TRUE. If no current or insufficient current is circulating (less than ≈10 mA), the signal changes its state to FALSE. As the BIS is based on full redundancy, the user system has to supply redundant signals. Beam operation will be stopped if at least one of the two USER_PERMITs is FALSE. The redundant USER_PERMIT signals are retransmitted from the *CIBU* to the distant *BIC* via copper cables also using the RS-485 standard.

[b] Safety integrity level (SIL) is defined as relative level risk reduction provided by a safety function, or to specify a target level of risk reduction. Four SILs are defined, with SIL4 being the most dependable and SIL1 the least.

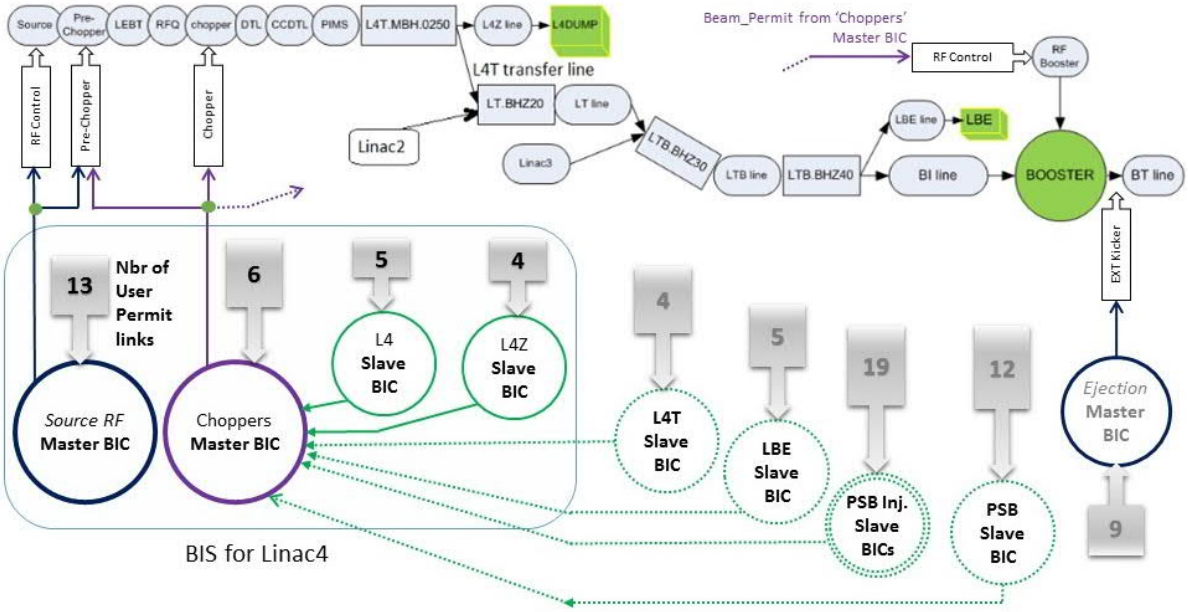

Fig. 3.41: Layout of the BIS deployed for the Linac4 and the PS booster.

3.9.2 The warm magnet interlock system

The warm magnet interlock controller (WIC) system is the CERN standard solution to assure the protection of resistive magnets against overheating and also serves as an interface between the power converters of the resistive magnets and the BIS. The WIC system has been chosen to protect the magnets of the Linac4 and its transfer line towards the booster. The *WIC* system is already deployed in many machines at CERN: the LHC, the transfer lines SPS-LHC, LEIR, HIE-Isolde, and the Linac3. The WIC system is one of the user systems of the BIC, discussed above.

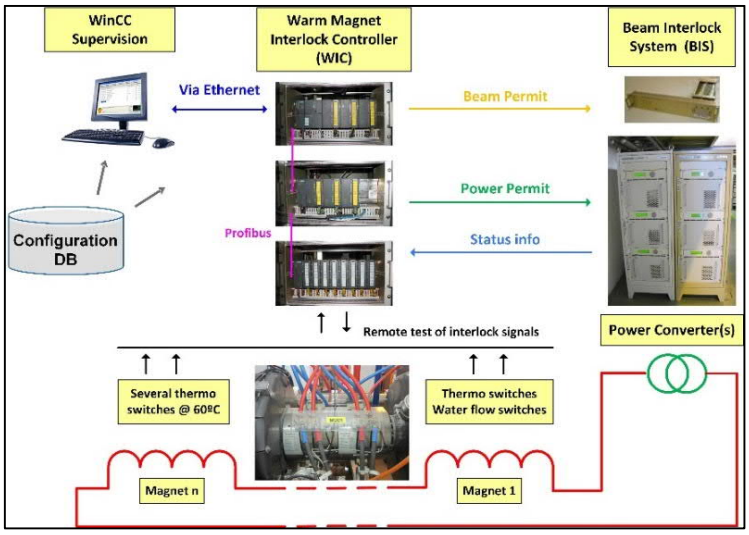

Fig. 3.42: Illustration of the WIC system architecture.

The air-cooled magnets are equipped with thermo-switches to protect the coils from overheating. Water-cooled magnets are equipped in addition to the thermo-switches with flow meters. The *WIC* system will inhibit magnet powering (by sending an interlock signal to the corresponding power converter) in case of an above expected temperature increase on the coils

or in case of lacking cooling water flow. In addition, it will remove the beam permit signal towards the BIS in case of active interlocks from any of the magnets or the associated power converters (Fig. 3.42).

The WIC is based on the use of programmable logic controllers (PLC). In order to maximize the safety of the system, the Siemens "F" Series PLC is used, offering a self-checking safety environment that ensures system integrity. The *WIC* system performs self-testing of its hardware and software to detect failures and memory corruption. It moves into a safe state upon detection of an abnormal behaviour. The fail-safe state always results in the passivation of the PLC outputs, switching off all power converters.

The *WIC* system is connected to the control system network and is monitored via a dedicated SCADA application based on the generic program components already in use in the other WIC deployments at CERN.

The *WIC* system consists of several crates: power supplies, controller crate connected together with one or several input/output crates mostly containing the Siemens I/O modules. Patch-panels and a series of magnet interlock boxes are equally required.

Two *WIC* systems are deployed for Linac4 magnet protection: one for the protection of the Linac4 magnets and one for the protection of the transfer line magnets. Each WIC system provides its own redundant USER_PERMIT signals to the BIS. About 90 magnets of Linac4 and its transfer line are connected to the two WIC controllers. In return they are connected to approximatively 75 power converters.

3.10 Survey

All the components that require an alignment by the survey are equipped at minimum with survey reference points (fiducials) and a tilt reference surface. The supports of the elements dissociate the movements in the horizontal and vertical planes.

The Survey team helped with the definition and placement of the fiducials/supports and was included in the approval of the final designs.

Appropriate theoretical and design data, together with measured parameters were the basis for survey activities. For beamline elements, the spatial position and orientation data were extracted from MADX Survey beamline definition files. Additional parameters necessary for the large-scale metrology are extracted from the layout drawings for the machines. The positions of the survey reference targets, and other parameters necessary for the large scale metrology work, are extracted from the drawings for each of the modules and elements to be aligned.

A geodetic survey reference networks has been established both above and below ground, as a reference for the measurement and control of the installations. The points in the network have been measured and their coordinates are determined in the CERN coordinate system (CCS). At the start of the civil engineering works, a geodetic reference network has been established on the surface. This network has ensured the correct position and orientation of the Linac4 tunnels and buildings with respect to the existing installations, and was adapted and used during the determination of the underground geodetic reference network.

At the start of the infrastructure installation in the accelerator tunnels, a network of geodetic survey reference points, equipped with the CERN standard survey reference sockets, has been established. This includes both reference points in the floor, which will be provided with a cover flush with the floor surface (GGPSO), several additional points on the tunnel walls (REF) and five pillars along the Linac4 (GPP). The pillars (Fig. 3.43) were designed such that they can be easily removed and precisely replaced in the same position. The complete network is determined in the CSS and measured

by total stations, laser trackers and direct levelling. The geodetic network of the area was updated periodically.

The line-of-sight hole, from the LINAC4 transfer line through to the existing transfer line from LINAC2 (LT) provides a direct link to points already known in the CCS. This aperture is used to link the both linacs and will guarantee the final position of LINAC4 transfer line and the good connection with the BHZ.20 magnet on the Linac2 side.

Fig. 3.43: Survey pillar.

References

[1] E. Hogenauer, A class of digital filters for decimation and interpolation, ICASSP'80, Denver CO, USA, pp. 271-274, doi: 10.1109/ICASSP.1980.1170846.

[2] G.F. Franklin, D.J. Powel and M. Workman, *Digital control of dynamic systems*, 3rd ed. (Pearson, Indianapolis, IN, 2005).

[3] Ph. Baudrenghien *et al.*, The LHC Low Level RF, EPAC06, Edinburgh, United Kingdom, 2006, pp. 1471–1473.

[4] C. Ziomek and P. Corredoura, Digital I/Q demodulator, PAC95, Dallas TX, USA, pp. 2663–2665, doi:10.1109/PAC.1995.505652.

[5] N. Schwerg, *Radioeng.* **21** (2012) 892, https://www.radioeng.cz/fulltexts/2012/12_03_0892_0897.pdf

[6] M.C.A. Aguglia Davide, A solid state high voltage klystron anode modulator design – an alternative to tetrode solutions, IET European Pulsed Power Conference, 2009, doi:10.1049/cp.2009.1672.

[7] OPERA Simulation Software, Dassault Systèmes, http://www.operafea.com

[8] T. Zickler *et al.*, Status of the new Linac4 magnets at CERN, IPAC2011, San Sebastián, Spain 2011, pp. 2436–2438.

[9] L. Vanherpe and T. Zickler, *IEEE Trans. Appl. Supercond.* **26** (2016) 4004304, doi:10.1109/TASC.2016.2539203.

[10] G. Golluccio *et al.*, Magnetic measurements of permanent and fast-pulsed quadrupoles for the CERN Linac4 project, IPAC10, Kyoto, Japan, 2010, pp 313–315.

[11] P. Arpaia *et al.*, A measurement system for fast-pulsed magnets: a case study on Linac4 at CERN, IEEE Instrumentation and Measurement Technology Conference, Austin TX, USA, 2010, pp. 153-156, doi:10.1109/IMTC.2010.5488290.

[12] L. Vanherpe *et al.*, *IEEE Trans. Appl. Supercond.* **24** (2014) 4000805, doi:10.1109/TASC.2013.2282302.

[13] A. Thonet, *IEEE Trans. Appl. Supercond.* **26** (2016) 4101404, doi:10.1109/TASC.2016.2532361.

[14] M. Buzio *et al*, *IEEE Trans. Appl. Supercond*. **22** (2012) 4004304, doi:/10.1109/TASC.2012.2185670.

[15] Kasaei *et al.*, Small-diameter rotating coils for field quality measurements in quadrupole magnets, 20th IMEKO TC4 International Symposium and18th International Workshop on ADC Modelling and Testing Research on Electric and Electronic Measurement for the Economic Upturn, Benevento, Italy, 2014, pp 827–832.

[16] D. Tommasini *et al.*, *IEEE Trans. Appl. Supercond.* **22** (2012) 4000704, doi:10.1109/TASC.2011.2179391.

[17] L. Vanherpe and T. Zickler, *IEEE Trans. Magn*. **49** (2012) 5417, doi:10.1109/TMAG.2013.2270976.

[18] S. Deghaye *et al.*, CERN proton synchrotron complex high-level controls renovation, ICALEPCS09, Kobe, Japan, 2009, pp. 638–640.

[19] S. Deghaye *et al.*, OASIS, a new system to acquire and display the analog signals for LHC", ICALEPCS03, Gyeongju, Korea, 2003, pp. 359–361.

[20] M. Arruat *et al.*, Front-end software architecture, ICALEPCS07, Knoxville TN, USA, 2007, pp. 310–312.

[21] V. Baggiolini *et al.*, The technology and techniques for the PS/SL middleware: The whitepaper, CERN-SL-Note-2000-008 (2000).

[22] J. Serrano *et al.*, Nanosecond level UTC timing generation and stamping in CERN's LHC, ICALEPCS03, Gyeongju, Korea (2003), pp. 119–121.

4 Building and infrastructure

4.1 Building

The civil engineering design of Linac4 has been completed in December 2007, resulting in the general layout shown in Fig. 4.1. All structures have a design life of fifty years. The Linac4 is located in the CERN site of Meyrin, on Swiss territory, in the area formerly known as 'Mont Citron' between building 363 and the Rutherford Road (see Fig. 4.2).

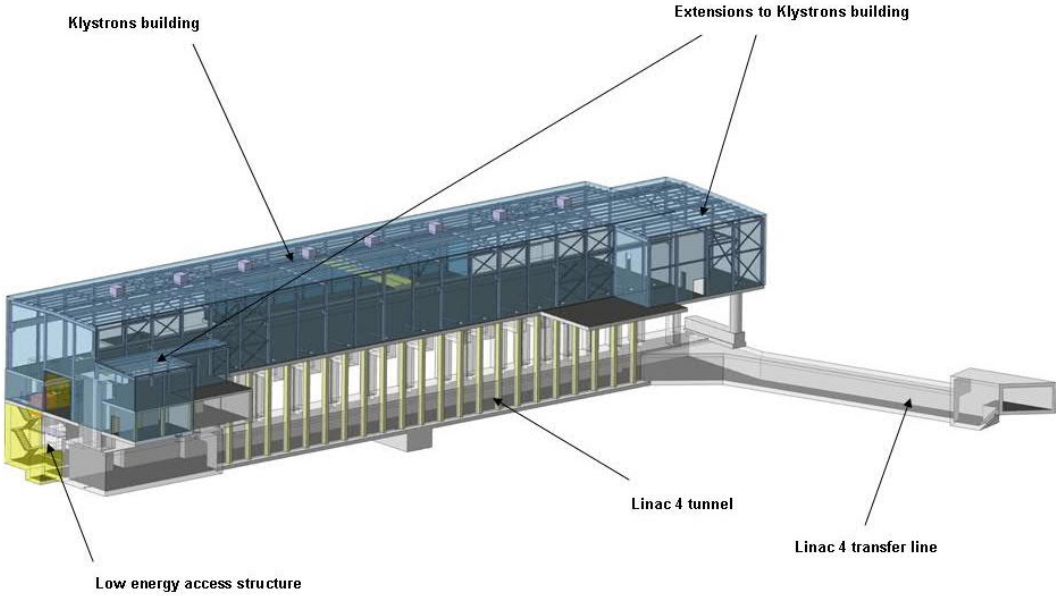

Fig. 4.1: Linac4 design.

Fig. 4.2: Building 400 (Linac4) location.

4.1.1 Geotechnical aspects and underground structures

The ground through which and in which the underground part has been excavated consisted of an artificial hill, 'Mont Citron' composed primarily of imported fill material from the PS accelerator

excavation in the mid-1950s. Beneath 'Mont Citron' there is a relatively thin superficial deposit of glacial moraine above a mixed sequence of molasse.

The molasse consists of irregular, sub-horizontally bedded tenses of rock with lateral and vertical variations from very hard and soft sandstones, to weak marl. Significant property variations occur between and within each gradational lens, making it difficult to assign parameters which are truly representative of the rock mass.

A geotechnical investigation campaign was carried out in August 2007, leading to the definition of specific excavation and support methods. The excavation works have been carried out using conventional methods with adequate cutting slopes in the tunnel area (see Fig. 4.3), and a piled wall anchored with pre-stressed anchor bolts in the low energy access area. Instrumentation and monitoring of excavations and existing structures, particularly the walls and slab of Linac2 were key elements of the construction process.

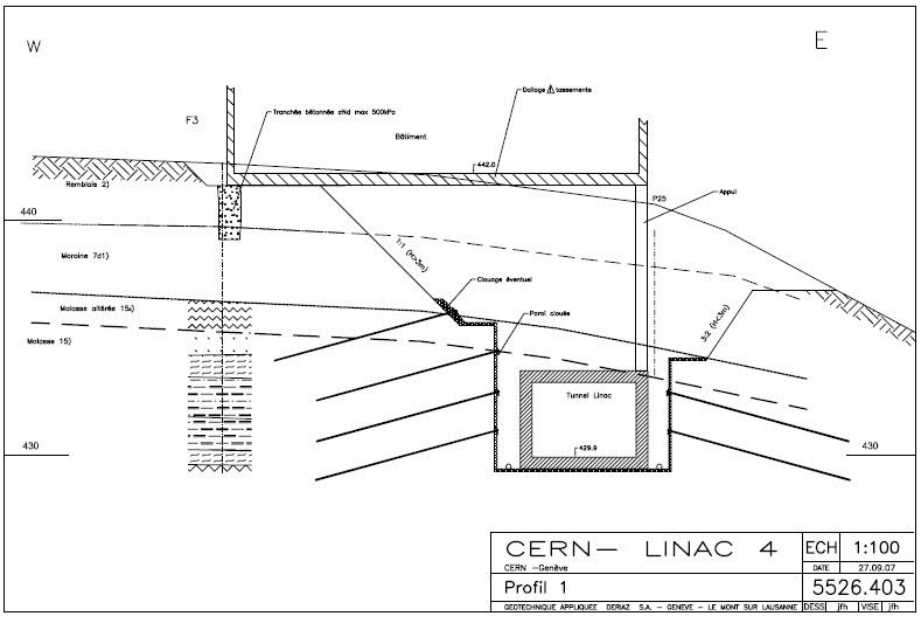

Fig. 4.3: Excavation works in the tunnel area.

All underground structures have been provided with an inner lining of concrete and are totally free from all visible signs of water ingress either from joints, cracks or elsewhere.

The **Linac4 tunnel** is approximately 100 m long and has internal dimensions of 4.45 m width and 3.20 m height. It is situated 12 m below finished ground level. The tunnel is connected with the surface via one access structure and several concrete ducts for guide waves and services, and with the Linac2, via the Linac4 transfer line. Its excavation is shown in Fig. 4.4, which is a photograph taken from the low energy side.

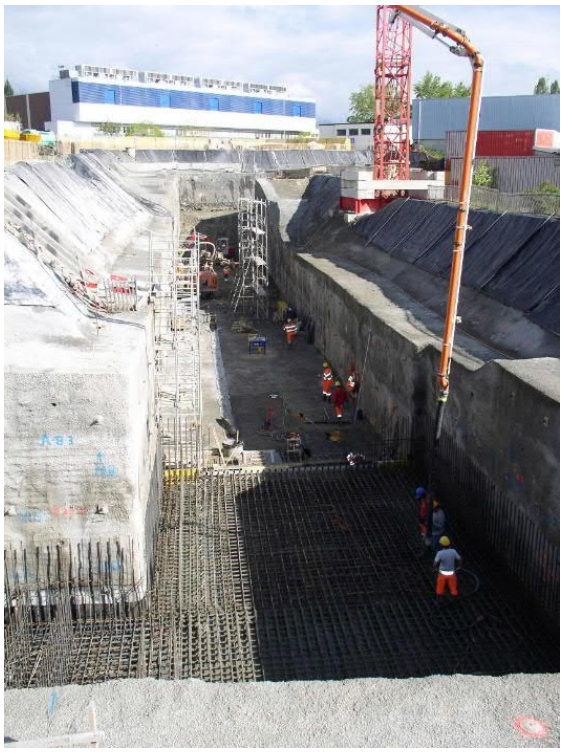

Fig. 4.4: Linac4 tunnel excavation works.

The **transfer line tunnel** connects the Linac4 tunnel to the existing Linac2 building, where the Linac4 beam joins the existing accelerator complex. The transfer line tunnel is approximately 49 m long and has internal dimensions of 2.8 m width and 3.1 m height. It is horizontal and situated 12 m below finished ground level. It passes under an existing technical gallery serving the PS booster, which was suspended above the open excavation and remained operational during the excavation works (see Fig. 4.5). The transfer line steps up to the same level as the existing Linac2 approximately 11 m before the junction, and is enlarged to allow the installation of an emergency door at the junction.

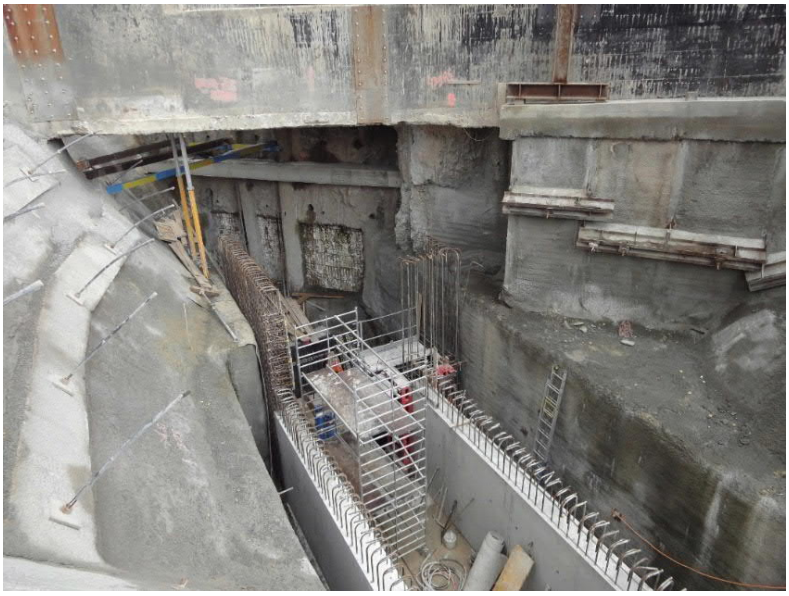

Fig. 4.5: Transfer line tunnel under the existing technical gallery.

The **low energy access structure** provides access for personnel, equipment and services into the Linac4 tunnel. It houses a lift shaft and a stairwell.

4.1.2 Surface structures

The Linac4 surface structures are built in steel frame with cladding, similar to existing CERN buildings.

The **klystrons building** houses the klystrons and their pulsed modulators, and all electronics racks and services needed for Linac4 operation. It is a steel frame with cladding approximately 100 m long and 18 m wide. The building has been equipped with a 10 t capacity gantry crane.

Two alignments of columns connect the building with the Linac4 tunnel in order to reduce settlements between both structures, see Fig. 4.6. The building during construction is shown in Fig. 4.7.

Fig. 4.6: Transverse section klystrons building and tunnel.

The building has two levels over the 'low energy' part of the linac to allow direct access from the road for delivery lorries. Three extensions of the building have been necessary to house additional racks, a control room, electrical equipment and cooling ventilation equipment.

Fig. 4.7: Klystrons building steel structure.

The building works for Linac4 started on 22nd October 2008 and were completed and delivered to CERN on 22nd October 2010, including car parking, roads, a new roundabout, surface water drainage, and landscaping of the area around the new klystrons building (Fig. 4.8).

Fig. 4.8: Klystrons building façade.

4.2 Cooling and ventilation

4.2.1 Cooling

All of the water pumping equipment is housed inside the Linac4 building, while the primary water is provided by chillers and cooling towers located outside the building. The cooling station is connected to the building's demineralized water distribution network (Fig. 4.9) and is equipped with pumps, heat exchangers, demineralization cartridges, and controls to feed the network.

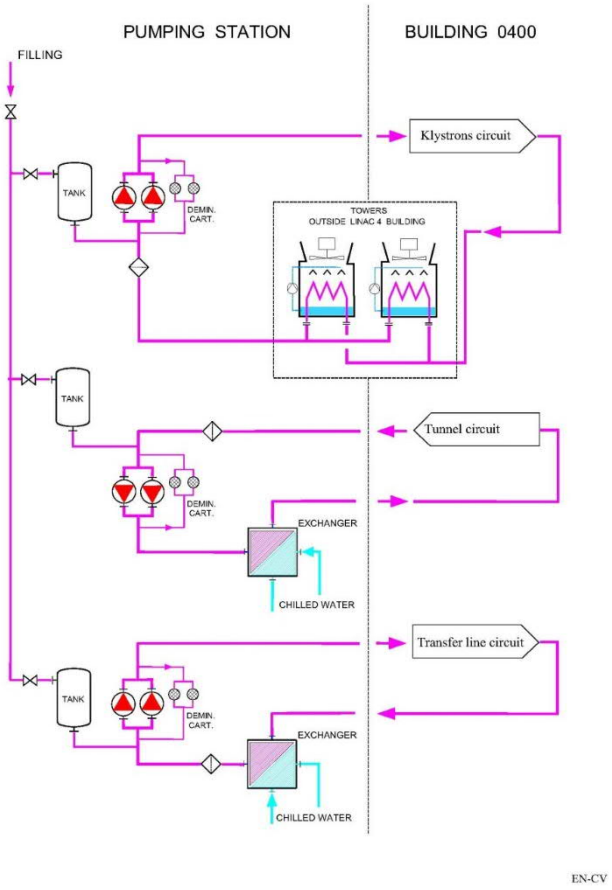

Fig. 4.9: Schematic diagram of the demineralized water pumping station.

The cooling demands for all of the equipment located in each circuit, so-called end users, are summarized in Table 4.1.

Table 4.1: Main parameters of the water circuits .

Identification	Total flow [m^3/h]	Power [kW]	Max. pressure [barg]	Water supply temperature [°C]
Klystron	154	300	10	22–25
Tunnel	21	50	10	20–23
Transfer line	16	44	15	22–25
RFQ	2	2	10	20–26
Chilled water	100	700	6	5–8

For the klystron circuit, two variable speed centrifugal pumps provide the pumping power with the necessary redundancy, each pump having the capacity to provide 100% of the required flow. The rotational speed of the pumps is controlled in order to have a fixed pressure difference across the main supply and return. A hybrid/adiabatic closed-circuit cooling tower is used for the primary water production.

In a similar way, variable speed centrifugal pumps provide the pumping power for each of the tunnel and transfer line circuits with the required redundancy. Given the water supply temperature

requirements, chilled water is used for the primary cooling. Due to the constraining temperature regulation requirements, a dedicated station is installed for cooling of the RFQ. This station provides demineralized water with an adjustable set point and an accurate temperature control of ± 0.2 K.

A chilled water plant provides the primary cooling necessary for the ventilation and air-conditioning systems and the 20 °C demi-water circuits. Two compressors, air-cooled chiller units, are installed outdoors. An additional reversible compressor supplies the ventilation unit of the Klystron Hall with hot water for the heating season and chilled water in case of high demand of cooling.

4.2.2 Ventilation and air conditioning

The Linac4 facility is divided into several ventilation areas or sectors, each has a dedicated heating, ventilation and air conditioning system according to its duty and safety requirements.

The indoors conditions requested by the project are summarized in Table 4.2. The internal loads, due to equipment or occupational activities inside the conditioned spaces are listed in Table 4.3.

Table 4.2: Indoor conditions to be maintained.

Identification	Temperature [°C] winter	summer	Dew point [°C]	Pressure control	Remarks
Klystron hall	20 ± 2	25 ± 2	-	Overpressure between the klystron hall and the tunnel/TL	Possibility to reach 30 °C during summer time
Access module	21 ± 2	25 ± 2	-	Overpressure (20 Pa when doors closed)	
Tunnel and TL	18 ± 1 (winter, no machine loads)	23 ± 1 (run)	Max. 12 °C (for summer conditions)	Overpressure between the klystron hall and the tunnel/TL	Max. ΔT of 5 K along the tunnel
Faraday cage	24 ± 1		-	-	-
Racks R-001	20 ± 2	25 ± 2	-	-	-

Table 4.3: Internal heat loads.

Identification	Loads from electrical equipment [kW]	Maximum number of people
Hall	405	50
Access module	15	10
Tunnel	15	50
Transfer line	7	50
Faraday cage	45	10
Racks (zone IV)	54	10
Control room	5	15

The general principles for heating, ventilation and air conditioning of the Linac4 sections were as follows.

Klystron hall: an air handling unit (AHU) supplies the air for the klystron hall through a duct network and air displacement grilles. The AHU works on recycled air with a minimum of fresh air to ensure air renewal inside the building. The amount of fresh air can be increased, in order to take advantage of free

cooling if necessary. Excess fresh air will escape outside the building through outlets located on the roof. Four extractors—located on the roof—will be used for the extraction of smoke. The fresh air intake, in case of fire emergency, will be ensured by the manual opening of the building doors.

Access module: one AHU maintains the access module at a positive overpressure by mechanical supply of pre-treated fresh air. A stand-by unit, although not fitted with air treatment equipment, only basic filtration and fan stages, will be installed to ensure redundancy of equipment in this safety related system.

Tunnel and transfer line: in machine mode (when the accelerator is in operation), an AHU works in recycling mode to maintain the ambient conditions. The tunnel and the transfer line are kept at a lower pressure than the klystron hall by means of an extraction unit which will continuously reject a fraction of the air flow-rate to the outside. In access mode, a minimum of pre-treated fresh air is supplied to ensure a renewal rate of the tunnel air above 2 volumes/hour. The excess of air is rejected outside and the remaining fraction is recycled through.

Faraday cage: two AHU located next to the Faraday cage extremity, ensure the ventilation of the volume. The air will come out through four supply air displacement grilles into the cold aisle (frontal side of the racks). The cool air enters the racks driven by their own fans, to be exhausted to the hot aisle (back side of the racks). The amount of fresh air can be increased, in order to take advantage of free cooling if necessary. Excess fresh air will escape outside the Faraday cage into the Klystron Hall through three outlets located on the roof.

Racks room R-001: an AHU supplies air through ducts mounted on the ceiling. The unit works on recycled air with a minimum of fresh air to ensure air renewal inside the room. The amount of fresh air can be increased, in order to take advantage of free cooling if necessary. Excess fresh air will escape outside the building through a decompression grill. In case of failure of the AHU, four wall mounted fan coils will ensure a minimum cooling.

4.3 Electrical systems

Following the definition of the electric requirements for the different subsystems of Linac4, the CERN Electricity group established a power load balance, listing all the identified systems of the project and their power supply requirements. Three separated systems functions were identified, personnel safety equipment, machine/accelerator equipment and general services for the infrastructure. The AUG (Arrêt D'Urgence Général) safety system was designed and implemented according to a detailed safety risk analysis.

4.3.1 High voltage electrical network

The ME84 electrical station, exclusively dedicated to the Linac4 complex and located inside building 400, is supplied upstream from the ME23 station which is part of the 18 kV ISOLDE loop. The ME23 electrical station located in building 214, supplies the Linac4 complex using three main buried power links. Two main 18 kV links dedicated to machine and general services equipment, and a third 400 V link dedicated to exclusively supply the safety network dedicated to power safety equipment.

Figure 4.10 shows the two 18 kV links dedicated to supply machine and general services equipment, and the ISOLDE Loop.

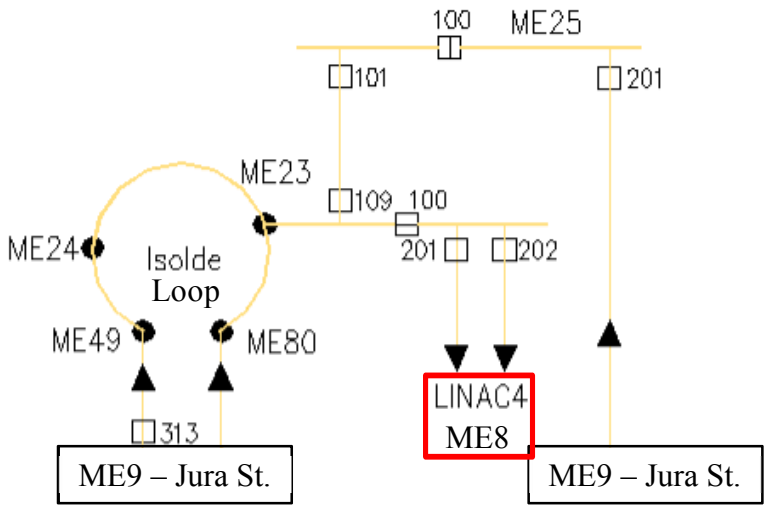

Fig. 4.10: HV electrical network supply for LINAC4 machine and infrastructure.

On the Meyrin site, an independent 18 kV diesel backup network is exclusively dedicated to power safety equipment. Three diesel gensets located in the ME9 electrical station are the source of the main 18 kV network. A 400 V power link is used to supply the Linac4 safety network, from the ME23 electrical station.

Figure 4.11 shows the 18 kV diesel backup network with its generators, and the supply of ME84 dedicated to the Linac4 complex.

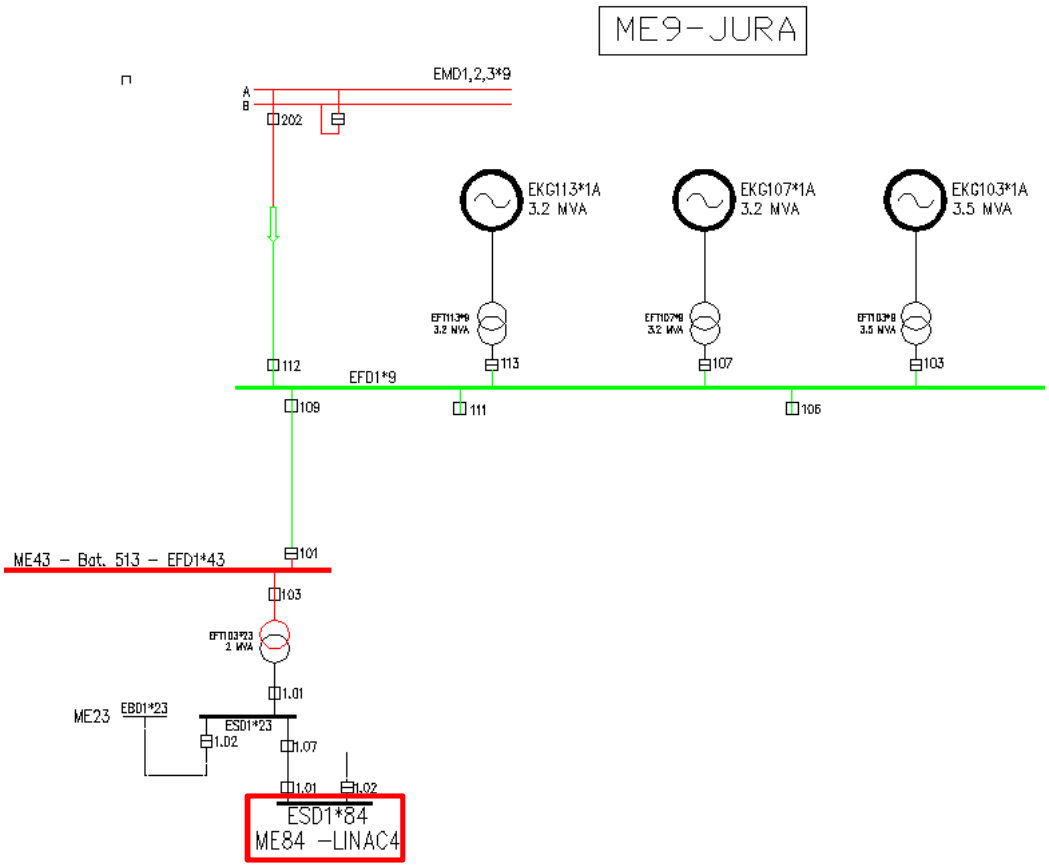

Fig. 4.11: HV and LV safety power network supplying the LINAC4.

4.3.2 Low voltage electrical network

The low voltage network for the Linac4 complex is composed of four main functional networks.

The diesel backup network takes its source from the ME23 station (LV link rated to 630 A) and is exclusively dedicated to supply safety equipment (lift, safety lighting, 48 Vdc for emergency stops, smoke extraction, fire and oxygen detection, etc.).

The machine and general services network take their source from a 2 MVA - 18/0.4 kV transformer located outside Linac4 hall.

The cooling and ventilation power network takes its source from a 2 MVA - 18/0.4 kV transformer located outside Linac4 hall. A LV interconnection link, rated to 1250 A, backup the cooling/ventilation to machine/general services switchboards. This link can be used in case of failure or maintenance on one of HV links or transformers.

The UPS network takes its source on a unique double conversion UPS rated to 200 kVA, with 10 minutes autonomy on batteries. The UPS network remains live in case of AUG *(Arrêt d'Urgence Général)* activation.

Figure 4.12 shows the main low voltage distribution for Linac4 complex.

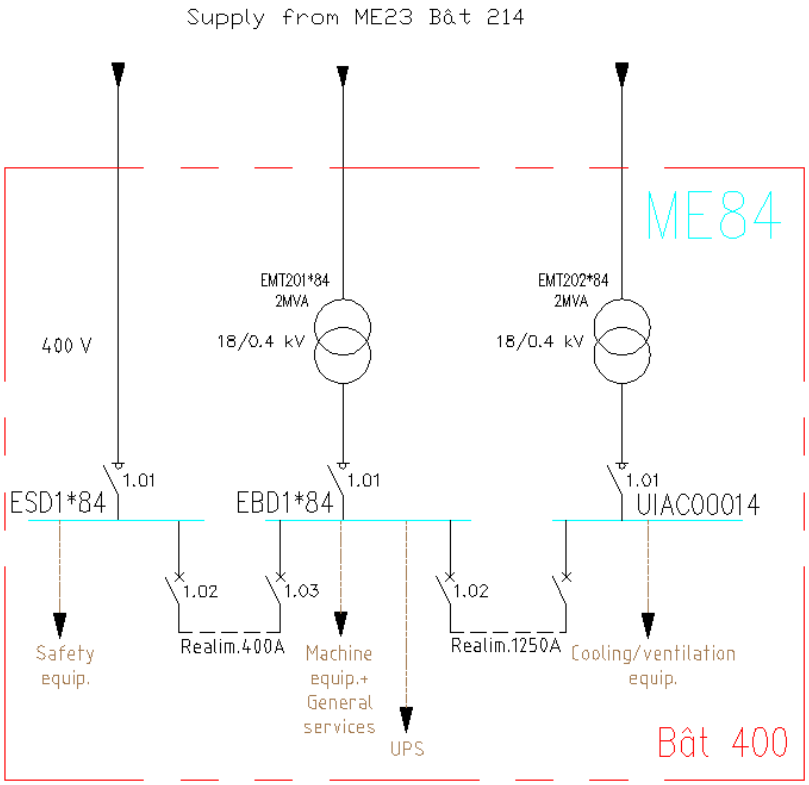

Fig. 4.12: Low voltage electrical network for LINAC4.

5 Safety, commissioning, and decommissioning

5.1 Radiation protection

5.1.1 Parameters and operational scenario considered in the radiation protection studies

The Linac4 was designed to replace the Linac2 as the injector for the PS booster whilst keeping the option open of serving as the front-end of a future superconducting proton linac (SPL). As presently installed, the Linac4 hardware only allows a maximum power of 5.1 kW and in its current configuration the PS booster can only accept a maximum beam power of 2.85 kW (1.2 s pulse spacing). The civil engineering layout of Linac4 (with respect to shielding) was dimensioned already taking into account a possible future operation for the SPL at higher duty cycle, whereas all operational and environmental studies were performed for the Linac4 as an injector for the PS booster.

The Linac4 design is such that, even under SPL conditions, hands-on maintenance must be ensured. The analysis of particle losses was done for a full-SPL duty cycle (~ 384 kW) and the highest possible operating beam current. Several random distributions of errors (alignment, focusing, accelerating field, etc.) showed that for the SPL beam power, beam losses would occur at 22 beam loss points along the beam line, with the highest beam loss rate localized at the end of the CCDTL section (Fig. 5.1). At this location, the beam loss rate corresponds to a loss power of 0.92 W. From experience, a beam loss power of up to 1 W per metre is considered as acceptable in a linear accelerator, still allowing for hands-on maintenance. For the time being the present Linac4 hardware will only allow a maximum power of 2.85 kW. Theoretically, with respect to this study losses would be reduced by about a factor 200. However, a conservative value of 0.1 W per beam loss point was assumed, and in the calculation losses were considered to occur at seven locations (loss points: 2 at DTL, 2 at CCDTL, 3 at PIMS).

5.1.2 Stray radiation levels and shielding design

The civil engineering layout is designed to cope with SPL beam power. The beam line is shielded by more than 8 m of earth and concrete towards the surface and the klystron hall, reducing the stray radiation to negligible values in areas accessible during Linac4 operation. However, secondary particles might stream through ducts, i.e., cable and ventilation ducts, access shafts and the 15 waveguide ducts connecting the underground area with the klystron hall. As an example, the layout of the ducts connecting the Linac4 tunnel to the klystron hall is shown on the left panel in Fig. 5.1. A ‘normal’ beam loss of 1 W (SPL case) will result in ambient dose equivalent rates of less than 100 nSv/h in the klystron hall, e.g., near a wave guide duct as it can be seen on the right panel in Fig. 5.1. In case of a full beam loss of 5.1 kW (maximum power for the Linac4 as an injector to the PS booster), the accidental dose rate could reach about 500 µSv/h. Various protection systems including the radiation monitoring system RAMSES will immediately switch off the beam in case of abnormal losses.

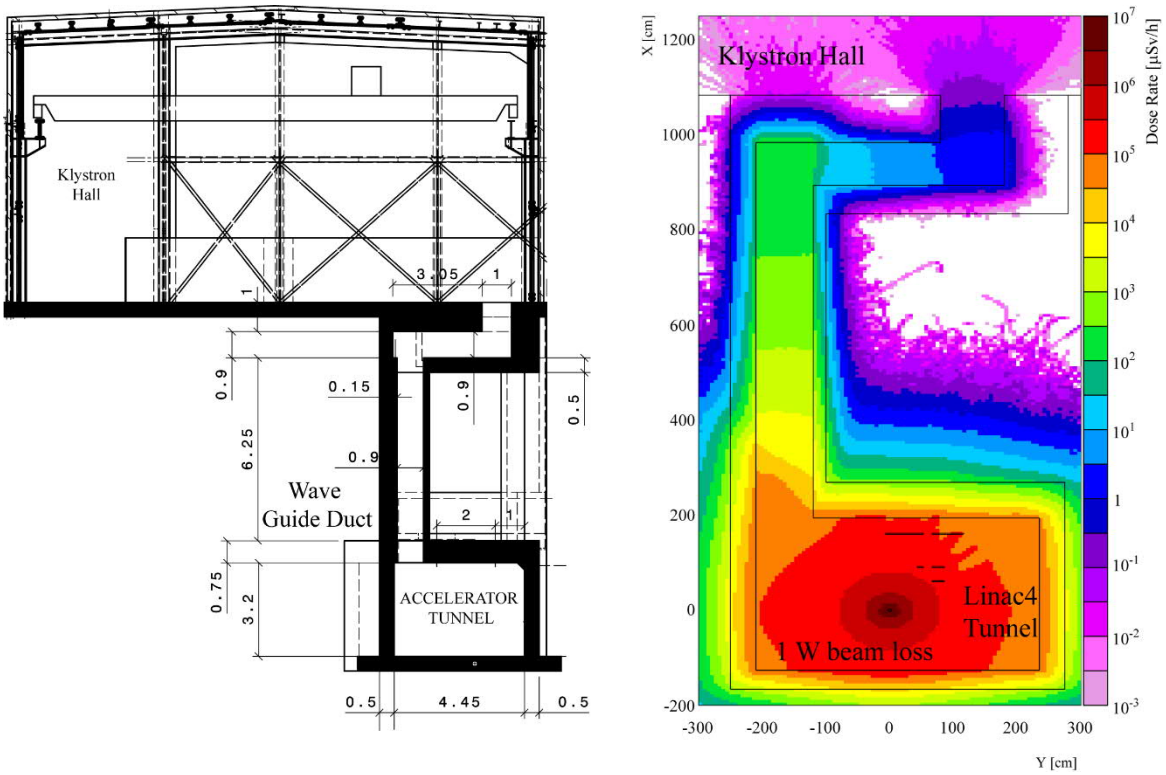

Fig. 5.1: Stray radiation in case of 1 W beam loss at the location of a waveguide duct.

The ambient dose equivalent rate inside the accelerator tunnel during beam operation as PS booster injector can exceed several hundreds of Sv/h in case of a full beam loss of 5.1 kW. During normal operation, the ambient dose equivalent rates inside the tunnel reach levels of some hundred mSv/h. The access safety system interlocks combined with procedures prevents the presence of personnel during beam operation.

5.1.3 Activation of equipment and residual dose rate levels

The Linac4 accelerator components, the surrounding structure, cooling water and air will become radioactive due to the nuclear reactions created by the beam particles in the respective materials. The radionuclide inventories were calculated with the code FLUKA, and the residual dose rates caused by the radioactive decay of the radionuclides have been determined in function of the cooling time.

5.1.3.1 Activation of the main beam dump

The main beam dump will be the most activated component in the Linac4 beam line. The design of the beam dump was optimized for beam operation and radiation protection [1]. The replacement of the dump core in case of failure during normal Linac4 operation and after one day of cooling would result in a collective dose of 30 µSv.

5.1.3.2 Activation of the beam line

The estimation of the induced radioactivity in the accelerator components is particularly important for the maintenance and repair activities, and finally for the disposal of radioactive waste. The residual activation was calculated with FLUKA, using a detailed geometrical model of the accelerator and estimated normal beam losses. The irradiation profile was derived from the present Linac2 yearly schedule but assuming 7000 hours of operation per year instead of the 5000 hours of Linac2. The activation will not be uniformly distributed along the beam line (see Fig. 5.2 for the beam line section

including the PIMS cavities). The dose rates after 30 years of operation and measured at 10 cm distance reach some few µSv/h in the DTL section and not more than 100 µSv/h in the CCDTL and PIMS sections, even without any cooling.

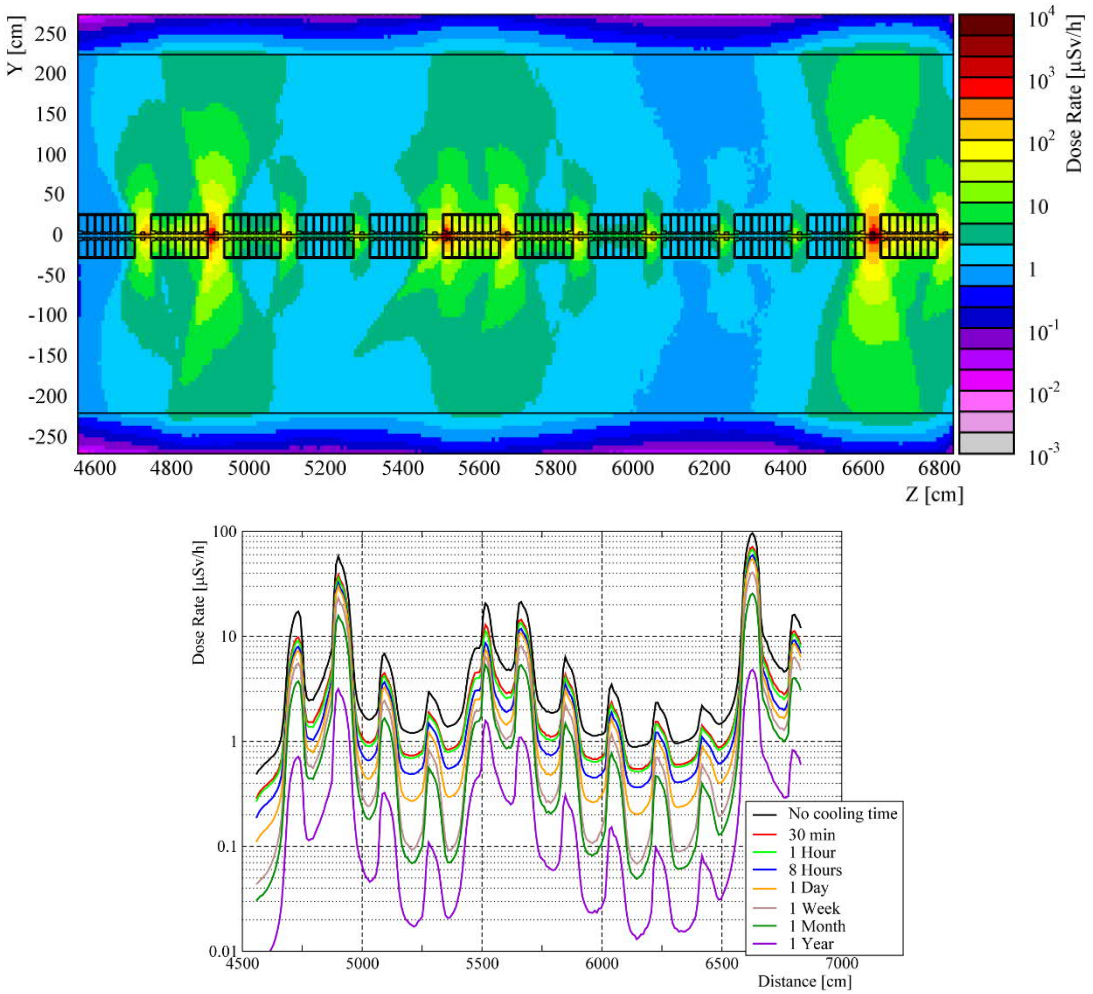

Fig. 5.2: Residual dose rates at 10 cm from the PIMS tank on a profile parallel to the beam axis after 30 years of operation. The top colour plot corresponds to the residual dose rate just after the beam stops (no cooling time).

5.1.3.3 Activation of cooling water

The water-cooling system of Linac4 comprises four different closed circuits filled with demineralized water. One is used for the klystrons on the surface. This water is not exposed to any hadronic radiation field and therefore will not be activated. The activation of the water in the RFQ cooling circuit will be negligible as the beam energy stays well below the threshold for typical nuclear reactions on oxygen nuclei. The third circuit cools the accelerating structures (DTL, CCDTL, and PIMS), whereas the fourth one cools the main beam dump. Assuming that the demineralized water will not be exchanged for the entire lifetime of the facility's beam dump circuit, FLUKA simulations result in a total activity of 8 MBq of Tritium and a specific activity of 5 kBq/l [2]. This value is well below the exemption limits given in the present and future Swiss Radiation Protection Ordonnance. The production of the ^{7}Be will be in the order of 30 MBq. It can be assumed that the major part of ^{7}Be will be trapped by the ion-exchange resins of the filter cartridges. The cooling circuits of the accelerating structure and the beam dump will be equipped with sampling outlets to allow regular routine measurements of the radioactivity.

5.1.3.4 Air activation and air management

The heating ventilation and air conditioning (HVAC) system will maintain the Linac4 tunnel in under-pressure (20 Pa) towards the surface areas to confine the radioactive air inside the tunnel and to achieve a controlled, continuous release (2000 m^3/h) via the stack. The air volume is renewed by fresh air every 40 minutes, as such limiting the build-up of long-lived radionuclides. The fresh air is injected into the high energy area of the Linac4 and extracted from the low energy area at the position of the Linac4 source to maximize the radioactive decay of the radionuclides before being released into the environment. The total activity released during the Linac4 commissioning presents the envelop case for one year of Linac4 operation. During the commissioning, 60 GBq will be released, resulting in a negligible dose to the public (20 nSv/year). A flush cycle of 16,000 m^3/h for 15 minutes will be performed before any access to the tunnel will be granted to limit the exposure of personnel.

5.1.3.5 X-ray from accelerating cavities and klystrons

The strong electric fields in an RF cavity will result in field emission effects, the liberated and accelerated electrons will produce bremsstrahlung when impinging on matter. This effect is particularly pronounced during the conditioning of the cavities. Several cavities are installed in the Linac4 (RFQ, buncher cavities, DTL, CCDTL, and the PIMS). The dose rate levels were measured during the RF conditioning tests. In case of DTL, CCDTL, and PIMS dose rates ranging from μSv/h to tens of mSv/h are observed and, consequently, access to the tunnel is prohibited during such tests. Radiation levels during conditioning of the RFQ allow the classification of this part of the tunnel as a supervised radiation area. The klystrons are shielded with lead and the radiation levels were measured during dedicated tests. The dose rates did not exceed 1 μSv/h at 10 cm distance.

5.1.4 Operational radiation protection aspects

The radiation levels in and around the Linac4 are measured by six high-pressure hydrogen ionization chambers (PAXL) in areas accessible during beam operation. They are installed close to the wave guide ducts, the cable duct, the material shaft, and the klystron gallery. Radiation alarms are transmitted to the Linac4 control room to inform the operator of abnormal radiation levels. Local alarm units warn the personnel. An additional hydrogen monitor is installed in the accessible part of the Linac2–Linac4 interface. Six open air plastic chambers (induced activity monitors PMI) are installed inside the accelerator tunnel during beam off to monitor the radiation levels due to residual radioactivity when the beam is switched off. They are installed in areas where higher beam losses are supposed to occur.

One ventilation monitoring station (MS) and one ventilation aerosol sampler measure the releases of radioactivity into the environment. All monitors are connected to the supervision system of RAMSES.

The Linac4 accelerator tunnel is classified as a supervised or controlled radiation area – as function of the measured ambient dose equivalent rates. The areas at the surface, such as the cooling and ventilation technical rooms, the buffer area and the klystron area, are classified as supervised radiation areas. The radiation veto of the access control system allows RP to control the access into the Linac4 tunnel as function of the radiation risks. Based on lessons learned from Linac2 operation, the annual, operational collective dose is not expected to exceed 500 man. μSv.

5.2 General safety

A key objective of the Linac4 project was to ensure that the level of safety for the people and the environment is maintained during all project phases (simulations, design, prototyping, installation, commissioning, operation, and dismantling), as demonstrated in the Linac4 Safety File.

Particular attention was given to minimizing beam losses in the linac and at the PSB injection, favouring technical solutions which minimize the dose rates in accordance with the ALARA principle (keep doses to persons as low as reasonably achievable) and limit the amount of radioactive waste. Some examples are:

- The machine design is highly modular, to permit an easy exchange of components and to avoid repair of machine parts 'in situ', with the goal of minimizing the dose to the personnel involved in installation, maintenance, and dismantling operations.
- The accelerator beam optics design aims at concentrating beam losses on a few shielded and protected elements (collimators and dumps), thus minimizing distributed loss and reducing the number of activated components.
- The design of the components more likely to be activated as the main dump assembly has been done considering the different operations for handling and dismantling on the basis of the ALARA principle.

5.2.1 Safety documentation

All technical aspects of Linac4 safety are covered by the appropriate safety documents: the Launch Safety Agreement and the Linac4 Safety File.

5.2.1.1 Launch Safety Agreement

The Launch Safety Agreement (LSA) covers the conventional safety aspects at the start of the project. It results from a launch safety discussion with the Project Leader, the Departmental Safety Officers (DSO), the Project Safety Officer (PSO), and the correspondent from the HSE (Health, Safety, Environment) Unit. After the launch safety discussion, the HSE correspondent releases the Launch Safety Agreement that provides the following information:

- Description of the facility, systems/processes.
- Preliminary identification of the safety hazards and risks.
- Identification of the CERN safety rules and host state regulations applicable to the facility, systems/processes.
- Tailored safety advice on hazard control measures.
- List of safety checks (including safety checks required to grant safety clearance) on the relevant facility, systems/processes that shall be carried out by the HSE Unit during the facility life cycle.
- Minimal contents of the Safety File needed to meet the Safety requirements.

The LSA may be reviewed and updated during the different phases of the facility, systems/sub-system's lifecycle. Any changes to the safety requirements are integrated through the ECR process.

5.2.1.2 Linac4 Safety File

The Safety File is established and maintained during the project life cycle. It consists of four main parts:

- Descriptive: description of the facility/process.

- Demonstrative: addresses hazard and safety risk identification; risk evaluation and risk analyses; risk responses; technical risk control measures; organizational risk control measures.
- Operational: inventory of all operational documents needed in order to optimize the exploitation of the facility, especially in terms of safety.
- Records experience and monitoring (REM): shall receive all the feedback linked to the development of the facility, accidents, or incidents and any other new development.

5.3 Decommissioning

Linac4 is the first accelerator project at CERN that integrates a decommissioning strategy and plan. The main objective of the plan is to minimize the radiation dose to the personnel during the decommissioning phase by integrating in the design appropriate dismantling procedures and by leaving instructions and documentation for the future decommissioning. Additionally, the plan aims to estimate the amount of radioactive waste and optimize its disposal, analysing within the project the financial impact of the future disposal.

The decommissioning plan is based on the assumption that Linac4 will be operated at the design beam parameters for LHC high luminosity during a period of about 30 years. After the operation cycle, the accelerator will be stopped and will remain under controlled access during a radiation cool-down period of a few years; the removal of all Linac4 components from the tunnel and the surface building will follow, leaving in operation the electrical distribution network and the cooling and ventilation infrastructure. The objective of the decommissioning will be to leave the building and tunnel available for another use, such as a new accelerator, an experiment, a workshop or as storage space.

The accelerator design integrates some basic principles intended to facilitate the future dismantling. The mechanical design of the linac is modular, the components being grouped in modules assembled at the surface and installed into the tunnel; this approach facilitates installation and maintenance, but at the same time will simplify the decommissioning operations, minimizing the amount of work to be done in the tunnel. In the beam optics design the principle of localizing beam losses in a few shielded and protected elements (collimators and dumps) has been applied, thus minimizing distributed losses and reducing the number of activated components. The first collimator is placed in the 3 MeV chopper line, at an energy below the activation limit for most metals; in the same line, a dump removes particles that would be lost at capture in the PSB bucket. Along the linac, a conservative beam dynamics design has been followed, with the goal of minimizing beam loss and activation of the accelerator components. Taking into account these considerations, the inventory of radioactive elements to be dismantled at the end of Linac4 lifetime will only include:

- the slightly activated accelerator components between 3 and 160 MeV, consisting of about 20 m^3 of stainless steel and copper, with small amounts of magnetic material (SmCo) likely to be more activated because of the presence of cobalt;
- the elements of the transfer line (4 m^3 of vacuum chambers and small magnetic and diagnostics components, plus five large bending magnets) whose level of activation will depend on the operating conditions;
- the components that will intercept the beam at high energy, main dump, and beam stopper. The overall activated volume is large because it includes the shielding; activation levels will be relatively high and decommissioning of these elements has to be carefully studied and planned.

5.3.1 Decommissioning of the main beam dump

The main dump is made of a graphite core press-fitted into a stainless-steel jacket that incorporates the water cooling. The external support and the ancillary systems are made of aluminium alloy, to reduce to a minimum its activation. The whole device is surrounded by a shielding designed after a set of

specific activation simulations, made of layers of different materials to contain the ionizing radiation escaping the device in nominal operating conditions. The mechanical design foresees a procedure for the emergency replacement of the entire device or of a particular component minimizing the dose to the operators, with operators remaining at safe distance and with the possibility of exchanging operators if needed. The same procedure can be used for the decommissioning of the device. Leak-tight quick connections / disconnections for vacuum and water are employed everywhere and positioned in locations far enough from the radiation source (the core). Once the shielding is assembled and in place, it will be dismantled only for disposal at the end of the Linac4 life. The total weight of the shielding with the dump and the table is lower than 40 tonnes.

The shielding can be opened on one side using a movable table (Fig. 5.3); the internal part (part of the iron shielding and the dump) can then be removed for disposal; this operation may take up to a few hours of work and can be made at distance with appropriate tooling. Once opened, the part to be removed is handled by a temporary crane in the tunnel, and subsequently parked in a radiation-controlled area and processed for radiation waste disposal.

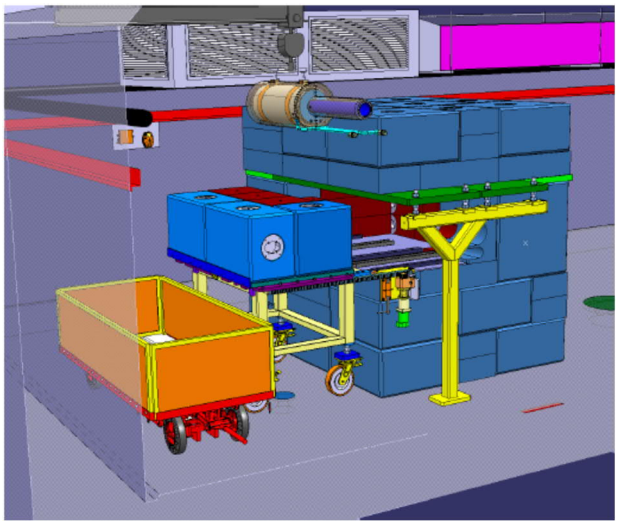

Fig. 5.3: Removal of the main dump for decommissioning.

Calculations of residual dose rate in the dump components and in the surrounding environment after 30 years of operation and two years of cooling-down time are presented in Fig. 5.4, for the complete dump, after removing the concrete shielding, and after removing the steel shielding. The maximum residual dose rate in the three cases is about 1, 10, and 100 μSv/h respectively. A time analysis indicates that the dose rate decreases drastically in the first days following the beam stop and more gently in the following months; while there is little or no difference in the dose rate outside the shielding after one or two years, the activity of the inner core is still slightly decreasing between one and two years. The optimum time for decommissioning is estimated according to these calculations to be more than two years. Accordingly, to the present CERN exemption limits, practically the entire dump assembly (core and shielding) will be classified as radioactive waste; the wall behind the dump will not be considered as radioactive. The shielding can be separated into its basic components, which will be disposed of as radioactive waste or reused based on activation measurements.

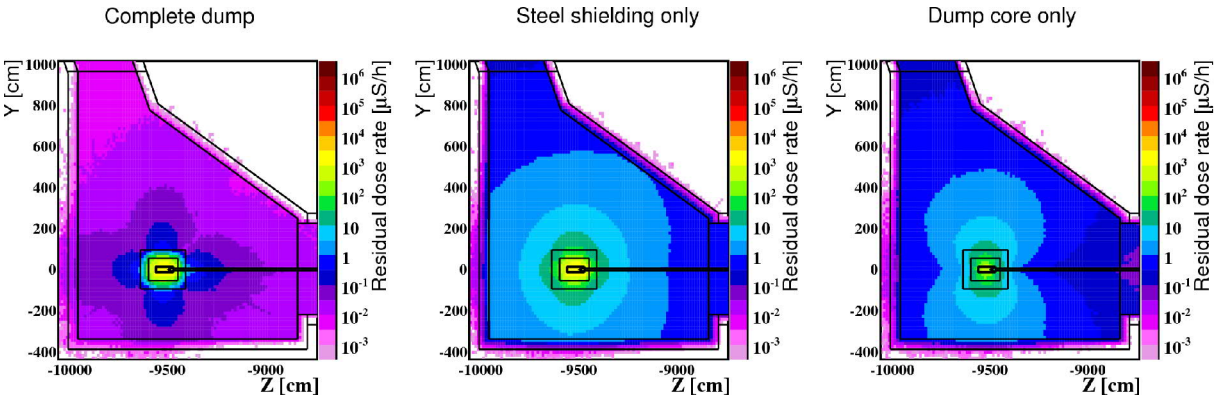

Fig. 5.4: Residual dose rates of the main dump after 30 years of operation and two years cooling time.

5.3.2 Decommissioning of accelerator components

The decommissioning strategy is based on a set of simulations performed using a detailed geometrical model of the accelerator. Although the precise Linac4 irradiation profile based on the sequence of shut-down and operation periods is impossible to predict, a simplified profile was derived from the present Linac2 yearly schedule. The beam loss pattern considered in the Linac4 Safety File has been used for the simulations, taking a conservative value of 0.1 W beam loss per 'hot spot' along the machine. The calculation of the induced radioactivity was performed in positions representative of typical aperture restrictions in the various sections of Linac4. To illustrate the results, Fig. 5.5 presents the case of the PIMS section, which presents the highest activation. The plot shows the ratio between the specific activity and the exemption limits for CERN design studies as a function of cooling time, integrated over all radioisotopes and for the main components of the accelerator.

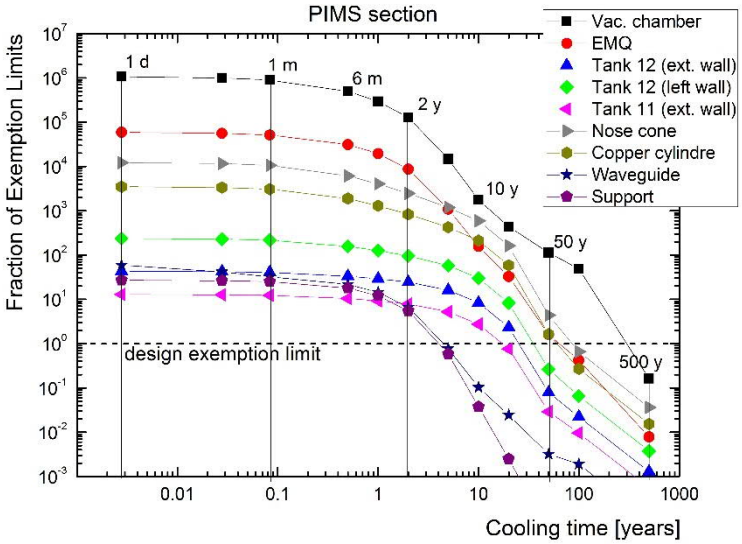

Fig. 5.5: Specific activity as fraction of CERN design exemption limit as a function of cooling time for the PIMS components.

This study indicates that the dose rates in the DTL are rather low while the CCDTL and PIMS are more critical. After one month of decay time the DTL dose rate decreases below 1 µSv/h and never exceeds 10 µSv/h even immediately after shutdown; in the other sections, the quadrupoles can present dose rates up to 100 µSv/h. On the other hand, the dose rate decreases quickly far from the beam loss points reaching 0.1 µSv/h in one month of cooling time.

Using as a reference the results of the simulations, we can define a dismantling procedure based on the following steps:

a) Wait for a minimum of two years after the end of Linac4 operation before starting the dismantling activities. After this time, the supports, waveguides and all ancillaries will be below the exemption limits and can be disposed of as non-radioactive equipment; the activity inside DTL and CCDTL tanks will be low enough to allow the dismantling of the tanks with a minimum collective dose to the workers; and the activity of the dumps will have appreciably decreased.

b) Remove the 23 accelerating structures with their supports and vacuum chambers and bring them to a workshop equipped for handling radioactive equipment. The estimated dose rate at 10 cm distance ranges between almost zero and a maximum of about 1 μSv/h in few specific spots.

c) After removing the accelerator components, take the main dump out of its shielding following the dismantling procedure, put the entire dump assembly in a special container and prepare it for special waste disposal. This operation, if performed two years after the end of the operation, would lead to a maximum collective dose of 5 μSv.

d) In the workshop, remove the accelerating structures from their supports, open them up and separate radioactive from non-radioactive components. In order to minimize the collective dose, only mechanical disassembly will be performed on active parts, avoiding the cutting of welds for activated parts; this procedure is facilitated by the design of the accelerating tanks that privileges mechanically assembled components. In case of dose rate higher than 200 μSv/h, the unit will be left as it is.

e) In the tunnel, dismantle all components of the transfer line classified as radioactive and remove the activated part of the dump shielding.

As an example, it is possible to compute the expected collective dose during the dismantling of the DTL, which is considered to be one of the most complex for the presence of SmCo material inside the drift tubes. The dose resulting from opening the tanks and removing all drift tubes would amount approximately to (expected dose at surface × number of activated tubes × time required for drift tube removal × persons involved) = (10 μSv/h × 74 × 0.25 h × 2) = 370 μSv. The collective dose for the other two accelerating structures is expected to be lower.

The activation simulations provide an approximate estimation of the inventory of radioactive material produced after the decommissioning of Linac4 (Table 5.1).

Table 5.1: PSB proton beam characteristics for LHC, from LIU TDR.

Activation level	Activity	Quantity
Very low	< 100 Bq/g	2.7 m^3
Low or medium	> 100 Bq/g	0.8 m^3

References

[1] E. Mauro, M. Silari, *Nucl. Instrum. Meth.* **A605** (2009) 249, doi:10.1016/j.nima.2009.03.250.

[2] A. Ferrari *et al.*, FLUKA: A multi-particle transport code, CERN-2005-10, INFN-TC-05-11, SLAC-R-773 (2005), doi:10.2172/877507.

A Appendix

A.1 Measurements and commissioning

The commissioning of Linac4 was structured in six phases of increasing energy, intended to assess the beam quality after each accelerating section with the help of extra diagnostics located on a movable bench. This approach enabled progress in beam commissioning before complete installation of the hardware and optimization of the beam throughput at each stage. Most important it also enabled a cross check of the information from the permanent diagnostics against more detailed information from the temporary diagnostics and, therefore, the validation of a strategy to set up and diagnose possible faults when the Linac4 is operational.

The six phases of commissioning include dedicated beam measurements at the energy of 45 keV, 3 MeV, 12 MeV, 50 MeV, 100 MeV, and finally 160 MeV. Two benches were used during the Linac4 commissioning. A 'low-energy' bench, used at 3 and 12 MeV which allows direct measurement of the transverse emittance with a slit and grid (or laser and diamond detector) and direct measurement of the energy spread with a 28° bending magnet followed by a profile harp. A 'high-energy' bench was employed for the measurements at 50 and 100 MeV, which contains: a) three profile harps and three wire scanners at the appropriate phase advance (about 60 degrees) for an indirect emittance measurement; b) a bunch shape monitor and a lasing station (which allows transverse profile measurement via stripping); and c) two monitors for time-of-flight and beam centre position.

A.1.1 Direct measurements

The important result of the campaign at 3 and 12 MeV is that the direct method of slit and grid (or laser-diamond) and the indirect method based on emittance reconstruction from profiles give the same overall value for the emittance. Even more important, both the direct and indirect emittance measurements give the same orientation of the emittance within a range of 10%, which is a very important information for the matching of the beam to the structures downstream. With this result we have validated the model of the machine on which emittance reconstruction techniques rely and the correspondence between direct and indirect methods. The success of this campaign is also due to the method applied for the reconstruction that is more sophisticated than a standard matrix inversion. In particular, for Linac4 were developed a 'forward method' that extends the accuracy of the classic emittance reconstruction techniques to space charge dominated regimes, and the tomographic method that allows phase space density information to be calculated from the profile. These two methods combined allow for a full knowledge of the beam parameters without relying on direct emittance measurements. An example of a direct emittance measurement compared with a reconstructed emittance is given in Fig. A.1.

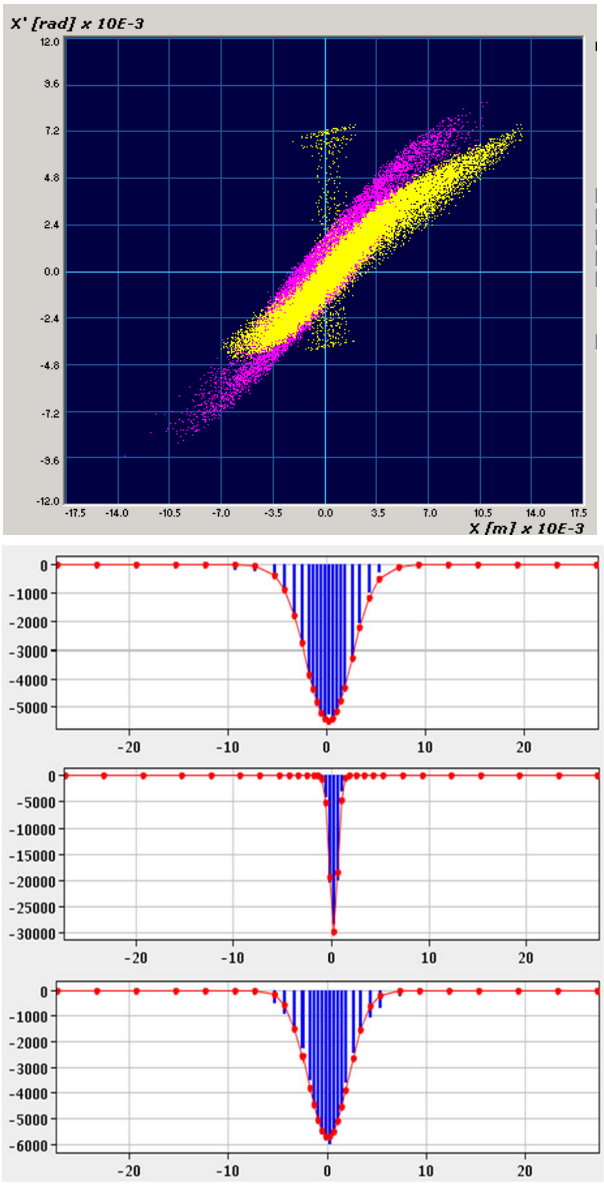

Fig. A.1: Transverse emittance measured with slit-and grid (yellow) compared to expectation (pink) at 12 MeV.

A.1.2 Indirect measurements

Following the measurements performed after the first DTL tank at 12 MeV, a period of installation of about ten months has led to the second type of measurement campaign. After the installation of the remaining DTL structures, the beam energy of 50 MeV no longer allows direct emittance and energy spread measurements. Several RF structures are installed in one period and the beam is passed through the unpowered RF structure to measure its quality at each energy step. This part of the commissioning has been accompanied by very accurate simulations as the beam in certain cases would travel 20 m without any acceleration before being measured in the bench. Backtracking techniques have also been employed and a combination of backtracking/forward tracing was employed to verify the consistency of the measurement. Emittance measured on the high energy bench is deduced from three (or more) profile measurements. An optimal phase advance between the profiles, located at 0.7 and 0.9 m from each other allows for a very accurate reconstruction. Emittance measured at 50 and 80 MeV are shown in Fig. A.2.

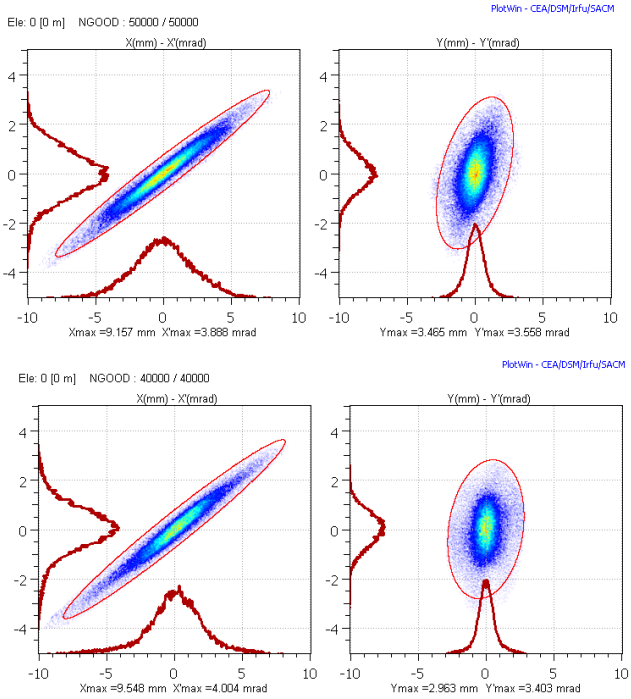

Fig. A.2: Estimated transverse emittance (top) compared to measured values at 80 MeV (bottom).

A.1.3 Setting of RF cavities' phase and amplitudes

One of the challenges of Linac4 during operation is to be able to set 22 phases and 23 amplitudes for the RF cavities without dedicated longitudinal beam diagnostics. To address this issue a dedicated campaign of finding beam-based signatures (indirect measurements of beam longitudinal parameters) was put in place after each structure. For the RFQ, plotting the transmission as a function of the RF voltage is sufficient to find the nominal amplitude. For the bunchers, a combination of beam loading observations, (to find the two RF zero crossings) and transverse beam sizes on a wire scanner enables the identification of the correct phase. Transmission through the DTL RF bucket is a good indication of the buncher amplitude and phase. For the DTL,CCDTL and in the future for the PIMS, a system based on measuring the average beam energy as a function of the cavity phase was validated as an accurate method to complement RF pick-up calibrations. In particular, a simple yet surprisingly precise method of measuring the beam energy gain through a cavity was the measurement of the beam loading. As the cavity is regulated so as to have a constant voltage, the low level RF systems responds to the presence of the beam depending on the phase between the cavity and the beam. The LLRF system will increase/decrease the power in the cavity (Power forward) depending on whether the beam is accelerated and therefore takes power from the cavity, or is decelerated and therefore gives power to the cavity. Figure A.3 shows the power of the cavity as the beam passes through the accelerating phase or at the decelerating phase. By measuring the difference in power (ΔP) and the beam current (I) at a downstream transformer the energy gain ΔE can be calculated via the formula

$$\Delta E = \frac{\Delta P}{I}.$$

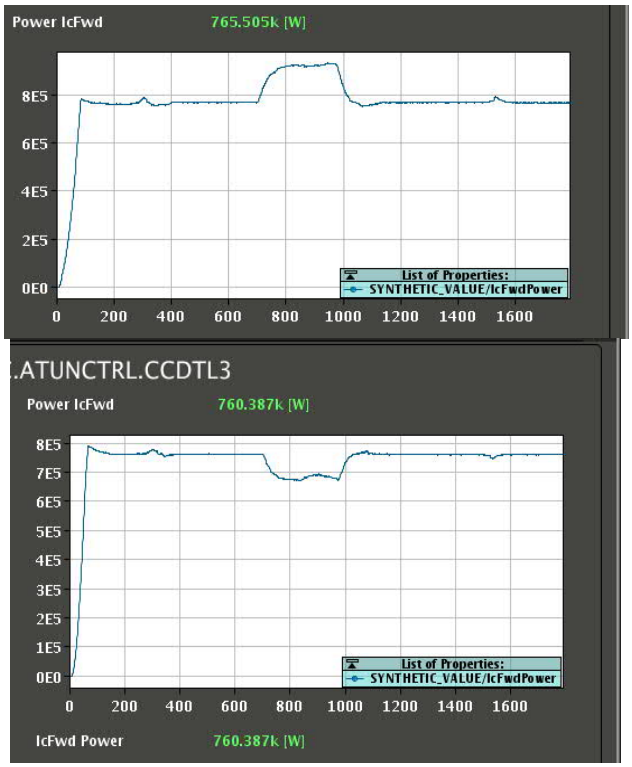

Fig. A.3: Forward power in CCDTL cavity number 3 when the beam is at the accelerating phase (top) or at the decelerating one (bottom).

Applying the above technique to the Linac4 CCDTL, has allowed to cross calibrate phase and amplitudes of the seven cavities. An example is shown in Fig. A.4.

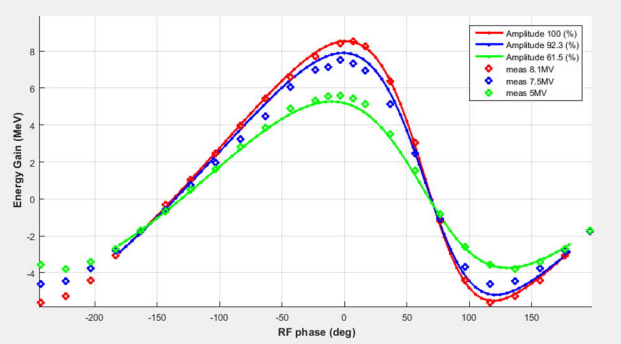

Fig. A.4: Energy gain in CCDTL cavity number 3 for three different amplitudes as a function of phase. Solid lines are simulation and dots are energy measurements deduced from beam loading observations.

For increased precision, the same measurement was repeated with a pair of pick-ups, which allow the measurement of the time of flight. Some pick-ups are located in between cavities and some are located on the bench. During the measurements, all the cavities downstream of the one being measured were switched off and detuned. The results are shown in Fig. A.5.

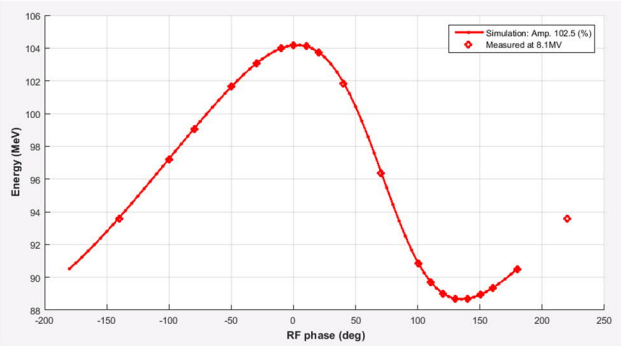

Fig. A.5: Energy gain in CCDTL cavity number 7 for three different amplitudes and varying phases. Solid lines are simulation and dots are energy measurements deduced from time-of-flight measurements.

A.2 Upgrade strategies

The Linac4 project was defined within an upgrade plan that was continuously evolving; its design incorporates a wide flexibility, intended to satisfy several options for the future development of the CERN accelerator facilities. The general design strategy was to specify the accelerator parameters for the PSB with LHC and ISOLDE as main users, leaving margin in some parameters for future upgrades if this was possible without large investment costs.

A.2.1 Energy upgrade

The upgrade in energy requires adding additional accelerating modules after the PIMS section and needs the construction of a new tunnel in the prolongation of the Linac4 tunnel, as considered in the SPL study (Fig. A.6). While the Linac4 tunnel could be excavated from a trench, an extension will have to go under the Computer Centre (Building 513) and be made using a tunnelling machine. The concrete wall at the end of the Linac4 tunnel, behind the main dump, has been constructed to be easily removed in case of an extension. The vertical level of the Linac4 beam has been fixed at 2.5 m below the level of the PS complex accelerators to leave sufficient margin between a future extension and the basement of Building 513 to avoid radiation concerns in Building 513. A vertical chicane in the Linac4 transfer line brings the beam to the PSB level.

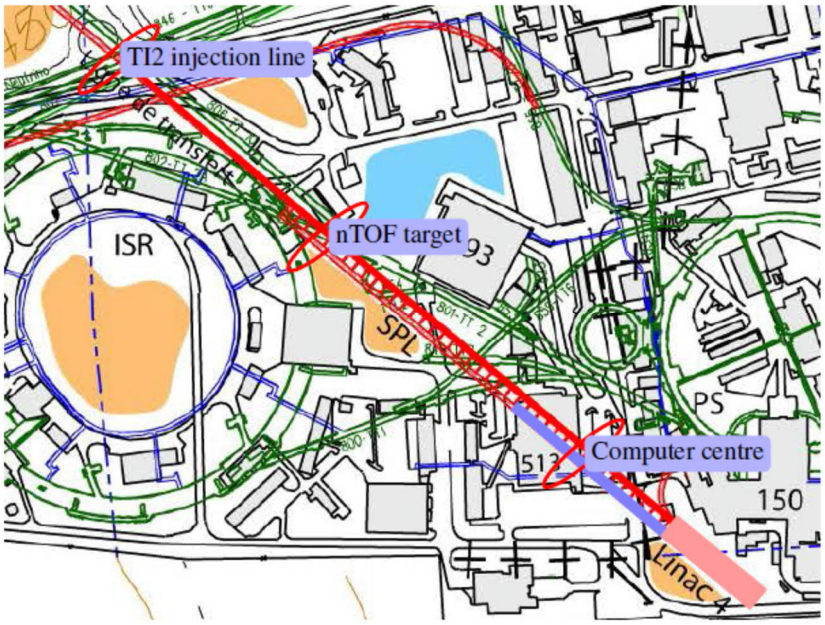

Fig. A.6: The SPL tunnels (accelerator and services) in the prolongation of Linac4.

A.2.2 Beam current upgrade

Linac4 has been designed to accelerate a current of 40 mA, averaged within the beam pulse. To achieve this current after chopping an ion source capable of producing about 70 mA of H^- ions in an emittance compatible with the acceptance of the RFQ is required, a value beyond the capabilities of present ion sources. The present ion source can produce 40 mA within the acceptance of the RFQ, giving 25 mA of pulse current; this leaves a margin for a 60% increase in beam current with a new ion source.

The limitation to 40 mA comes from the RF system; the use of old LEP klystrons on the CCDTL modules is the main limitation for RF power and therefore for beam current, while the future replacement of the LEP klystrons with new klystrons at 2.8 MW peak power will allow this limit to be reconsidered. The theoretical beam dynamics limitation from space charge is 52 mA (after chopping).

A.2.3 Pulse length upgrade

While the PSB distributor is designed for a maximum pulse length of 600 μs, most of the Linac4 power converters have been specified for possible use in a future low power (e.g., low repetition rate) SPL at 1.2 ms pulse length. This is in particular the case of the klystron modulators that allow an RF pulse duration of 1.2 ms. Increasing pulse duration up to this limit is relatively simple requiring only an upgrade of the 3 MeV injector power converters, which were specified before the definition of the low-power SPL for a maximum pulse length of 600 μs.

A.2.4 Repetition frequency upgrade

In the original plan, Linac4 was required to be compatible with future operation at 50 Hz repetition frequency, for use in the proton driver of a neutrino or radioactive ion facility [1]. The maximum pulse length in this case was 0.8 ms, giving a duty cycle of 4%. Considering the uncertainty in the parameters and the need to keep a safety margin, all accelerating structures have been designed and built for a maximum duty cycle of 10%. In the present configuration, only the cooling required for operation as PSB injector has been installed, and an extensive upgrade of the cooling system will be required if the duty cycle is increased. The new Linac4 klystrons have been specified for a 6% beam duty cycle (50 Hz and 1.2 ms), this parameter having a minor impact on the cost; the old LEP klystrons were built for CW operation. However, pulsing the RF at a higher repetition frequency will require replacing all modulators.

The shielding of the Linac4 tunnel was also dimensioned for the beam loss related to high duty cycle operation; this provides a margin in the operation for the PSB and makes possible a future upgrade. In the tunnel cross-section, a provision has been left for the additional cooling pipes required for high-duty operation (Fig. A.7); in the surface building, additional space is foreseen for the larger power converters.

Table A.1 summarizes the main interventions required on Linac4 to make operation at high duty cycle possible.

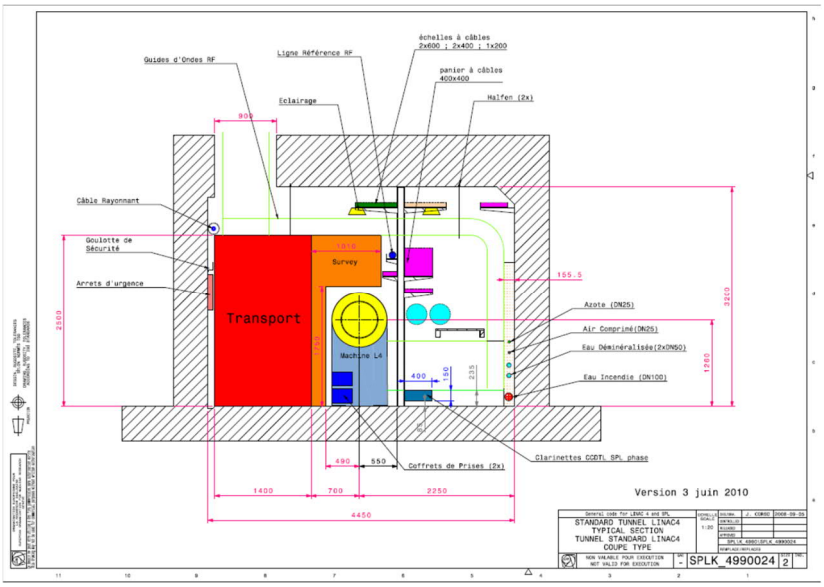

Fig. A.7: Cross-section of the Linac4 tunnel showing the planned position of the additional cooling pipes required for high duty cycle operation, in the technical corridor to the right of the accelerating structures (light blue).

Table A.1: Main modifications to the Linac4 accelerator (excluding the transfer lines) for high duty cycle operation.

Element	Location	Intervention
Ion source	Tunnel	New source for high duty cycle
RFQ and accelerating structures cooling	Tunnel	Add cooling pipes and improve cooling configuration, add cooling to tuners and couplers
Main cooling pipes	Tunnel	Add cooling pipes and distribution in the technical corridor for larger water flow
Main dump	Tunnel	Replace with a dump dimensioned for high beam power
Electromagnetic quadrupoles	Tunnel	Replace the air-cooled quadrupoles with water-cooled or permanent
Beam diagnostics	Tunnel	Upgrade for higher average current
Cooling station	Building	Upgrade for larger power
Klystrons modulators	Building	Replace for higher repetition frequency
Power converters	Building	Replace for higher repetition frequency
Electrical distribution	Building	Upgrade for larger power
Buncher amplifiers	Building	Upgrade for higher duty cycle

A.3 Selection of CERN EDMS internal documents related to Linac4

A.3.1 Chapter 2

2.1 1585312, 1519468, 1586866, 1521020, 1261469, 1585317, 980861, 1525272, 1525292, 1584094, 1584821 and 1509956.

2.8 1187543 and 1291572.

A.3.2 Chapter 3

3.2 1057463, 1256894, 1366039, 1373207 and 1301655.
3.5 1405391, 1525044, 977112, 1159270, 1183024, 1265033, 998731, 1137518, 1232370, 1183023, 1492698, 1252682, 1269423 and 1274890.
3.6 1866793.
3.7 1173438 and 1149687.
3.9 567256, 1016233, 636589 and 1319721.
3.10 991526 and 1004277.

A.3.3 Chapter 4

4.1 874712, 875307, 904354, 904350 and 904353.
4.3 1001010, 1000528, 1108361 and 1084036.

A.3.4 Chapter 5

5.1 1316656, 1182648 and 1263477.
5.2 1181158, 1227231, 1280472, 1280745 and 1280750.
5.3 1316656.

A.4 Parameter list

The following parameter list refers to the Linac4 baseline design of August 2012.

A.4.1 General linac parameters

Ion species	H^-
Overall linac length	76.33 m
Output energy	160 MeV
Bunch frequency	352.2 MHz
Maximum beam pulse length	600 μs
Chopper beam-on factor	65 %
Nominal chopping scheme	229 bunches transmitted / 123 removed
Source current, nominal	40 mA
Linac current, nominal after chopping	25 mA
Linac current, maximum	40 mA (for source current 62 mA)
Transverse emittance	0.4 π mm mrad (rms, normalised)
Number of particles per pulse	1.5×10^{14}

A.4.2 Operating modes

	Normal for PSB	*Maximum for PSB*	*Linac test*
Pulse repetition frequency	0.83 Hz	1.1 Hz	2 Hz
Pulse spacing	1.2 s	0.9 s	0.5 s
Beam duty cycle	0.05%	0.066%	0.12%
Average beam current	12.5 μA	16.5 μA	30 μA
Average beam power	2 kW	2.64 kW	4.8 kW

A.4.3 Error tolerances from beam dynamics

Values at 1σ	
Quadrupole gradient	± 0.5 %
Quadrupole displacement	± 0.1 mm
Quadrupole rotation (x,y)	± 0.5°
Quadrupole rotation (z)	± 0.2°
Cavity field phase	± 1°
Cavity field amplitude	± 1 %

A.4.4 Ion source

Type	RF surface
Max. Repetition rate	2 Hz
Extraction voltage	45 kV
RF frequency	2 MHz
Max. RF power	100 kW

A.4.5 Low Energy Beam Transport

Focusing elements	2 solenoids
Length	1.955 m

A.4.6 Radio Frequency Quadrupole

Input energy	45 keV	
Output energy	3.0 MeV	
RF frequency	352.2 MHz	
Beam current at input	70 mA	
Design RF duty cycle	10%	
Voltage	78.27 kV	
Modulation factor	1.0–2.4	
Beam peak power	210 kW	for 70 mA
Max. RF peak power	700 kW	1.2 computed + beam
Max field on pole tip	34 MV/m	1.84 Kilpatrick
Transmission	95%	
Number of klystrons	1 (1.3 MW)	
Number of cells	300	
Length	3.06 m	
Beam aperture	3.2–1.8 mm	
Vacuum	10^{-7} mbar	

A.4.7 Chopper line (Medium Energy Beam Transport)

Beam energy	3 MeV	
Peak current	66.5/62 mA	Input/Output
Average pulse current	66.5/40 mA	Input/Output
Chopper plate voltage	700 V	
Effective chopper plate voltage	>500 V	seen by beam
Chopper rise/fall time	< 2 ns	10–90 %
Chopper repetition rate	1–2 Hz	
Maximum chopping factor	40 %	

Chopper deflection angle	7 mrad	
RF frequency buncher cavities	352.2 MHz	
Maximum buncher voltage	150 kV	
RF peak power per buncher	16–18 kW	
Number of buncher cavities	3	352.2 MHz
Number of chopper structures	2	inside quadrupoles
Number of quadrupoles	11	
Length of chopper plates	400 mm	
Chopper plate distance	20 mm	
Length	3.7 m	
Beam collimation	appr. 7%	controlled beam loss on internal dump

A.4.8 Drift Tube Linac

Input energy	3 MeV
Output energy	50.26 MeV
RF frequency	352.2 MHz
Design RF duty cycle	10%
Beam current during pulse	40 mA
Beam power	1.89 MW
Total RF power	4.928 MW
Number of tanks	3
Focusing scheme	FOFODODO
Total length	19.1 m
Transition to CCDTL	0.67 m
Beam aperture	20 mm
Quadrupole type	PMQ
Quadrupole length Tank1	45 mm
Quadrupole length Tank2	80 mm
Number of quadrupoles	112
Outer drift tube diameter	90 mm
Inner quadrupole diameter	22 mm
Vacuum	10^{-7} mbar

	Tank 1	*Tank 2*	*Tank 3*	
Output energy	11.88	31.45	50.26	MeV
Length	3.896	7.341	7.255	m
Number of quadrupoles	39	43	31	
Accelerating field	3.1	3.3	3.3	MV/m
Maximum surface field	1.6	1.4	1.3	Kilpatrick
Synchronous phase	-35 to -24.5	-24	-24	Deg
Peak RF power	0.988	2.001	1.939	MW
Number of klystrons	1 (1.3 MW)	1 (2.8 MW)	1 (2.8 MW)	
Cells per tank	39	42	30	
Effective shunt impedance ZT^2	43.76	52.44	50.75	MΩ/m
Q-value Q_0	39123	43383	42965	
Nominal tank voltage V_0T	10.34	21.65	20.90	MV
Cavity copper losses	633.10	1218.29	1186.71	kW

A.4.9 Cell-Coupled DTL

Input energy	50.26 MeV
Output energy	102.9 MeV
RF frequency	352.2 MHz
Beam current during pulse	40 mA
Design RF duty cycle	10 %
Accelerating field E_0	2.7–3.6 MV/m
Maximum surface field	1.6–1.7 Kilpatrick
Synchr. phase	-20°
Total beam power	2.1 MW
RF power per module	0.95–1.0 MW
Total RF power	7.0 MW
Number of klystrons	7 (1.3 MW)
Cells per cavity	3
Cavities per module	3
Coupling cavities per module	2
Number of cavities	21
Number of modules	7
Number of quadrupoles	21 (14 PMQ, 7 EMQ)
Focusing scheme	FODO
Length	25.0 m
Transition to PIMS	1.2 m
Beam aperture	28 mm
Vacuum	10^{-7} mbar

	Module1	*Module2*	*Module3*	*Module4*	*Module5*	*Module6*	*Module7*	
Cavity length	2.14	2.32	2.48	2.64	2.79	2.93	3.06	m
Output energy	57.15	64.54	72.07	79.90	87.76	95.58	102.94	MeV
Voltage V_0T	7.59	7.91	8.01	8.33	8.35	8.33	8.36	MV
Q_0	40400	41600	44200	41500	41700	41800	42500	
ZT^2	40.6	39.8	40.1	38.5	36.5	34.5	33.3	MΩ/m
Beam power	285	297	301	313	314	313	295	kW

A.4.10 PI-Mode Structure

Input energy	102.9 MeV
Output energy	160 MeV
RF frequency	352.2 MHz
Average beam current	40 mA

Design RF duty cycle	10%	
Accelerating gradient E_0T	3.74 MV/m	cavities 1 to 10
Accelerating gradient E_0T	2.92 MV/m	cavities 11 and 12
Maximum surface field	33 MV/m	1.8 Kilpatrick
Synchronous phase	-20°	
Total beampower	2.3 MW	
Total RF power	11.0 MW	
Number of klystrons	8 [1.3 MW] + 2 [2.8 MW]	
Cells per cavity	7	
Number of cavities	12	
Number of quadrupoles	12 (EMQ)	
Focusing scheme	FODO	
Length	21.5 m	
Beam aperture	40 mm	
Vacuum	10^{-7} mbar	

	Cavity1	*Cavity2*	*Cavity3*	*Cavity4*	*Cavity5*	*Cavity6*	
Length	1.298	1.326	1.350	1.373	1.395	1.418	
Voltage V_0	4.805	4.909	4.995	5.078	5.159	5.242	MV
Output energy	107.4	112.0	116.7	121.5	126.3	131.3	MeV
Q_0	20800	21032	21222	21319	21452	21810	
ZT^2	24.622	24.881	25.103	25.203	25.358	25.750	MΩ/m
Beam power	181	185	188	191	194	197	kW
Cavity losses	739	747	753	763	771	782	kW

	Cavity7	*Cavity8*	*Cavity9*	*Cavity10*	*Cavity11*	*Cavity12*	
Length	1.440	1.462	1.484	1.505	1.524	1.540	
Voltage V_0	5.327	5.400	5.476	5.551	4.387	4.433	MV
Output energy	136.3	141.3	146.5	151.7	155.8	160.0	MeV
Q_0	21835	22154	22175	22477	22557	22673	
ZT^2	25.771	26.110	26.121	26.442/	26.509	26.621	MΩ/m
Beam power	200	203	206	209	165	167	kW
Cavity losses	784	795	796	796	490	493	kW

A.4.11 Transfer line

Input energy	160 MeV	
Output energy	160 MeV	
Total length	177.6 m	to PSB entrance
Total length of new section	70.9 m	to LT.BHZ20
Number of RF cavities	1	

Cavity voltage	0.7 MV	
Power per cavity	60 kAV/20 kW	apparent power/dissipated power
Number of quadrupoles	17+18	new + old
Quadrupole aperture	50 mm + 45 or 70 mm	new + old
Number of bendings	5 + 2	new + old
Vacuum	10^{-7} mbar	

A.4.12 Layout

Section	Element	Description	Beam energy at input	Input position (from source)	Length (incl. intertank)	Length of acc. structure	Length of section	Focusing elements	Diagnostics elements	Steering elements	Real estate acc. gradient	Overall length
			[MeV]	[m]	[m]	[m]	[m]				[MeV/m]	[m]
L4L	L4L.NFHR.0111	Ion source	0	0	0.485		9.324					76.329
	L4L.LEBT.1101	LEBT	0.045	0.48	1.955			2 solenoids	1 BCT 1 SEM 1 FC	2 HV		
	L4L.ACRFQ.2101	RFQ	0.045	2.44	3.233	3.06					0.97	
	L4L.LMEBT.3101	MEBT (chopper line)	3	5.673	3.651			11 EMQ 3 RF	2 BCT 2 WS 1 BPM	2 HV		
L4D	L4D.ACDT.0125	DTL tank 1	3	9.397	4.039	3.966	19.127	39 PMQ 1 EMQ	1 BPM	1 HV	2.47	
	L4D.ACDT.0225	DTL tank 2	11.88	13.571	7.618	7.41		43 PMQ	1 BPM	1 HV		
	L4D.ACDT.0325	DTL tank 3	31.45	21.126	7.47	7.325		30 PMQ				
L4C	L4C.ACCD.0125	CCDTL module 1	50.26	29.062	3.308	2.697	25.004	1 EMQ 2 PMQ	1 BPM 1 BCT 1 BLM 1 SEM	1 HV	2.11	
	L4C.ACCD.0225	CCDTL module 2	57.1	32.117	3.229	2.871		1 EMQ 2 PMQ	1 BPM 1 BLM 1 WS			
	L4C.ACCD.0325	CCDTL module3	64.6	35.346	3.395	3.037		1 EMQ 2 PMQ	1 BPM	1 HV		
	L4C.ACCD.0425	CCDTL module4	72.1	38.741	3.552	3.194		1 EMQ 2 PMQ	1 BPM 1 BLM 1 WS			
	L4C.ACCD.0525	CCDTL module5	79.9	42.293	3.703	3.345		1 EMQ 2 PMQ	1 BPM	1 HV		
	L4C.ACCD.0625	CCDTL module6	87.8	45.996	3.844	3.486		1 EMQ 2 PMQ	1 BPM 1 BLM 1 WS			
	L4C.ACCD.0725	CCDTL module7	95.6	49.84	3.973	3.615		1 EMQ 2 PMQ	1 BPM	1 HV		
L4P	L4P.ACPM.0125	PIMS cavity 1	102.9	54.186	2.121	1.39	22.874	1 EMQ	1 BPM 1 BCT 1 BLM 1 SEM	1 HV	2.50	
	L4P.ACPM.0225	PIMS cavity 2	107.4	55.899	1.74	1.417		1 EMQ				
	L4P.ACPM.0325	PIMS cavity 3	112.0	57.578	1.773	1.511		1 EMQ	1 BPM	1 HV		
	L4P.ACPM.0425	PIMS cavity 4	116.7	59.427	1.802	1.464		1 EMQ	1 BLM 1 WS			
	L4P.ACPM.0525	PIMS cavity 5	121.5	61.236	1.831	1.486		1 EMQ	1 BPM	1 HV		
	L4P.ACPM.0625	PIMS cavity 6	126.3	63.074	1.862	1.51		1 EMQ	1 SEM			
	L4P.ACPM.0725	PIMS cavity 7	131.3	64.942	1.889	1.531		1 EMQ	1 BPM	1 HV		
	L4P.ACPM.0825	PIMS cavity 8	136.3	66.838	1.919	1.554		1 EMQ				
	L4P.ACPM.0925	PIMS cavity 9	141.3	68.764	1.945	1.573		1 EMQ	1 BPM	1 HV		
	L4P.ACPM.1025	PIMS cavity 10	146.5	70.715	1.974	1.596		1 EMQ	1 BLM 1 WS			
	L4P.ACPM.1125	PIMS cavity 11	151.7	72.694	1.998	1.615		1 EMQ	1 BPM	1 HV		
	L4P.ACPM.1225	PIMS cavity 12	155.8	74.698	2.02	1.631		1 EMQ				
L4T(1)		Line section 1	160.0	0	7.476		7.476	2 EMQ	1 BCT 2 BPM 2 SEM 1LPM	3 HV		70.934
	L4T.MBH.0250	Bending magnet 1	160	7.476								
L4Z		Line section dump	160	7.476	4.466		7.466		1 BCT 1 BLM 2 SEM			
L4T(2)		Line section 2	160	7.476	4.1		63.458	2 EMQ	1 BLM	1 HV		
	L4T.MBH.0450	Bending magnet 2	160	11.576								
		Line section 3	160	11.576	4.1			2 EMQ	1 SEM			
	L4T.MBH.0650	Bending magnet 3	160	15.676								
		Line section 4	160	15.676	25.9			4 EMQ	2 BCT 4 BPM 2 BLM	4 HV		
	L4T.ACDB.1075	Debuncher	160	41.576								
		Line section 5	160	41.576	8.95			2 EMQ	1 BCT 3 BPM 2 BLM 1 SEM	2 HV		
	L4T.MBV.1250	Bending magnet 4	160	50.526								
		Line section 6	160	50.526	10			3 EMQ	1 BLM	2 HV		
	L4T.MBV.1550	Bending magnet 5	160	60.526								
		Line section 7	160	60.526	10.408			2 EMQ	1 BCT 2 BPM 2 BLM	1 HV		
LT	LT.BHZ20	Bending magnet	160	70.934								

References

[1] F. Gerigk (ed.), Conceptual design of the low-power and high-power SPL: a superconducting H^- Linac at CERN, CERN-2014-007 (2014), doi:10.5170/CERN-2014-007.